MODELING AND CONTROL OF A HYBRID ELECTRIC DRIVETRAIN FOR OPTIMUM FUEL ECONOMY, PERFORMANCE AND DRIVEABILITY

DISSERTATION

Presented in Partial Fulfillment of the Requirements for

the Degree Doctor of Philosophy

in the Graduate School of The Ohio State University

By

Xi Wei, M.S.

* * * * *

The Ohio State University
2004

Dissertation Committee:	Approved by
Professor Giorgio Rizzoni, Adviser	________________________________
Professor Vadim Utkin, Co-Adviser	________________________________
	Advisers
Professor Stephen Yurkovich	Graduate Program in Mechanical Engineering

ABSTRACT

Automotive manufacturers have been striving for decades to produce vehicles which satisfy customers' requirements at minimum cost. Many of their concerns are on fuel economy, road performance and driveability. Improving fuel economy is both a political concern of alleviating dependency on foreign fuel and a customer preference of reducing vehicle operating cost. Consumers also expect vehicles to provide satisfactory performance with desirable driving comfort. Improvements on all these aspects may contribute to lower emissions as well if the vehicle is designed and controlled properly.

A hybrid electric vehicle (HEV) is one of the most promising alternatives to a conventional engine-powered vehicle which satisfies increasing customer requirements mentioned above. However, how much the hybrid vehicle is better than the conventional one depends heavily on its control strategy. The involvement of the electric machine for HEV traction offers the possibility to provide the total tractive force in different ways. Investigations indicate that how to allocate the total tractive force between the engine and the electric machine has significant influences on vehicle fuel economy, performance and driveability. Therefore, designing an optimal control strategy which considers all three criteria is of great interest.

Model based control design requires control oriented models and the complexity of these models are determined by their applications. The control oriented models need to be sufficient to evaluate the control criteria and easy enough for control strategy development. Vehicle fuel economy and performance are related with power allocation in the steady state while human perceptible driveability issues are in the frequency range of a few hertz. Since the control strategy is developed in two steps (finding the solution for the best fuel economy first and then taking driveability into account), two models, i.e.,

the quasi-static model and the low-frequency dynamic model are built for each step in the control design. Simulation results demonstrate that these two models are effective to capture the main behaviors of the vehicle and to evaluate fuel economy, performance and driveability respectively.

Defining objective metrics for vehicle fuel economy, performance and driveability is also very important. Evaluations in both simulations and real vehicles require objective and quantitative measures. Subjective and descriptive metrics cannot be easily implemented in simulations and evaluations vary with changing time or evaluators. Vehicle fuel economy is estimated under various city, highway and some other user-defined driving schedules. Performance criteria consist of acceleration/deceleration performance, gradeability and towing capability. Driveability measures deal with pedal responsiveness, operating smoothness and driving comfort, which include interior noise level, jerk, tip-in/tip-out response, Maximum Transient Vibration Value (MTVV), acceleration Root Mean Square (RMS) value and Vibration Dose Value (VDV). Numerical references and some interpretations for these metrics are also presented in this dissertation.

The optimal control solution is then found hierarchically with the help of Pontryagin's minimum principle based on models, i.e., solving vehicle fuel economy optimization first and then taking driveability into consideration. Meeting power requests always has the highest priority which guarantees good vehicle performance. Fuel economy optimization contains three steps: finding the optimal solution for known constant power requests, for known time-varying power requests and for unknown time-varying power requests with short-term predictions. An innovative interpretation of the minimum principle is applied when minimizing fuel consumption for the vehicle with constant battery parameters and fixed CVT ratio under constant power requests. This so-called sliding optimal control which switches between two control values has been theoretically proven to be the optimal solution. The control strategy developed with the minimum principle is compared with a simple heuristic one and simulation results demonstrate an improvement on vehicle fuel economy.

Dedicated to my parents and my husband

ACKNOWLEDGMENTS

I would like to express my sincere gratitude to my adviser Dr. Giorgio Rizzoni for leading me into the automotive field. I have been impressed by his beautiful sharp mind. His guidance and experience as well as his trust have provided a continuous inspiration for this dissertation.

It is my great pleasure to have Dr. Vadim Utkin to be my co-adviser. His invaluable guidance and unique way of thinking has opened my eyes to a new world. I also enjoyed all the discussions and chatting between us.

I would like to thank Dr. Lino Guzzella for all his advices and nice discussions. I am also very thankful to Dr. Yurkovich for reviewing this work.

I would like to express my appreciation to my best friends Yubing Xie and Yanfei Liu for sharing my laughs and tears. Being friends of you is one of the most beautiful parts of my life in America. I also acknowledge all the fellow students at the Center for Automotive Research and Intelligent Transportation for their assistance in numerous problems.

Finally I am very indebted to my parents and Feng for their constant support and encouragement. It is impossible to go through all the difficulties without your love.

VITA

March 16, 1973 …………………………..	Born – Shanghai, China.
July 1995 ………………………………….	B.S. Mechanical Engineering and Electrical Engineering, Dalian University of Technology, Dalian, China.
July 1998 ………………………………….	M.S. Mechanical Engineering, Tsinghua University, Beijing, China.
1998 – present …………………………….	Graduate Teaching and Research Associate, The Ohio State University, Columbus, OH.

PUBLICATIONS

Research publications

1. Wei X., Rizzoni G., 2004, "Modeling of Hybrid Electric Vehicles for Various Optimization Applications", *ASME Transaction, Journal of Dynamic Systems, Measurement, and Control.*

2. Wei X., Guzzella L., Utkin V., Rizzoni G., 2004, "Model-based Fuel Optimal Control of Hybrid Electric Vehicle Using Variable Structure Control Systems", *ASME Transaction, Journal of Dynamic Systems, Measurement, and Control.*

3. Wei X., Utkin V., Rizzoni G., 2004, "Sliding Optimal Control for Hybrid Electric Vehicle Energy Management Optimizations", *IFAC FISITA F2004F060.*

4. Wei X., Rizzoni G., 2004, "Objective Metrics of Fuel Economy, Performance and Driveability", *SAE paper 2004-01-1338*.

5. Wei X., Pisu P., Rizzoni G., Yurkovich S., 2003, “Dynamic Modeling of a Hybrid Electric Drivetrain for Fuel Economy, Performance and Driveability Evaluations”, *Proceedings of ASME International Mechanical Engineering Congress and Exposition 2003, Washington D.C.*

6. Wei X., Rizzoni G., 2001, “A Scalable Approach for Energy Converter Modeling and Supervisory Control Design”, *Proceedings of ASME International Mechanical Engineering Congress and Exposition 2001, New York, NY*.

7. Rizzoni G., Guezennec Y., Brahma A., Wei X., Miller T., 2000, “VP-SIM: A Unified Approach to Energy and Power Flow Modeling Simulation and Analysis of Hybrid Vehicles”, *Proceedings of the 2000 Future Car Congress*, *Arlington, Virginia*.

FIELDS OF STUDY

Major Field: Mechanical Engineering

Specialization: system dynamics, modeling and control of automotive powertrains, hybrid electric vehicles, driveability objective metrics.

TABLE OF CONTENTS

Page

Abstract………………………………………………………………………… ii

Dedication ………………………………………………………………………... iv

Acknowledgments……………………………………………………………..... v

Vita…………………………………………………………………………………... vi

List of Figures…………………………………………………………...…... xi

List of Tables………………………………………………………………...…… xiv

Abbreviates……………………………………………………………..……… xv

CHAPTERS:

CHAPTER 1 INTRODUCTION 1
1.1 Motivation and Problem Statement 1
1.2 Contributions of the Research... 8
1.3 Organizations of the Dissertation... 9

CHAPTER 2 LITERATURE REVIEW AND BACKGROUND 10
2.1 Modeling and Simulation.. 10
2.2 Modeling of a Hybrid Electric Drivetrain... 14
2.3 Control 17
2.3.1 Supervisory Control Strategies for Hybrid Electric Vehicles................... 18
2.3.2 Control Algorithms for Improving Performance and Driveability........... 28
2.3.3 Optimal Control Theory Overview 30
2.4 Summary 34

CHAPTER 3 OBJECTIVE METRICS FOR FUEL ECONOMY, PERFORMANCE AND DRIVEABILITY 36
3.1 Introduction to Fuel Economy, Performance and Driveability Evaluation Criteria 36
3.2 Objective Metrics for Fuel Economy.. 40

3.2.1 Fuel Economy Metrics 40
3.2.2 Numerical References of Fuel Economy Metrics 43
3.3 Objective Metrics for Performance 45
3.3.1 Performance Metrics 45
3.3.2 Numerical References of Performance Metrics 47
3.4 Objective Metrics for Driveability 48
3.4.1 Driveability Metrics 48
3.4.2 Numerical References of Driveability Metrics 53
3.4.3 Relationship between Subjective and Objective Driveability Metrics 55
3.5 Summary 56

CHAPTER 4 MODEL DESCRIPTION 57
4.1 Drivetrain Model for Fuel Economy Optimization 57
4.1.1 Internal Combustion Engine 58
4.1.2 Electric Machine 66
4.1.3 Battery 71
4.1.4 Torque Converter (TC) 72
4.1.5 Continuously Variable Transmission (CVT) 75
4.1.6 Final Drive (Differential) 78
4.1.7 Vehicle Longitudinal Dynamics 78
4.1.8 Controller 79
4.1.9 Driver 80
4.2 Drivetrain Model for Fuel Economy, Performance and Driveability Optimization 80
4.2.1 Engine 81
4.2.2 Integrated Starter/Alternator (ISA) 87
4.2.3 Torque Converter 88
4.2.4 Continuously Variable Transmission (CVT) 90
4.2.5 Driveshaft 91
4.2.6 Brake-By-Wire (BBW) 92
4.3 Summary 92

CHAPTER 5 OPTIMAL CONTROL STRATEGY DEVELOPMENT 94
5.1 Optimal Control for Best Fuel Economy 101
5.1.1 Control Problem Formulation 103
5.1.2 Optimal Control for Constant Power Requirement 104
5.1.3 Optimal Control for Time-Varying Power Requirement 125
5.1.4 Optimal Control with Predicted Driving Conditions 133
5.2 Optimal Control Considering Fuel Economy, Performance and Driveability 139
5.2.1 Problem Formulation 140
5.2.2 Relationship of Control Variables with Performance and Driveability Measures 143
5.3 Summary 148

CHAPTER 6 CONCLUSIONS AND FUTURE WORK 149
6.1 Conclusions 149
6.2 Future Work 152

APPENDIX A ADDITIONAL DRIVING CYCLES AND PERFORMANCE MANEUVERS ……………………………………………………..…………..…... 153

APPENDIX B MODEL IMPLEMENTATION ………….…………………………….... 155

Bibliography…………….…………….…………...……………………………………….. 167

LIST OF FIGURES

Figure: Page

Figure 1.1 Schematic of an HEV powertrain ... 5
Figure 1.2 Model hierarchy based on time scale ... 6
Figure 2.1 Model hierarchy for a parallel HEV ... 14
Figure 2.2 A schematic of zeroth-order model for a parallel HEV ... 15
Figure 2.3 A schematic of low-order model for a parallel HEV ... 17
Figure 2.4 Hierarchical control in an HEV ... 18
Figure 2.5 Techniques for reducing engine fuel consumption ... 20
Figure 2.6 Engine peak efficiency line ... 22
Figure 2.7 Engine lowest fuel consumption line ... 23
Figure 3.1 Torque hole during shifting [65] ... 39
Figure 3.2 Federal Urban Driving Schedule (FUDS) ... 41
Figure 3.3 Federal Highway Driving Schedule (FHDS) ... 41
Figure 3.4 Fuel economy of 2003 model year vehicles ... 44
Figure 3.5 Tip-in response ... 52
Figure 3.6 Horizontal Vibration Exposure Limit ... 54
Figure 3.7 Vertical Vibration Exposure Limit ... 54
Figure 3.8 Time Dependency of Vibration Exposure Limit ... 55
Figure 4.1 Schematic of engine basic functions ... 59
Figure 4.2 Engine efficiency map of a 2.2 L SI engine ... 60
Figure 4.3 Engine fuel consumption map of a 2.2 L SI engine (g/s) ... 61
Figure 4.4 Schematic of the input-output relationship of an energy converter ... 63
Figure 4.5 Scaled Willans line model of a gasoline engine (2.2 L) ... 66
Figure 4.6 Efficiency map of a 30 kW (peak) induction machine ... 67
Figure 4.7 Scaled Willans line model of an electric machine (30 kW induction) ... 70
Figure 4.8 Battery Model Schematic ... 71
Figure 4.9 Torque converter stator operation ... 73
Figure 4.10 Torque converter performance curves [107] ... 74
Figure 4.11 A push-belt CVT ... 75
Figure 4.12 Shifting of a push-belt CVT [109] ... 76
Figure 4.13 CVT efficiency map ... 76
Figure 4.14 Control strategy for the baseline vehicle ... 80
Figure 4.15 Schematic of a SI gasoline engine (after Kim [107]) ... 81
Figure 4.16 Block diagram of automotive powertrain dynamics (after Rizzoni [107]) ... 82

Figure 4.17 Effect of manifold pressure on intake air mass flow rate 84
Figure 4.18 Torque converter characteristics.. 90
Figure 5.1 Optimal control solving procedure 94
Figure 5.2 Example #1: state trajectory under sliding optimal control........................... 97
Figure 5.3 Example #1: sliding optimal control trajectory 97
Figure 5.4 Example #2: Hamiltonian versus control variable 100
Figure 5.5 Example #2: state trajectories under sliding optimal control 100
Figure 5.6 Hamiltonian versus engine power 112
Figure 5.7 Hamiltonian versus engine power 112
Figure 5.8 Optimal control for vehicles with batteries of different internal resistance .. 115
Figure 5.9 Fuel consumption savings comparing HEV, ... 116
Figure 5.10 State trajectories under sliding optimal control.. 117
Figure 5.11 Flow chart of solving optimal control for constant power requests 118
Figure 5.12 Optimal control for constant speed and torque requirement 119
Figure 5.13 Optimal engine torque, battery SOC and co-state variable for a 120-second long constant torque request trip (T_{req} = 29.94 N·m) 120
Figure 5.14 Hamiltonian versus engine torque (T_{req} = 29.94 N·m) 121
Figure 5.15 Zoom-in Hamiltonian versus engine torque (T_{req} = 29.94 N·m) 121
Figure 5.16 Optimal engine and ISA torques for constant power requests 123
Figure 5.17 Optimal CVT ratio for constant power requests (variable battery parameters) 123
Figure 5.18 Fuel Improvement of an HEV with Different Control Strategies over a Conventional Vehicle for Constant Power Requests 124
Figure 5.19 Flow chart of solution method for optimal control for variable power requests 126
Figure 5.20 Optimal engine operating points on fuel consumption map (FUDS).......... 127
Figure 5.21 Optimal electric machine operating points on efficiency map (FUDS)...... 127
Figure 5.22 Optimal transmission ratio (FUDS).. 129
Figure 5.23 Battery state of charge under optimal control (FUDS) 129
Figure 5.24 Optimal engine operating points on fuel consumption map (FHDS).......... 130
Figure 5.25 Optimal electric machine operating points on efficiency map (FHDS)...... 131
Figure 5.26 Optimal transmission ratio (FHDS).. 131
Figure 5.27 Battery state of charge under optimal control (FHDS) 132
Figure 5.28 Schematic of the prediction window in the optimal control problem 133
Figure 5.29 Optimal engine operating points on fuel consumption map (FUDS) (prediction window)... 135
Figure 5.30 Optimal electric machine operating points on efficiency map (FUDS) (prediction window)... 135
Figure 5.31 Optimal transmission ratio (FUDS) (prediction window).......................... 136
Figure 5.32 Battery state of charge under optimal control (FUDS) (prediction window) 136
Figure 5.33 Optimal engine operating points on fuel consumption map (FHDS) (prediction window)... 137
Figure 5.34 Optimal electric machine operating points on efficiency map (FHDS) (prediction window)... 138

Figure 5.35 Optimal transmission ratio (FHDS) (prediction window)......................... 138
Figure 5.36 Battery state of charge under optimal control (FHDS) (prediction window) 139
Figure 5.37 Vehicle jerk for the baseline vehicle under hard-acceleration/deceleration test 145
Figure 5.38 Vehicle jerk with limited control derivatives 147

Figure A.1 New European Driving Cycle ……………………………………………...153
Figure A.2 Japan 1015 Driving Cycle …………………………………………..……153
Figure A.3 0 ~ Top Speed ~ 0 Acceleration Test ……………………………..……...154
Figure A.4 30 ~ 50 mph Acceleration Test ……………………………………..…...154
Figure A.5 50 ~ 70 mph Acceleration Test ……………………………………….....154
Figure A.6 Gradeability Test ……………………………………………...……....154

Figure B.1 Actual vehicle velocity in hard acceleration/deceleration test...................... 158
Figure B.2 Vehicle behaviors during launch simulated in the quasi-static model.......... 159
Figure B.3 Vehicle behaviors during launch simulated in the dynamic model 160
Figure B.4 CVT torques, speeds and ratio simulated in the quasi-static model 160
Figure B.5 CVT torques, speeds and ratio simulated in the dynamic model.................. 161
Figure B.6 Vehicle acceleration profile for the first 5 second during lunch.................. 162
Figure B.7 Vibration dose value and acceleration RMS value...................................... 162
Figure B.8 Battery State of Charge.. 163
Figure B.9 System frequency analysis when TC is locked... 164
Figure B.10 System frequency analysis when TC is unlocked...................................... 165

LIST OF TABLES

Table: Page

Table 2.1 Design Techniques for Improving Fuel Economy 19
Table 3.1 Vehicle Driveability Scorecard [61] 37
Table 3.2 Vehicle Driveability Ratings and Descriptions [63] 38
Table 3.3 Vehicle Performance References 48
Table 3.4 Comfort Reaction to Vibration Environments (ISO 2631-1 1997) 53
Table 5.1 Control Strategies for Different Torque and Speed Requirements 102
Table 5.2 Effects of the Derivative of the Control Variables on Fuel Economy, Performance and Driveability Measures 144
Table 5.3 Limits of the Control Variable Derivatives for the Controller Considering Fuel Economy, Performance and Driveability 147

Table B.1 Vehicle Parameters 157
Table B.2 System Resonances When the TC is Locked or Unlocked 165

ABBREVIATIONS

ABS	Anti-Lock Brake system
AFR	Air Fuel Ratio
ANN	Artificial Neural Network
BBW	Brake-By-Wire system
BP	Back Propagation
CI	Compression Ignition
CVT	Continuously Variable Transmission
DOE	Degree Of Freedom
EC	Energy Converter
ECMS	Equivalent Consumption Minimization Strategy
ECU	Engine Control Unit
EGR	Exhaust Gas Recirculation
EM	Electric Machine
EPA	Environmental Protection Agency
ES	Energy Storage
ET	Energy Transformer
ETB	Electronically Controlled Throttle Body
ETC	Electronic Throttle Control
EV	Electric Vehicle
FD	Final Drive
FHDS	Federal Highway Driving Schedule
FTP	Federal Test Procedure
FUDS	Federal Urban Driving Schedule
GIS	Geographical Information System

GPS	Global Positioning System
HEV	Hybrid Electric Vehicle
HIL	Hardware-In-the-Loop
ICE	International Combustion Engine
ISA	Integrated Starter Alternator
ISO	International Standard Organization
LQR	Linear Quadratic Regulator
MTVV	Maximum Transient Vibration Value
NEDC	New European Driving Cycle
NiMH	Nickel Metal Hydride
NYCC	New York City Cycle
OOL	Optimal Operating Line
PID	Proportional, Integral and Differential
RMS	Root Mean Square
SA	Spark Advance
SI	Spark-Ignition
SOC	State of Charge
SIL	Software-In-the-Loop
SUV	Sport Utility Vehicle
TC	Torque Converter
UDDS	Urban Dynamometer Driving Schedule
VDV	Vibration Dose Value
VVT	Variable Valve Timing

CHAPTER 1

INTRODUCTION

1.1 Motivation and Problem Statement

Human desires for improving living quality motivate the introduction of thousands of inventions and new technologies. The desire to move around brings us space, sky, marine and ground transportation tools. Among them, automobiles are dominating in daily travel [1] and will reach 2.5 billion by the year of 2050 [2]. However, the challenge for automotive manufacturers is more of making vehicles competitive than meeting the growing quantity demand. Customers make decisions in purchasing by evaluating how well the vehicle satisfies his or her requirements, which on the other hand tells how competitive the vehicle is on the market.

Automobile customers' concerns are rather comprehensive and these include cost, performance, driveability, durability, safety, space, appearance, etc. besides mobility. Much attention of daily commuters and travelers is focused on fuel economy, road performance and driveability. Improving fuel economy is not just a customer preference of reducing vehicle operating cost. More importantly, it saves energy for the whole world and alleviates the dependency of this country on foreign fuel. The energy crisis especially the oil shortage forced us to seek for candidates to replace engines and for techniques of converting other energy into engine usable fuel as well [3]. The fuel economy in these cases represents the total energy consumption and it is often translated into gasoline equivalent fuel economy for fair comparisons with that of the gasoline-powered vehicles. In addition to good fuel economy, consumers also expect their vehicles to provide satisfactory performance with desirable driving comfort. Extremely poor performance and driveability may cause severe safety and health problems. Due to environmental protection concerns, the government has issued legislations and tax incentives for automakers and car buyers to encourage more vehicles with less exhaust gas emissions to be driven on the street. Improvements on fuel economy, performance and driveability may contribute to lower emissions if the vehicle is designed and controlled properly.

Progress in either powertrain design or control may help to achieve good fuel economy, performance and driveability, but the coordination between control and design will bring even better results. Developing a control strategy is significant if the controlled subject has potentials for such improvements and enough freedom for control engineers to work on. In a conventional vehicle with an internal combustion engine (ICE), these targets are mainly reached by shifting transmission gears and adjusting engine inputs, such as fuel injection, spark advance (SA), exhaust gas recirculation (EGR), etc. When targets upgrade, researchers may need to explore alternative powertrains if further improvements are restricted by the limitation of the current one.

An electric vehicle (EV) was once considered as a promising alternative for a conventional vehicle due to good overall efficiency, low audible noises and zero on-board emissions. EVs are actually cleaner even when comparing the pollution from electricity generation power plants with that from petroleum industries plus individual moving tailpipes. However, a vehicle driven by electric machines (EMs) alone is not attractive because of its short driving range on a single charge and long charging time limited by battery technologies. An EM is also more expensive per unit power than an ICE. These drawbacks seemed to keep the EM out of vehicle tractions. In fact, the EM is quite suitable for moving vehicles because it has torque characteristics matching the vehicle torque request curve, i.e., high torque at low speeds for accelerations and less torque when cruising speed is reached. Moreover, an EM responds much faster than an ICE does which may compensate for torque deficiency during shifting and smooth out most of the transients. A natural idea of combining the ICE with the EM for vehicle propulsion brings the hybrid electric vehicles (HEV) into reality. Unlike fuel cell and natural gas cars, the HEV can be built with existing technologies and need little change in energy supply infrastructure and individual refuel stations. Therefore, hybridization is still a feasible solution for today even though this idea dates back to 1905 [3].

Hybrid, in the arena of automotive research, means a vehicle is powered by at least two different types of energy sources or converters with one on-board for traction purpose. Unless otherwise specified, in this dissertation hybrid vehicle implies a hybrid-electric vehicle, indicating that one of the energy sources is electric. The EM in the HEV is used to supplement the power supplied by the ICE and the energy stored in chemical fuel is supplemented by the use of electrochemical energy from the batteries. This coordination permits downsizing the engine to work inside the optimal region under most operating conditions. In addition, the HEV can provide regenerative braking, on-board electrical power generation and limited all-electric traction capabilities. All of these advantages result from the additional degree of freedom of hybridization, but this flexibility and diversity increase the complexity of the HEV drivetrain design and control. However, it is this flexibility that makes optimizing fuel economy, performance and driveability more challenging and meeting updated customer expectations possible.

There are three types of HEVs depending on the powertrain configuration. The ICE and the EM can work alone or together in a *parallel hybrid* while the EM can work as either a motor or a generator. The mechanical coupling between these two energy converters prevents the decoupling of the engine speed with the vehicle speed. Although we lose the possibility of always operating the engine in its most efficient region, the parallel hybrid is generally more efficient than the others. The vehicle can also go home even when the traction battery is completely discharged. In a *series hybrid*, the engine is used either to charge the battery through the generator or to supply the circuits to reduce the battery load. The motor directly drives the vehicle and thus has to be sized for the maximum power request. The engine and the generator also need to be sized to meet this request unless this vehicle is only used for short trips. Dual EMs plus at least one full-sized machine increases the cost and the total mass of the vehicle. The losses from multiple energy conversions further decrease the overall efficiency even though people are benefiting from running the engine efficiently due to the electrical isolation between the engine and the wheels. The *power-split hybrid* combines the positive aspects of both the series and the parallel hybrid. A planetary gear set that acts as an electrically controlled variable transmission (ECVT) connects the engine, the motor, the generator and the differential. Hence, the engine operates at optimum load and the whole system can achieve high performance, good driveability and less energy consumption. The complexity of the powertrain, however, leads to high cost and that makes it difficult to earn reasonable profit with a competitive price. All HEVs allow downsizing the combustion engines and recovering kinetic energy through regenerative braking.

Energy storage devices in the HEV could be electric, such as batteries and super/ultra capacitors, or mechanical, i.e., flywheels. The HEV can be classified according to battery operations as well. In a charge sustaining HEV, the battery state of charge (SOC) is well maintained in a certain range, while a charge depleting HEV may discharge the battery to the minimum level and then recharge it using either the engine or the wall outlet. The charge sustaining hybrid is usually more desirable since convenient and fast recharging for the charge depleting hybrid has not been realized yet.

The degree of hybridization describes how much the electric machine is involved in vehicle propulsion and it is defined as the ratio of the EM power over the total power of the ICE and the EM, as shown in equation (1.1).

$$\text{Degree of Hybridization} = \frac{P_{EM}}{P_{ICE} + P_{EM}} \times 100\% \tag{1.1}$$

Two examples in the extreme case are the conventional vehicle with the hybridization degree of 0 and the pure electric vehicle with the hybridization degree of 1. In contrast to "strong" or "regular" hybrid, "mild" or "soft" hybrid means the power from the electric side accounts for a small portion of the total available power, i.e., less than 15 - 20%.

Increasing demand for auxiliary electric-powered devices, such as electric power steering, active suspension, electric brakes, catalyst heaters, etc., tends to double or triple the current vehicle electric load [4]. An integrated starter/alternator (ISA) with a 42V system is able to meet this requirement at low cost and is becoming popular around the world. A propulsion system with an ISA coupled to an engine directly or by a belt is referred to as a "mild" hybrid. The mild hybrid offers slightly better fuel economy than the conventional vehicle, but costs much less to produce than the regular hybrid. The ISA itself cannot move the vehicle, but it can assist in propulsion especially during accelerations. It also allows the engine to shut down at idle. This saves more fuel and consequently cuts down emissions.

The continuously variable transmission (CVT) is another attractive technology and has recently become more practical with improvements in technology. The CVT is effective in achieving continuously smooth shifting and enables the engine to operate in its most efficient region. The side effect is that it decreases available torque reserve and may have undesirable impacts on driveability before the engine is recalibrated [5]. Frijlink and Schaerlaeckens suggested that if we combine an ISA with a CVT, the ISA can compensate for this deterioration with torque boost capability [5]. Therefore, thorough investigations on a charge sustaining, parallel hybrid powertrain, which consists of a spark-ignition (SI) internal combustion engine (ICE), an ISA, a torque converter (TC), a CVT, a final drive (FD), a driveshaft, a brake-by-wire (BBW) system and wheels, (as it is sketched in Figure 1.1), is of great interest. This study focuses on a front-wheel drive mid to full size passenger sedan as the baseline vehicle.

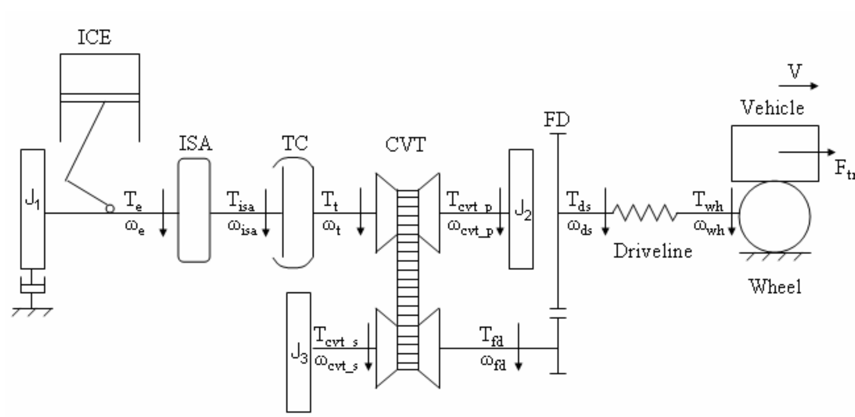

Figure 1.1 Schematic of an HEV powertrain

This hybrid electric drivetrain with a downsized engine, an ISA and a CVT has potentials to satisfy today's increasing demands on fuel economy, performance and driveability. However, realization of these improvements depends, in part, upon proper control of the vehicle. Unlike that in a conventional engine-powered vehicle, the control in an HEV is recognized as two levels of control actions: supervisory control and component control. The supervisory controller functions primarily as an energy management unit, splitting power request between chemical (fuel) and electrical (batteries or super/ultra capacitors) energy sources. The lower level component controller receives commands from the supervisory controller to generate detailed control instructions for its actuators. The optimal control strategy in the HEV is usually found hierarchically: finding the optimal solution for fuel economy and performance first and then taking driveability into consideration.

Model-based control design is widely used by control engineers in many fields and obviously it requires a control-oriented model. A system model is classified as static/quasi-static (zeroth order), low-frequency dynamic, high-frequency dynamic and distributed model based on time scale, as it is shown in Figure 1.2.

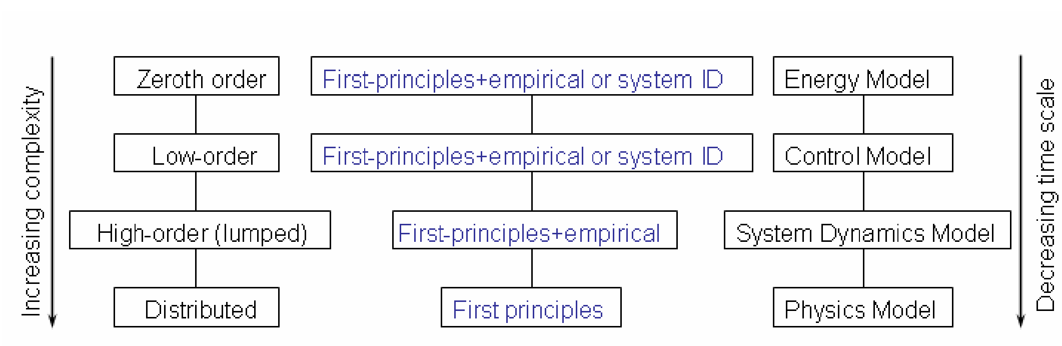

Figure 1.2 Model hierarchy based on time scale

The resources to quantify these models can be from experimental data, empirical equations or first principle derivations. Unlike the low-order model which contains ordinary differential equations and is often used to solve for control problems, the zeroth order model, i.e. the energy model, calculates energy flow in the drivetrain using algebraic equations. Both the zeroth and low-order models can be built with first principle derivations plus empirical equation or system identification techniques. Further decreasing the time scale keeps experimental methods out of modeling since a distributed physical model can only be built by using first principles. Individual cylinder engine model [6, 7], five-state electric machine model [8], high-order battery dynamic model [9], Hrovat and Tobler's TC model [10] and detailed CVT model [11] are all categorized as the high-frequency dynamic model. These models are of high-order and they are excessively complicated for standard control design [12]. However, control engineers can always design a controller based on a simplified quasi-static or low-frequency, low-order dynamic model, as shown in the literature [11, 13-17], and then test this controller with the high-frequency dynamic model if hardware validation is not available.

The "best" model is the one that represents all the phenomena that are relevant to the intended purpose with the lowest complexity and expenses. Due to the existence of model uncertainty and disturbance, no model is perfect. However, if a model captures the main behaviors of a physical system with satisfactory accuracy, we consider that it is acceptable and valid. Obviously, a model can only be evaluated after its application has been determined. Consider, for example, the problem of optimizing fuel economy and driveability in a HEV. A quasi-static model is adequate to analyze and optimize fuel economy and performance [18-20], but it is definitely not sufficient to evaluate driveability issues. The dynamics of driveability are in the frequency range from zero to a few hertz in a real vehicle, thus we need a low-frequency dynamic model for the optimization problem considering driveability. Using the low-frequency dynamic model to optimize fuel economy and performance increases the complexity of the problem and may cause the problem unsolvable.

Vehicle fuel economy is mainly determined by the supervisory control strategy which could be globally optimized, for example, using dynamic programming [21].

Alternatively, the global optimum can be approximated by a local optimum, as done in the Equivalent Consumption Minimization Strategy (ECMS) [22]. Besides the more analytically based optimizations methods, control strategies can also be heuristically based, as with rule-based controllers [23], fuzzy logic [24], artificial neural networks [25], etc.

In any real vehicle knowledge of future driving conditions is always either limited or non-existent, making a truly globally optimal solution impossible. However, the case where all driving conditions are known in advance still provides a rich topic for study. The HEV energy management problem can be solved in a series of steps: beginning with known driving cycles (both constant and variable power requests) and then proceeding to real driving scenarios with limited predictable future driving conditions. This research focuses on building the models for optimal control strategy development, establishing objective control criteria and developing the control strategy using Pontryagin's minimum principle to achieve optimum vehicle fuel economy considering performance and driveability. Modeling and control of exhaust emissions are not in the scope of this dissertation.

1.2 Contributions of the Research

The primary objective of this research is to propose a model based control algorithm for a parallel hybrid electric vehicle to optimize fuel economy while considering performance and driveability. A supervisory controller deals with energy management in a hybrid electric vehicle and solves for the minimum fuel consumption with battery state of charge constraints. Based on Pontryagin's minimum principle, the controller presented in this dissertation achieves lower fuel consumption and similar or better performance and driveability compared with the baseline vehicle. This optimal control solution is applicable for known driving cycles and unknown driving maneuvers with short-time predictions. Minimizing emissions is not the goal here.

Since the control strategy is developed hierarchically and tested based on models, this dissertation also provides two drivetrain control oriented models, the quasi-static and the low-frequency dynamic, for different steps in solving the energy management optimization problem. Objective metrics and numerical references of fuel economy, performance and driveability which are useful to formulate control criteria are introduced as well.

1.3 Organizations of the Dissertation

There are six chapters in this dissertation. Chapter 1 includes the introduction to this research and also the contribution of this work. Related topics, including modeling and control of the hybrid electric vehicle are reviewed in Chapter 2. Chapter 3 then covers objective metrics of fuel economy, performance and driveability, focusing on those used for this research. Chapter 4 presents two control oriented models for the hybrid drivetrain, one for fuel economy optimization and one for optimization considering driveability as well as fuel economy. Chapter 5 describes the development of control strategies for best fuel economy for both constant and time-varying power requests, for power requests with predictable future driving conditions, and for the case which considers fuel economy, performance and driveability. Finally, Chapter 6 concludes the dissertation and also proposes future work.

Appendix A provides some driving cycles and driving maneuvers used in the simulator except for the most commonly used ones, i.e., the FUDS and the FHDS cycles. Model implementation and simulation validation results are in Appendix B.

CHAPTER 2

LITERATURE REVIEW AND BACKGROUND

2.1 Modeling and Simulation

Many designers use models in the product development process, especially in automotive industries where shortening development cycle and reducing cost is critical under high competition pressure. Validated models which represent system characteristics accurately allow designers to explore options using virtual instead of physical systems and hence reduce resource investments significantly. Rapid prototyping is feasible especially when computers are involved. Simulations accelerate powertrain design and control development in the early stage of the vehicle design process and certainly require mathematical models. Considering model inaccuracy, simulation error and environmental disturbances, designs need to pass experimental tests before they are finalized. Experimentations also play a role in tuning and calibrating simulation-based designs, especially for vehicle controllers [26].

There are a variety of ways to classify a system model according to the following criteria:

- Linearity: linear, nonlinear;
- Time scale: static/quasi-static, low-frequency dynamic, high-frequency dynamic and distributed physical;
- Resources: experimental data, empirical equations, first principle derivations;
- Degree of freedom (DOF): single DOF, multi DOF (multi-body);

- Continuity: continuous, discrete;
- Domain: time-based, event-based;
- Parameter property: lumped, distributed;
- Modeling language: quantitative, qualitative (linguistic, descriptive);
- Explicity: explicit model, gray box, black box (Artificial Neural Network, ANN).

The diversity of model types makes modeling not an easy task and hence modelers need to choose the proper model according to their intended goals. In general, models are getting more complex and more accurate when the time scale is decreased and the parameter number is increased. Models with nonlinearity, high-frequency dynamics and/or distributed parameters are better representations of real systems since that is how systems behave in reality. It usually takes longer to establish a new model from first principles than from experimental data, either by using the raw data directly with look-up tables/maps or by extracting system input-output relationships with curve fitting techniques. However, the model based on first principles is not restricted to a specific application and it saves storage memory used in the other two cases. The model written in descriptive language cannot be implemented in computers unless it is translated into numerical expressions.

Sophisticated models increase modeling difficulty and developing time. Furthermore, simulations based on complex models may lengthen the execution time and make real-time processing impractical. Reasonable assumptions and simplifications can reduce model complexity, but at the price of losing modeling accuracy. Therefore, modelers need to make a compromise between these two factors to select models which are best suitable for their applications. The “best” model is the one that represents all the phenomena a real system exhibits with the lowest complexity and expense. Due to the existence of model uncertainty and disturbance, no model is perfect. However, if a model captures the main behaviors of a physical system with satisfactory accuracy, we consider that it is acceptable and valid. It is obvious that a model can only be evaluated after its application and inaccuracy tolerance have been determined.

There does not exist a set of theories in the modeling area as complete as that in the control area. Thus, modelers usually build models based on previous researches, their own modeling experiences and understandings of the real systems. In general, modeling domain and continuity are determined according to the nature of the system. Applications then help to decide how much nonlinearity and dynamics should be involved and what kind of parameters should be used. Models must be programmable if one uses computers for design exploration. In powertrain design space search with automated modeling, modular, scalable and composable models of all alternative powertrain components are required as well [27].

Since models will substitute real systems in the design process, these models need to be validated through testing on dynamometers or prototypes. The Hardware-In-the-Loop (HIL) approach [28, 29], which is often used for control unit validation and testing, such as Engine Control Unit (ECU), offers a fast, inexpensive, flexible, repeatable and safe testing approach. The basic concept of the HIL is to combine certain elements of the actual system with high-fidelity models of the other elements executed on real-time computers in a closed loop. In the late stage of the vehicle component or control strategy design processes, the HIL allows fast validation and comparison of the design alternatives. Hardware involvement also reduces modeling load and simulation inaccuracy. Physical components are preferred when accurate models are difficult to build or simulation does not provide reliable results. However, simulation is desirable if the actual system is too costly. When the driver is brought in the loop, it becomes the Man/Operator-In-the-Loop system.

The Software-In-the-Loop (SIL) [30] has all the testing components running in real-time computers and permits repeatable sensitivity study eliminating hardware parameter variations and disturbances. This approach allows one to use cheap computers entirely instead of employing some hardware components and interface connections which sometimes have cost and availability problems. The conventional simulation also runs in computers entirely but offline and it neglects the communication and the calculation time which are critical in the real system. Both the HIL and the SIL are useful alternatives of the conventional model-based simulations.

Simulation is a powerful tool in design processes for shortening product development cycles, reducing resource investments and cost, and easing design option explorations. In the vehicle powertrain design, the design space filled with candidates need to be evaluated and decreased to the minimum size before physical prototypes are built. Automated modeling with design space search is a feasible solution and becomes practical when using digital computers. Since there exist modeling inaccuracy and hardware uncertainty, simulation is mainly used in the early stage of the design process to extract the designs that are inferior even in simulations. Obviously, any design needs to be tested in real systems before it is finalized for mass production. In addition to evaluating designs, simulation is also useful in guiding designs, e.g. system analysis, parametric study and sensitivity study. Moreover, real-time simulation finds applications in model validation and design calibration by using the HIL and the SIL methodologies.

A simulator should be at least accurate and portable. Modular layout and hierarchical organization with user-friendly interface constitute a good simulator structure which keeps the programmers organized and makes it easy for users to understand. In order to save simulation running time, designers should reduce model complexity and improve simulation implementation besides exploiting fast computers. As mentioned earlier, model accuracy and complexity are contradictory to each other. Simulation speed is sacrificed if the desirable accuracy has not been achieved. Many simulations used for automotive powertrain component design are implemented in MATLAB®/SIMULINK®. When the variable concerned cannot be expressed in an explicit form, such as the derivative of a variable is a function of this variable itself, the simulator contains algebraic loops which have to be solved iteratively. The iteration reduces the simulation speed and it may be avoided by reformulating the problem in a causal form. In addition, equations containing explicit differentiation may amplify high-frequency dynamics in the system. This might be solved by rewriting the equations if the derivatives of all the other variables are already available. Certainly, the derivatives of all the other variables are not solved by taking a derivative but by using an algebraic equation or by integrating an algebraic equation. It is a general rule for MATLAB simulators that trying not to introduce explicit differentiation unless it is inevitable. The "for-loop" in MATLAB also takes long time to run and it may be replaced with matrix operations.

2.2 Modeling of a Hybrid Electric Drivetrain

The control objective of this research is to minimize fuel consumption while considering performance and driveability. The optimal control strategy to achieve this objective can be found in two steps: finding the optimal control for the minimum fuel consumption first and then taking driveability into consideration. This consequently requires two powertrain models, one for each step in the control problem.

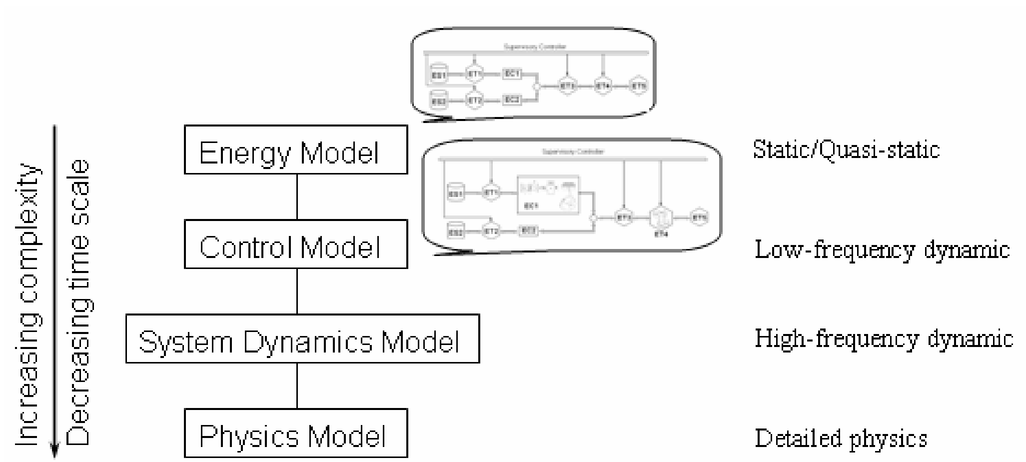

Figure 2.1 Model hierarchy for a parallel HEV

As mentioned in Chapter 1, there exists model hierarchy based on time scale, i.e., zeroth-order, low-order, high-order and distributed models. The zeroth-order model, also referred to as the static/quasi-static model, is sufficient to calculate energy flows in the powertrain and suitable for fuel economy optimization problem. When driveability is taken into consideration, the low-order model is required. Figure 2.1 shows the model hierarchy for a parallel HEV where the energy model corresponds to the static/quasi-static model and its generic structure is depicted in Figure 2.2.

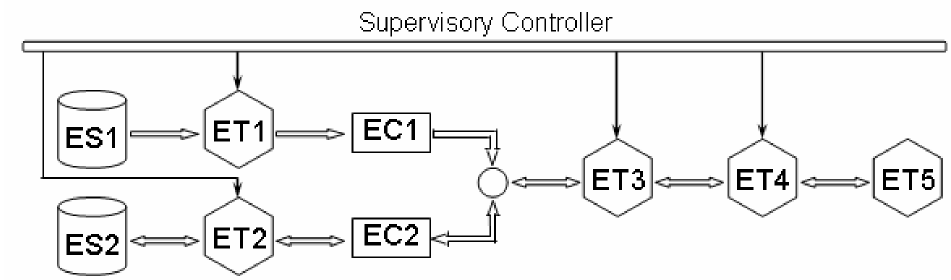

Figure 2.2 A schematic of zeroth-order model for a parallel HEV
(ES: energy storage device; ET: energy transformer; EC: energy converter)

The most commonly used two energy converters in the parallel HEV shown above are the engine (EC1) and the electric machine (EC2). Correspondingly, the energy storage devices are the fuel tank (ES1) and the battery or super/ultra capacitors (ES2). "ET1" to "ET5" represents fuel injector, power amplifier, clutch/torque converter, transmission and differential (final drive). Unlike that in the mechanical (engine) path where the energy can flow in only one direction, the energy in the electrical (electric machine) path can flow in two directions: the energy may flow from the battery to the wheels when the electric machine works as a motor and the kinetic energy at the wheels or the mechanical energy of the engine can flow back to recharge the battery when the electric machine works as a generator. The supervisory controller controls "ET1" and "ET2" to split energy requirement between the engine and the electric machine, and also "ET3" and "ET4" for appropriate gear ratio.

The proper model for vehicle fuel economy optimization is the static/quasi-static model which describes power input-output relationship of powertrain components with efficiency or power losses. The engine and the electric machine use maps or the Willans line model to express the efficiency. This efficiency depends on both the operating speed and torque. While in the transmission and the final drive, constant efficiency and gear ratio are considered to describe the relation between the input and output speeds and torques. The transmission efficiency is sometimes expressed as a 3D map indexed by the gear ratio, speed and load torque. As the secondary energy source in the vehicle, the battery uses current integration to estimate the state of charge (SOC). The discharging and recharging power are both bounded as well as the battery SOC. Here, the SOC limits allow for operating the battery without being damaged. In this quasi-static model, the vehicle model is the only one that contains dynamics to calculate the vehicle speed from torque.

When driveability is considered in finding the optimal control strategy, the quasi-static model introduced above is no longer sufficient. Dynamics of vehicle driveability are in the frequency of a few hertz in a real vehicle and thus it requires a low-frequency dynamic model which has the proper time scale. The objective driveability metrics used in this research include jerk amplitude, acceleration RMS, MTVV, VDV values and tip-in response as defined in Chapter 3. Figure 2.3 depicts the extended picture of the control model in Figure 2.1. Most of the powertrain components shown above are modeled as actuators with first or second order dynamics plus saturations and some nonlinearity. The engine (EC1) is approximated with mean-value model which has been broken down into four subsystems: throttle, intake, combustion and crankshaft. The electric machine (ET2) with its controller behaves like a first order system, i.e., the output torque follows its command after a delay. Furthermore, the rotational dynamics of the transmission (ET4) are also captured in this low-frequency dynamic model. Both the quasi-static and low-frequency dynamic models are introduced in details in Chapter 4.

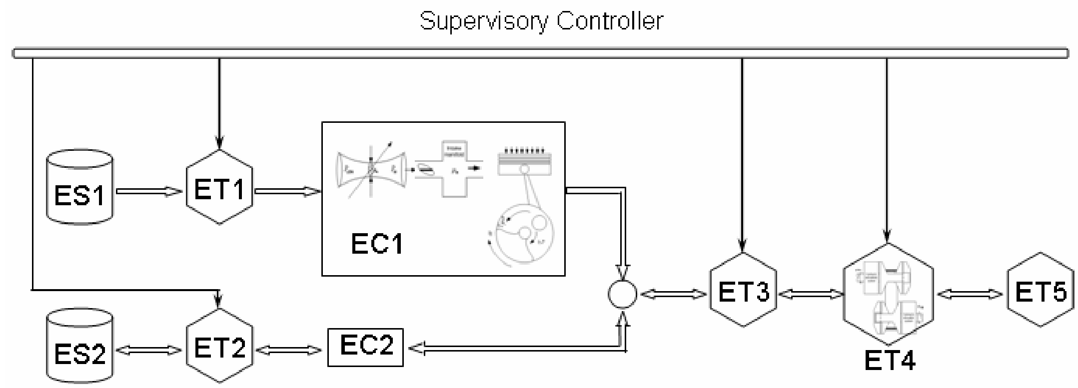

Figure 2.3 A schematic of low-order model for a parallel HEV
(ES: energy storage device; ET: energy transformer; EC: energy converter)

2.3 Control

Control in the hybrid electric vehicle is recognized as two levels of control actions: supervisory control and component control, as shown in Figure 2.4. The supervisory controller translates driver's intentions into power requirements and coordinates powertrain components to achieve certain objectives. Common objectives include minimizing fuel consumption and emissions while maintaining or improving performance and driveability. In reality, sufficient safety, limp home capability, etc. are also considered for production vehicles. The component controller, on the other hand, receives commands from the supervisory controller and generates detailed control instructions for its actuators.

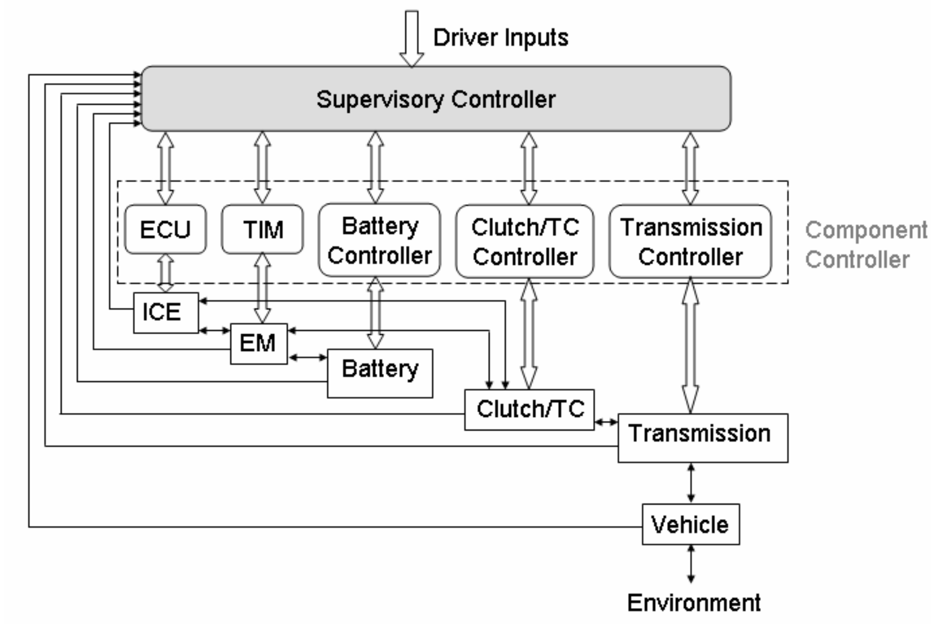

Figure 2.4 Hierarchical control in an HEV

2.3.1 Supervisory Control Strategies for Hybrid Electric Vehicles

The supervisory controller functions as an energy management unit which splits power requirements between the engine and the electric machine as well as determines the transmission gear ratio. Improving fuel economy and reducing emissions are the two primary objectives for supervisory control strategy design. Since emissions modeling and control are not the subjects of this dissertation, only strategies for improving fuel economy are discussed below.

Minimizing power losses implies higher efficiency and less fuel consumption. This is accomplished through optimizing powertrain design and control. Powertrain optimal design is composed of configuration design and component design. Not only the drivetrain architecture and each component need to be power efficient, but these components need to be matching in type and size to obtain high overall efficiency. Table 2.1 lists some techniques for improving the vehicle fuel economy in design.

Design Aspects		Technology or Design Modification
Powertrain configuration		Hybridization
Engine	Improving thermal efficiency	Turbocharged direct-injection diesel engine
		Supercharging
	Improving mechanical Efficiency	Low friction lubricant
	Improving thermal and mechanical efficiency	Variable X engine (variable displacement, variable valve timing, variable compression ratio, variable geometry turbocharger) [31]
Transmission		Manual transmission
		Continuously variable transmission
Vehicle		Aerodynamic drag reduction
		Lower rolling resistance tires
		Smaller frontal area
		Ultra-light steel or aluminum body for less weight
Accessories		Humidity sensor for air conditioning [31, 32]
Electric aspect		X-by-wire (drive-by-wire, steering-by-wire, brake-by-wire)
		42 V system

Table 2.1 Design Techniques for Improving Fuel Economy

Engine size is an important factor for vehicle fuel economy. Figure 2.5 shows the fuel consumption map of two engines with different displacement. The power difference between these two engines is roughly identified as the torque difference since they have the same speed range. The fuel consumption of the smaller engine is close to that of the larger one in the lower torque region. It is obvious that using a smaller engine reduces fuel consumption. The engine in a conventional vehicle is the only power source and is usually sized based on the most stringent power requirement, such as acceleration, gradeability, or towing capacity. Consequently, the engine is inevitably oversized for everyday city and highway cruise, sometimes by as much as 10 times to the size needed for 62.5 mph (100 km/hr) coasting [33]. While in the HEV, the electric machine together with the traction battery acts as an energy buffer and it allows downsizing the engine and operating it at a lower constant torque. Exploiting the CVT, the ECVT or the series hybrid allows the engine to run at constant speed. Observing the figure below, it seems that minimizing the fuel consumption encourages operating the engine in the low speed, low torque corner. This is not true because people need to meet the power requirements at the wheels as well. Therefore, the optimal engine operating region is the most efficient region or the lowest fuel consumption region when the power request is satisfied. This comment, however, has not taken vehicle performance and driveability into consideration.

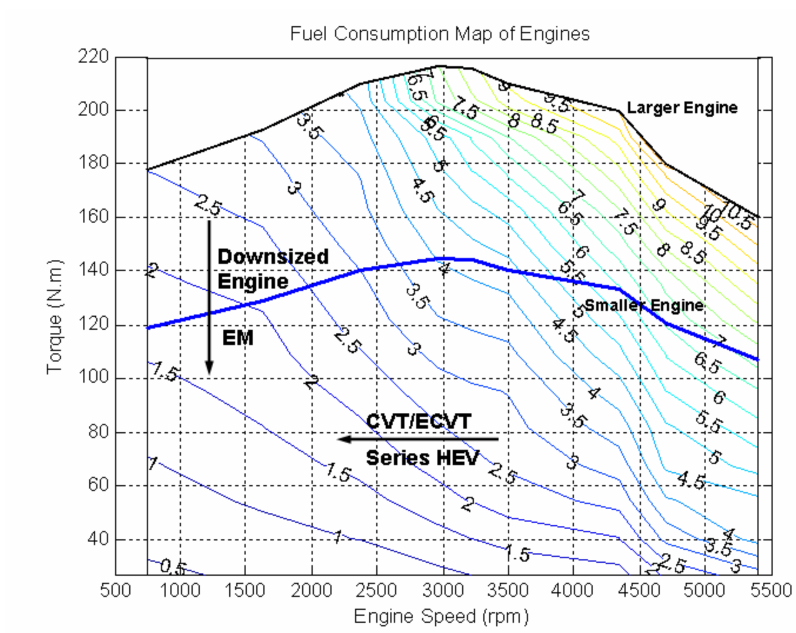

Figure 2.5 Strategies for reducing engine fuel consumption

For a conventional vehicle, transmission speed reduction ratio is determined as the one which satisfies vehicle power requirements at the highest efficiency. Only a few alternative operating points are compared in the vehicle with stepped transmission. If one can decouple the engine speed from the vehicle speed or the transmission ratio can vary continuously, alternative engine operating points may increase tremendously. When the EM is also employed for propulsion, transmission ratio may be determined by setting the engine operating points in its most efficient region based on known vehicle velocity and torque demands. The EM then compensates for the difference between the requested total torque and the engine output torque unless the battery SOC is outside of its acceptable operating region. An engine has optimal operating region instead of a single optimal point is because of the following reasons. First, there exists multi maximum efficiency or minimum fuel consumption points. Second, powertrain components all have physical limitations, such as engine and electric machine speed and torques limits, and transmission ratio limits. The battery SOC restricts the EM actual operating conditions and the engine operation has to be adjusted when other criteria (performance, driveability, etc.) are considered. It is evident that the last two reasons will shift the engine operation from the most fuel efficient region.

Improving fuel economy requires all powertrain components to operate in the most efficient region. If any of them is running outside of its desired region under perfect control, it indicates that the drivetrain components are not optimally matched. Other reasons of moving the engine optimal operating region outside of its most efficient region could be when performance, driveability and component physical limitations (i.e. speed and torque constraints, bounded transmission ratio) are considered.

In the HEV that has a function of recovering kinetic energy through braking, maximizing the regenerated energy is as important as minimizing the energy losses in the powertrain. Shutting down the engine during vehicle deceleration reduces the engine losses but it affects vehicle driveability and needs to be thoroughly controlled. Engine frequent start-stop enabled by the ISA together with 42 V system may save 8 ~ 25 % of fuel [34].

After the vehicle powertrain design is finished, control engineers begin to develop control algorithms to optimize vehicle operation. Numerous control strategies for best fuel economy in the literatures including OOL, LQR, dynamic programming, ECMS, rule-based, fuzzy logic, neural network, genetic algorithm and optimal control are introduced below.

Engine Optimal Operating Line (OOL) [35, 36] is a sequence of intersections of the constant engine power lines with the peak efficiency contours or the lowest fuel consumption curves if the efficiency or the fuel consumption is the only concern. Figure 2.6 and Figure 2.7 show the peak efficiency line and the lowest fuel consumption line of a 1.9 L gasoline engine.

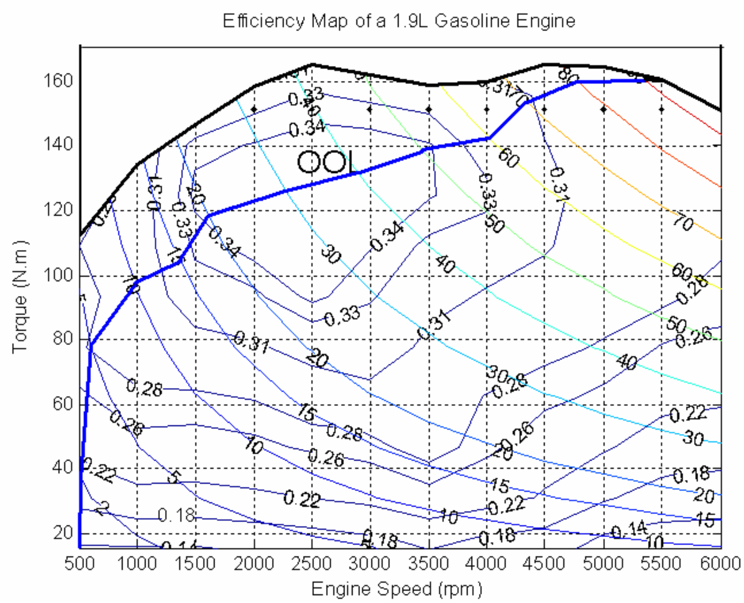

Figure 2.6 Engine peak efficiency line

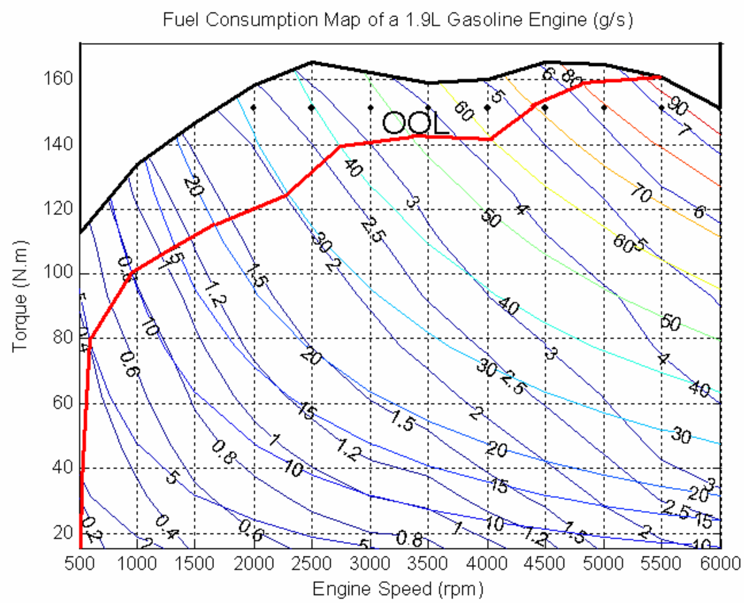

Figure 2.7 Engine lowest fuel consumption line

The actual operating line may be adjusted to a smoother curve for better engine performance. The peak efficiency and the lowest fuel consumption curves are essentially equivalent because the lowest fuel consumption will result in the highest efficiency at the same engine output power. When performance and driveability are taken into account, the OOL will certainly be shifted from the peak efficiency or lowest fuel consumption line.

In the literature [37], a parallel HEV is simplified as a linear, time-invariant system and the optimal operating line is solved by minimizing the penalties of the velocity tracking error and the control effort using Linear Quadratic Regulator (LQR). This method is only applicable for linear system with known reference velocity trajectory.

Dynamic programming [21] guarantees global optimality. It divides the given driving profile into many segments and solves for the optimal control in a backward recursive way. The optimal solution for the last segment N is solved first and then the calculation moves one step back to obtain the solution for the current step *N-1*. The cost function consists of weighted engine and electric machine energy.

$$J^*_{N-K,N} = \min_{N-K}\{g(x(N-K),u(N-K)) + J^*_{N-(K-1),N}[f(x(N-K),u(N-K))]\} \tag{2.1}$$

Where

$J^*_{N-K,N}$	optimal solution from *N-K* to *N* step,
$J^*_{N-(K-1),N}$	optimal solution from *N-K+1* to *N* step,
K	step index in calculation,
N	total number of sliced segments,
f	system state dynamic function,
g	cost function,
u	system control variables,
x	system states.

Dynamic programming is not applicable in real vehicles because it needs all the driving conditions to be known in advance and requires unaffordable real-time computational efforts. However, since it gives the optimal solution, dynamic programming offers a reference for comparison with other realistic optimization algorithms.

For a charge-sustaining HEV, Paganelli's Equivalent Consumption Minimization Strategy (ECMS) [22, 38] considers the electricity usage in the battery pack as another type of fuel consumption. Thus, the total fuel consumption includes this equivalent fuel consumption in addition to the actual one consumed by the engine. Determining the equivalent fuel consumption of the battery and the electric machine requires the analysis of all the components in the power converting path between the fuel tank and the electrical devices. The conditions under which future electricity will be generated are unknown at the instant electricity is being consumed, thus the average conversion efficiency is used. Global optimization is explicitly feasible only in simulations where the driving conditions are completely known. A sub-optimal solution that instantaneously minimizes the total fuel consumption is inevitable. Finally, a nonlinear battery SOC penalty function is used to adjust the power splitting between the engine and the electric machine.

Johnson’s approach [39] is intrinsically the same as Paganelli’s but she uses energy instead of fuel consumption. The electric energy is converted into the effective fuel energy before it is summed with the actual fuel energy. Then the total energy usage is minimized and the solution is adjusted considering the battery SOC as well.

Jalil et al. [23] proposed a rule-based control policy for a series hybrid according to engineering experience and intuition. Engine operating commands are determined based on vehicle conditions such as the battery SOC and are expressed using if-then logics.

Fuzzy logic [24] translates linguistic representations of control inputs and outputs into numerical representation with membership functions in the fuzzification and the defuzzification processes. A rule base that is constituted of control laws based on expert knowledge is utilized to generate control decisions. Therefore, the fuzzy logic control is inherently the same as the rule-based control.

As one of the intelligent control methods, Artificial Neural Networks (ANN) [25] represents system input-output relationship implicitly. The ANN usually consists of one input layer, one output layer and one or more hidden layers. Neurons in the adjacent layer are interconnected and each neuron receives the summed signal, passing through a sigmoid function, from neurons in the previous layer with different weights. For the same given inputs, the neurons are trained to give the outputs matching those of the real system. Training continues until the error between the outputs of the ANN and the training data is within a predetermined threshold. When the training data is extracted from the empirical data, real world imperfections and disturbances have already been considered. Back Propagation (BP) is widely used as one of the supervised learning techniques which adjust the neuron weights with known inputs and outputs.

Unsupervised learning methods, such as Kohonen, classify data into groups with each corresponding to a specific utility: function estimation, variable relationship investigation or decision making.

The genetic algorithm [40] is a stochastic global search technique that mimics the phenomena of natural biologic evolution. It is more suitable for nonlinear optimization problem than the calculus-based strategy since it does not require strong assumptions of continuity, differentiability and Lipschitz condition to hold. Chromosome representation and fitness function are defined to describe control candidates and to evaluate their status. Finally, the genetic operators select the probabilistic optimal solution using the heuristic crossover. When the interactions of design variables are not all considered, this approach does not ensure global optimality.

Kleimaier and Schroder [41] developed a computer program, DIRCOL, for numerical solutions of fuel economy optimization problem using optimal control method. However, this program is only for given driving cycles.

In summary, of the approaches discussed above the LQR is the only approach that is restricted to linear or linearized systems and the dynamic programming is the only one that gives global optimum but is not applicable in real vehicles. Neural networks, rule-based and fuzzy logic control do not provide optimal solutions unless the training data is from an optimized system or the rule base is optimized in advance. All control algorithms discussed above minimize fuel consumption based on engine and electric machine steady state maps.

Finding a global minimum of fuel consumption requires the entire trip to be known before conducting optimization. This is apparently not practical in reality. However, knowing the driving conditions in the near future, even only a few minutes ahead, may help to obtain better results than the case we know nothing about it. It is reported that a prediction horizon of 500 m saves 15 % of fuel [42]. Prediction is accomplished using either on-board measurements or historical data with statistical analysis. Telematics, such as the Global Positioning System (GPS) and the Geographical Information System (GIS), together with on-board radar system help in gaining traffic information, topological data and speed limits on the road [43]. General Motor's OnStar navigation system allows the user to plan a route to a destination and also to obtain information along the path. In the case where a vehicle is driven under habitual usage like commuting, an intelligent control algorithm based on fuzzy logic allows reliable estimation of road parameters at the point of departure [44]. ANN trained with historical loading conditions is also used for load forecasting [23]. Predictions become more accurate when the difference between the prediction and the actual load is corrected with the factor obtained from stochastic analysis, such as Kalman filtering, auto-regressive moving average and spectral expansion technique.

Driving mode is the first variable to be identified in the multi-mode driving control where control rules are established according to different driving modes. The Hamming network is used for the real-time driving pattern recognition [45]. A feed-forward layer stores the inner products between the current driving pattern and the representative ones and passes them to the competition layer. The recurrent "competitive" layer is composed of six neurons competing with each other to determine the winner. The only neuron with nonzero output indicates the representative driving pattern and that is the input for the multi-mode driving control.

Imperfections of the model-based control due to unmodeled dynamics and modeling error are mainly compensated in the calibration process, while adaptive control deals with parameter variations, i.e., parameter drifting caused by aging and unpredicted disturbances. Adaptations in system parameter identification may be achieved using more precise models in simulations [46]. However, observer-based control and the ANN are preferred in real systems. Observer-based controller increases control accuracy and robustness through constructing observers with adaptation techniques. Pole placement observers choose gains for desired steady state error, dynamic performance and noise rejection. Stochastic optimal observers, the Kalman filter and the extended Kalman filter, determine gains using noise models or solving an on-line matrix Riccati equation [47]. Stability and convergence can be evaluated by Lyapunov theory. Adaptations also appear in predictive control mentioned above. The ANN with self-learning property can adjust neuron weights when the driving conditions (driving style, area, time etc.) are changed. However, this self-tuning takes some time to stabilize and thus rapid changes of either the parameters or the operating conditions will be difficult to follow by the adaptive controllers. In addition, frequent and rapid changes of controller gains may lead to system instability.

Robustness is another desired property for a controller. For example, the controller should be insensitive to different driving cycles and be able to tolerate imprecise measurements and plant uncertainties caused by production tolerances and external disturbances. Robust H_∞ control offers optimal solution with good disturbance rejection. Disturbances with known attributes can be estimated with stochastic analysis. Sliding mode control forces the system to operate on a reduced order sliding surface under a discontinuous control which is implemented with an equivalent control. When the desired sliding surface is linear, the original nonlinear system is linearized. High gains used in the controller ensure stability and robustness. Sliding mode control is insensitive to parameter variations and shows complete rejection of disturbances.

2.3.2 Control Algorithms for Improving Performance and Driveability

Shorter acceleration time requires adequate power at least during acceleration while better gradeability and towing capability need large power for the whole trip. The torque reserve is defined as the difference between the current operating torque and the maximum torque at the same speed. The torque reserve of the engine and the EM are summed together as the total reserved torque for an HEV. After receiving an acceleration command, the engine and the EM tend to operate at larger speed and larger torque before the transmission shifts. Upshifting reduces the wheel torque and thus the vehicle acceleration will decrease if the allowable operating torque after shifting is not sufficiently larger than the actual operating torque before shifting, i.e., the torque reserve after shifting is not big enough to compensate for the wheel torque decrease due to the transmission ratio change. In contrast to the engine optimal fuel economy line which locates at high torque region and has low torque reserve, the engine optimal performance line is located at relative low torque region.

Increasing damping in the drivetrain helps to suppress the vibrations at the cost of dissipating more energy. Consistent acceleration with large amplitude ensures short acceleration time and small jerk. The acceleration delay and sag due to power deficiency maybe minimized by the electric machine fill-in torque [48] or power assistance. The EM which has fast response also helps to smooth torque fluctuations when the battery condition permits. Whenever the torque ripple is predicted or detected, the EM produces opposite torque to reduce this “ac” content or completely cancel the ripple [48-50]. The acceleration delay due to the system lag and the transportation delay cannot be eliminated completely unless the controller can predict the acceleration and react earlier.

Shifting of an automatic transmission involves releasing the offgoing clutch and engaging the corresponding oncoming clutch. Relative timing of the clutch operations affects the shifting comfort. If the oncoming clutch is brought in too early, the transmission output torque is reduced since the torque of the offgoing clutch is negative. This may cause the engine and the vehicle to stop in the extreme case. In contrast, late engagement of the oncoming clutch shows that the vehicle velocity is temporarily decreased since the torque is not transmitted. The engine speed is increased, however, due to the reduced engine load. The vehicle jerk for a nominal 1-2 gear shifting is less than ± 5 m/s^3 and an early or late oncoming clutch occurrence excite it to ± 25 m/s^3. A closed-loop clutch slip speed control algorithm reduces the jerk by keeping the slip set point as zero and its second derivative as a piecewise constant, i.e., speed slip is a smooth function. Increasing the engaging time further decreases the vehicle jerk but consumes more energy. [51]

Reducing the engine torque during shifting substantially improves shifting comfort and relieves the load on the shift elements. This is achieved by retarding the spark ignition and cutting off part or full fuel injection [52].

Lee et al. proposed an advanced gear shifting and clutching strategy for an automated manual transmission to reduce shift shock. The speed of the clutch plate that is attached to the engine and the speed of the other plate which connects the EM are synchronized before the engagement. This strategy is tested for upshifting and downshifting between 4th and 5th gears and it is observed that the torque variations are greatly reduced. [53]

Ciesla et al. [54] used fuzzy rules to have the CVT ratio changing rate to be big for acceleration from low vehicle speed for better performance and small for acceleration from high vehicle speed for smoother driving. Limiting the derivative of the CVT ratio according to the vehicle states shows smoother acceleration and hence lower jerk [55]. Upshifting the CVT too fast during the acceleration causes the temporary power drop and the non-minimum phase behavior. After the desired CVT ratio trajectory is determined, various control methods may be used to track this trajectory, such as decentralized PID [17], feedback linearization [56], backstepping [57], sliding mode [36, 58] and fuzzy logic [58].

2.3.3 Optimal Control Theory Overview [59, 60]

The objective of optimal control is to determine control signals that will cause the system to minimize or maximize some performance criteria while satisfying the physical constraints at the same time. Performance criteria, in general, is expressed by the cost function J as

$$J = h\left(x(t_f), t_f\right) + \int_{t_0}^{t_f} g\left(x(t), u(t), t\right) dt \tag{2.2}$$

for a system of $\dot{x} = f(x, u, t)$. The variables t_0 and t_f are the initial and final time, h and g are scalar functions. t_f may be fixed or free depending on the problem statement. Starting from the initial value $x(t_0) = x_0$ and applying the optimal control $u^*(t)$ for $t \in [t_0, t_f]$, the system will follow some state trajectory with minimum cost. (The superscript asterisk on x, λ and u represents the optimal trajectories for state, co-state and control variables)

Calculus of Variations

The calculus of variations is one branch of mathematics in solving optimization problems. $J(x^*)$ is a relative minimum if

$$\delta J = J(x) - J(x^*) = J(x^* + \delta x) - J(x^*) \geq 0 \tag{2.3}$$

Neglecting the penalty for the final state, this becomes

$$\delta J = \int_{t_0}^{t_f} \left(\frac{\partial g}{\partial x} \delta x + \frac{\partial g}{\partial \dot{x}} \delta \dot{x} \right) dt = \frac{\partial g}{\partial \dot{x}} \delta x \Bigg|_{t_0}^{t_f} + \int_{t_0}^{t_f} \left[\frac{\partial g}{\partial x} - \frac{d}{dt}\left(\frac{\partial g}{\partial \dot{x}} \right) \right] \delta x dt \tag{2.4}$$

Where, $\frac{\partial g}{\partial x} - \frac{d}{dt}\left(\frac{\partial g}{\partial \dot{x}} \right)$ is referred to as the Euler equation. Then, necessary conditions to achieve the minimum cost for different final state status are:

t_f and $x(t_f)$ are fixed

$$\frac{\partial g}{\partial x} - \frac{d}{dt}\left(\frac{\partial g}{\partial \dot{x}} \right) = 0 \tag{2.5}$$

t_f is fixed and $x(t_f)$ is free

$$\begin{cases} \frac{\partial g}{\partial x} - \frac{d}{dt}\left(\frac{\partial g}{\partial \dot{x}} \right) = 0 \\ \left. \frac{\partial g}{\partial \dot{x}} \right|_{t_f} = 0 \end{cases} \tag{2.6}$$

t_f is free and $x(t_f)$ is fixed

$$\begin{cases} \dfrac{\partial g}{\partial x} - \dfrac{d}{dt}\left(\dfrac{\partial g}{\partial \dot{x}}\right) = 0 \\ g - \dfrac{\partial g}{\partial \dot{x}}\dot{x}\Big|_{t_f} = 0 \end{cases} \tag{2.7}$$

t_f and $x(t_f)$ are fixed

$$\begin{cases} \dfrac{\partial g}{\partial x} - \dfrac{d}{dt}\left(\dfrac{\partial g}{\partial \dot{x}}\right) = 0 \\ \dfrac{\partial g}{\partial \dot{x}}\Big|_{t_f} = 0 \\ g - \dfrac{\partial g}{\partial \dot{x}}\dot{x}\Big|_{t_f} = 0 \end{cases} \tag{2.8}$$

The calculus of variations requires the functions to be continuous and differentiable and it does not solve for the case where control variable is bounded.

Pontryagin's Minimum Principle

Pontryagin's Minimum Principle is based on the calculus of variations, but it does not require the function to be continuous and differentiable. More importantly, it is applicable for bounded control as well.

Define λ as the co-state variable, then, the Hamiltonian is defined as

$$H\big(x(t),u(t),p(t),t\big) = g\big(x(t),u(t),t\big) + \lambda^T(t) f\big(x(t),u(t),t\big) \tag{2.9}$$

For all t ∈ [t_0, t_f] and for all admissible controls, minimizing the cost function *J* is thus equivalent to minimizing the Hamiltonian such that

$$H\left(x^*(t),u^*(t),\lambda^*(t),t\right) \le H\left(x^*(t),u(t),\lambda^*(t),t\right) \tag{2.10}$$

Necessary conditions of the optimal control $u^*(t)$ for the minimum Hamiltonian:

$$\begin{cases} \dot{x}^*(t) = \dfrac{\partial H}{\partial \lambda}\left(x^*(t),u^*(t),\lambda^*(t),t\right) \\ \dot{\lambda}^*(t) = -\dfrac{\partial H}{\partial x}\left(x^*(t),u^*(t),\lambda^*(t),t\right) \\ H\left(x^*(t),u^*(t),\lambda^*(t),t\right) \le H\left(x^*(t),u(t),\lambda^*(t),t\right) \end{cases} \tag{2.11}$$

$$\left[\frac{\partial h}{\partial x}\left(x^*(t_f),t_f\right) - \lambda^*(t_f)\right]^T \delta x_f + \left[H\left(x^*(t),u^*(t),\lambda^*(t),t\right) + \frac{\partial h}{\partial t}\left(x^*(t_f),t_f\right)\right]\delta t_f = 0$$

Sufficient condition for the minimum Hamiltonian:

$$\frac{\partial^2 H}{\partial u^2}\left(x^*(t),u^*(t),\lambda^*(t),t\right) > 0 \tag{2.12}$$

When the control variable is bounded or multiple minimum/maximum points exist, we need to compare the control solutions from equation (2.13) and also control boundaries to see which one is the actual optimal solution, i.e., which one leads to the minimum Hamiltonian.

$$\frac{\partial H}{\partial u}\left(x^*(t),u^*(t),\lambda^*(t),t\right)=0 \tag{2.13}$$

<u>*Additional necessary conditions for special cases:*</u>

If t_f is fixed and the Hamiltonian does not depend on time explicitly, then the Hamiltonian is a constant under the optimal control.

$$H\left(x^*(t),u^*(t),\lambda^*(t)\right)=C \tag{2.14}$$

If t_f is free and the Hamiltonian does not depend on time explicitly, then the Hamiltonian is zero under the optimal control.

$$H\left(x^*(t),u^*(t),\lambda^*(t)\right)=0 \tag{2.15}$$

2.4 Summary

The objective of this dissertation is to develop a control strategy to minimize fuel consumption while considering performance and driveability. The optimal control strategy is found in two steps, i.e., finding the control which leads to the minimum fuel consumption and best performance first and then taking vehicle driveability into consideration. Solving the control problem hierarchically requires two separate models: a quasi-static model for fuel consumption minimization and a low-frequency dynamic model for fuel consumption minimization considering performance and driveability. The quasi-static model describes energy losses in the powertrain and it is adequate to estimate vehicle fuel economy. Energy losses are generally described with efficiency coefficient or map except for battery where internal resistance is used. To simulate vehicle driveability, the model needs to show powertrain dynamics in the concerned frequency range. Therefore, a low-frequency dynamic model which simulates powertrain components as low-order dynamic systems with saturations and nonlinearity is required. The engine model is broken down into four low-order subsystems for easy modeling. In addition, the rotational dynamics of the transmission also shows contribution to the vehicle overall driveability and has to be included in the model.

Among the control strategy in the literature for the best fuel economy, dynamic programming is the only one that guarantees global optimality if the driving cycle is known in prior. However, it is not practical for real-time applications due to unaffordable computational efforts besides the unsolvable difficulty of knowing the entire future driving trajectory before the trip starts. Control rules written in fuzzy logic, rule-based and neural network controllers are generally not optimized, but from heuristic reasoning based on expert knowledge. Even though no global optimal solution exists when the future driving conditions are unknown, one of the optimal control theories, Pontryagin's minimum principle helps in finding a suboptimal or locally optimal solution if future driving conditions of a few minutes ahead can be predicted. This dissertation thus focuses on finding the optimal solution using Pontryagin's minimum principle. The detailed solution is shown in Chapter 5.

CHAPTER 3

OBJECTIVE METRICS OF FUEL ECONOMY, PERFORMANCE AND DRIVEABILITY

3.1 Introduction to Fuel Economy, Performance and Driveability Evaluation Criteria

Every product is born to meet some customer requirements. In general, how competitive the product is depends on how well it satisfies buyers' requests and how low the price is. Both sellers and buyers have their own metrics to estimate or evaluate this satisfaction.

Automobile customers have concerns on a variety of aspects. Whether a vehicle is affordable, safe, reliable and easy to drive may all affect the final decision of purchasing. However, customers often emphasize some requirements more than the others and different customers may have different emphases. Therefore, automotive manufacturers have designed various series of vehicles according to the majority favorites. For instance, passenger cars are more fuel efficient, sports cars have excellent acceleration, sport utility vehicles (SUVs) satisfy off-road drivers and pickup trucks offer good cargo towing capability. Hybrid electric vehicles have advantages for additional fuel savings and they are becoming popular among daily commuters.

For any of the vehicles mentioned above, it is necessary to formulate effective metrics for fuel economy, performance and driveability. The fundamental requirements for this metrics are objective and quantitative. Subjective evaluation is time consuming and expensive since it can only be done by a human driver after a physical vehicle is built. It also varies with changing time or evaluators and thus is neither reliable nor comparable to other evaluations. Descriptive metrics are not able to be implemented in simulations directly. Therefore, automotive engineers may lose the opportunities of using simulations in vehicle powertrain design and control development processes.

Fuel economy is usually estimated with various city, highway and user-defined driving cycles. Performance criteria include acceleration performance, stopping distance, gradeability and towing capability. Fuel economy and performance metrics are relatively well-established and some have been already applied in simulations and testing.

Unlike fuel economy and performance, driveability describes driver impression on the overall driving quality. Hence, it is conventionally evaluated subjectively. Subjective evaluation is done by trained drivers conducting specific tests and may need a reference vehicle for comparison. The rating can be generated by evaluators, computer ranking program or neural nets. Table 3.1 lists evaluating criteria on the responsiveness and the smoothness of a vehicle under transients and steady state operations [61].

Test Condition	Score	Comments
Start time		
Start quality		
Idle stability		
Idle NVH		
Idle drive		
Pullaway		
Tip-in/back-out (city)		
Tip-in/back-out (highway)		
Cruise 2000/3000 rpm		
Full load performance		
Acceleration from low to high speeds		
Pedal response		
Gearshifts		
Engine response in neutral		

Table 3.1 Vehicle Driveability Scorecard [61]

The computer program is able to calculate the ratings according to measured driver inputs and vehicle responses in different maneuvers [62]. Neural networks correlate subjective assessments with objective evaluations through extensive trainings with vehicle testing data as the inputs and evaluator scores as the outputs [63]. An example of the subjective ratings with the corresponding scores and explanations are shown in Table 3.2.

Score	Subjective Rating	Description
10	Excellent	Not noticeable even by experienced test drivers
9	Very good	Disturbing for experienced test drivers
8	Good	Disturbing for critical customers
7	Satisfying	Disturbing for several customers
6	Even satisfying	Disturbing for all customers
5	Adequate	Very disturbing for all customers
4	Defective	Felt to be deficient by all customers
3	Insufficient	Reclaimed as deficient by all customers
2	Bad	Limited vehicle operating only
1	Very bad	Vehicle not operating

Table 3.2 Vehicle Driveability Ratings and Descriptions [63]

Driveability measures should reflect the driver's audible and perceptible dissatisfactions resulted from undesirable engine operating quality (start quality, idle response), pedal response, acceleration tip-in/tip-out response and shifting quality. These dissatisfactions are often referred as hesitations, jerks, surges, sags, oscillations, noises, stumble, hunting, roughness, etc. by the drivers. Customer requirements on driveability also exhibit culture differences: Americans pay attentions to cruise quality and driving comfort; Europeans appreciate good acceleration performance and smooth gear shifting; and Japanese prefer slight vibrations and noises [64].

Establishing effective objective metrics for driveability is still an ongoing task. Some existing objective measures in the literature are introduced here. The torque hole illustrated in Figure 3.1 represents the torque deficiency during shifting [65]. Minimizing the width and the depth by using fill-in torque from an assisting device will help to level the hole. The overshoot in the shaft torque curve need to be reduced as well.

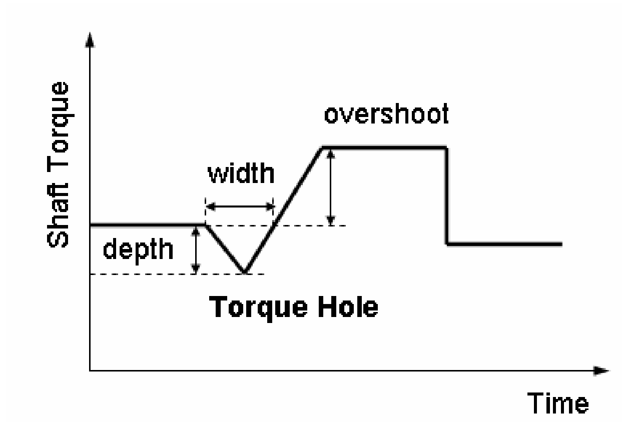

Figure 3.1 Torque hole during shifting [65]

The Vibration Dose Value (VDV) is an industrial standard describing the accumulative vibrations received during a period of time. Only the vibration in a certain frequency range that causes discomfort by human is considered. Furthermore, acceleration characteristics and jerk amplitude are also used to evaluate driveability.

This chapter summarizes the objective metrics of driveability used in this dissertation. The relationship between driveability subjective evaluations and objective measures is also introduced to show the validity of this metrics compared with a scorecard.

3.2 Objective Metrics for Fuel Economy

3.2.1 Fuel Economy Metrics

In addition to reducing the amount of imported fuel and consumers' fuel cost, improving fuel economy indicates less fuel consumption, which means less emissions and more conserved resources for future generations. Fuel economy is defined as volumetric fuel consumption per distance traveled in the unit of miles per gallon. Vehicle maintenance condition, driving pattern, traffic load, fuel quality, environmental (temperature, wind speed, etc.) and trip terrain conditions all have effects on the vehicle fuel economy.

Some drivers check the fuel economy of their cars by crude estimation. They record the odometer readings of two refuels. The difference between the two readings divided by the volume of the total fuel purchased between two refuels is the average fuel economy of the journey. Averaging results over several months eliminates short-term influences, such as unusual traffic conditions and fuel variations, but may bring in disturbances due to mechanical and seasonal changes. [66]

Automakers estimate the 'city' and the 'highway' fuel economy of a newly designed vehicle through testing prototypes by a professional driver under controlled laboratory conditions. After the U.S. Environmental Protection Agency (EPA) verifies manufacturers' estimates through partial retesting, these values are adjusted down 10% and 22% for the 'city' and the 'highway' respectively to make them closer to the average of real-world testing results. [67, 68]

'City' represents urban driving, in which a vehicle is started with a cold engine and driven in stop-and-go rush hour traffic. 'Highway' represents a mixture of rural and interstate highway driving in warmed-up vehicles, typical of longer trips in free-flowing traffic [69]. Standardized test procedures, also referred as driving cycles, were designed by the EPA for fuel economy and emissions tests. A driving cycle is a time history of the typical vehicle velocity profile simulating certain traffic condition and driving pattern. Federal Urban Driving Schedule (FUDS, also referred to as FTP72, LA4 and UDDS [70]) and Federal Highway Driving Schedule (FHDS or HWFET) shown in Figure 3.2

and Figure 3.3 represent typical daily driving conditions and are widely used by automotive engineers in the U.S.

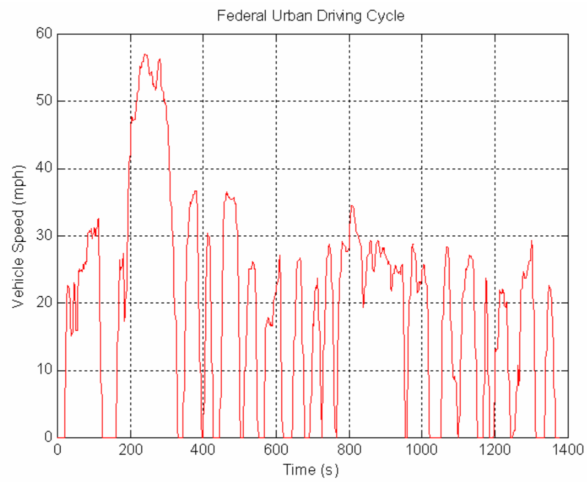

Figure 3.2 Federal Urban Driving Schedule (FUDS)

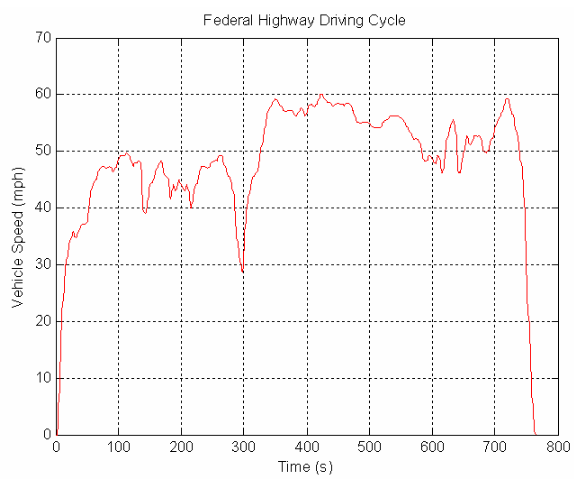

Figure 3.3 Federal Highway Driving Schedule (FHDS)

The FTP75 (Federal Test Procedure) is the FTP72 with an extended warm-engine running phase. The first 505 second of the FTP72 (which operates with a cold engine) is appended to itself after a 10 minute soak period with the engine shut off. The FTP75 is especially useful to compare emissions and fuel consumption under the same driving conditions with the cold and the warm engine. There also exist numerous other standard or customer defined driving cycles for different cities, countries or scenarios, such as New York City Cycle (NYCC), aggressive US 06, New European Driving Cycle (NEDC), Japan 10/15/1015, military driving cycles, etc. [71]. Dembski [72] and Gammariello [73] proposed some methodologies to generate realistic driving cycles with desired statistical properties.

The FUDS and the FHDS are often used in simulations to estimate the 'city' and the 'highway' fuel economy as well. To compare the simulation estimates with the real ones, one may either use the recorded actual vehicle velocity on real road as the driving cycle or apply predefined driving cycles in the vehicle on a test bed.

For vehicles powered by energy not from gasoline nor gasoline alone, gasoline equivalent fuel economy needs to be calculated to allow for fair comparisons. The gasoline equivalent fuel economy for a diesel powered and a hybrid electric vehicle is listed in equations (3.1) and (3.2). The fuel economy of vehicles with other alternative fuels can be calculated similarly by balancing the energy equation of the gasoline and the alternative fuel.

$$MPG_{diesel} = \frac{X \cdot H_{v\_gas} \cdot \rho_{gas}}{H_{v\_diesel} \cdot \rho_{diesel} \cdot V_{f\_diesel}} \tag{3.1}$$

$$MPG_{HEV} = \frac{X}{\frac{264.2 \cdot E_{elec}}{\eta_{elec} \cdot H_v \cdot \rho} + V_f} \tag{3.2}$$

Where,

X distance traveled in *miles*,

E_{elec} net electricity consumption in *MJ*,

H_v lower heating value of fuel in *MJ/kg*,

V_f volumetric fuel consumption in *gallons*,

ρ fuel density in kg/m^3,

η_{elec} average energy conversion efficiency from gasoline to electricity.

3.2.2 Numerical References of Fuel Economy Metrics

Figure 3.4 lists the highest and lowest fuel economy with corresponding vehicles in each class according to the EPA fuel economy database of 2003 model year vehicles [69].

Most of the MILE/GAL leaders in the above table are equipped with manual transmissions except for those marked with (A), which represents automatic transmissions. Similarly, the default transmission for the least fuel efficient vehicles is automatic except for those marked with (M). Manual transmissions are generally more efficient than automatic transmissions. All the violations seen in Figure 3.4 are due to the reason that the same vehicles with the other type of transmissions are not available on the market.

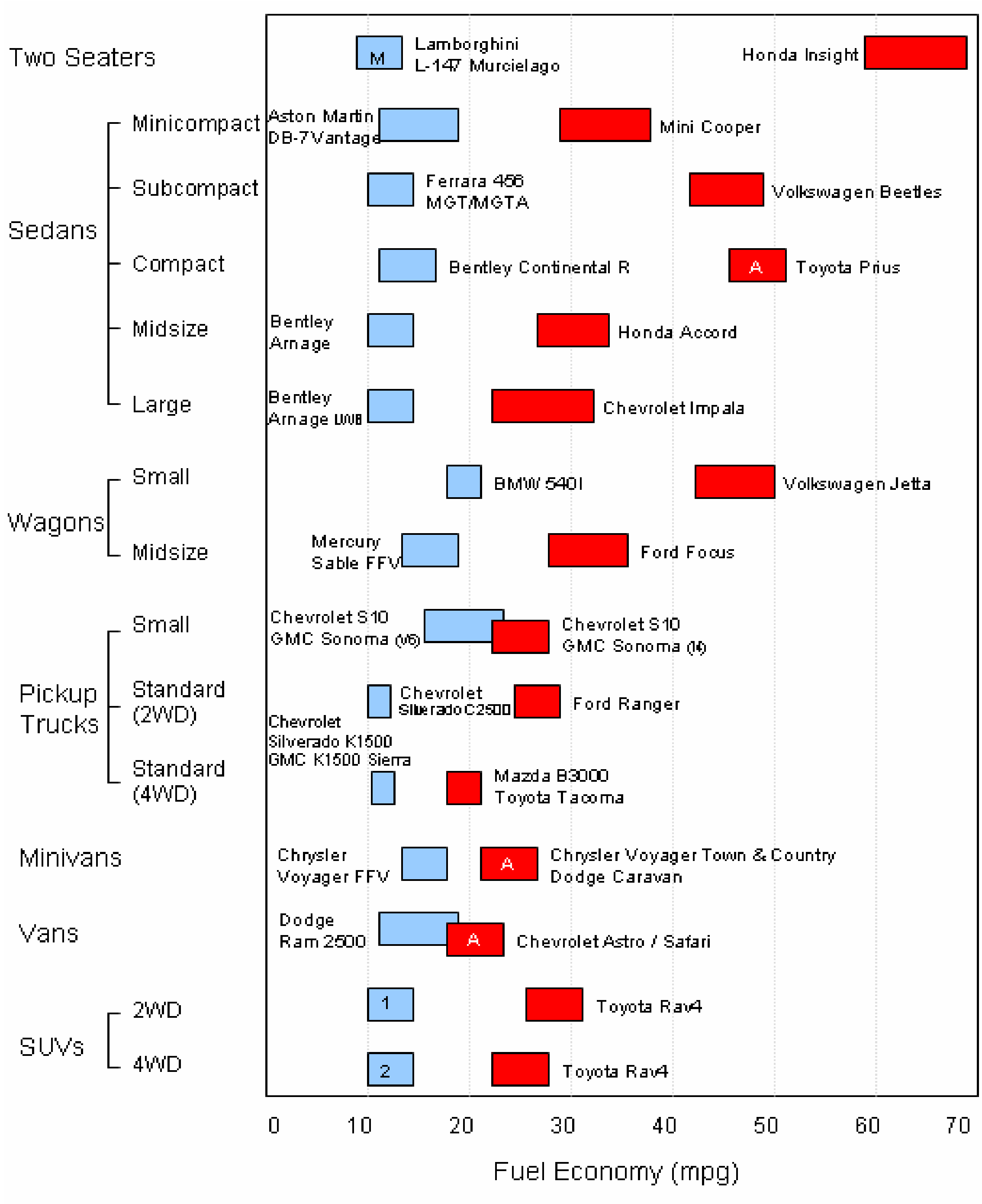

Figure 3.4 Fuel economy of 2003 model year vehicles

(1: Chevrolet K1500 Avalanche, Suburban GMC C1500 Yukon

2: Chevrolet K1500 Avalanche, Suburban, Tahoe/ GMC K1500 Yukon)

3.3 Objective Metrics for Performance

3.3.1 Performance Metrics

Vehicle performance metrics include acceleration time, top speed, stopping distance, gradeability and towing capability.

Acceleration Performance

0 to 60 mph acceleration is widely used to evaluate vehicle acceleration capability. It appears in almost every simulation tool which contains an acceleration test. 30~50 mph acceleration is designed to approximate a vehicle merging to highway and 50~70 mph acceleration simulates a passing event on highway. Acceleration capability sometimes is considered as a measure to escape from a danger.

Top Speed

Top speed is the maximum speed a vehicle can reach. For an HEV, it implies that the electric machine can only help in the first portion of the acceleration, but cannot assist during the whole acceleration from zero speed to top speed, if it is defined as the sustainable maximum vehicle speed. The top speed of a vehicle can be calculated through force balancing by considering vehicle acceleration as zero, see equation (3.3).

$$V_{\max} = \sqrt{2\frac{F_{tr\_\max} - MgC_r\cos(grade) - Mg\sin(grade)}{\rho_{air}C_dA_f}} \tag{3.3}$$

Where,

M vehicle mass in *kg*,

g gravity acceleration in m/s^2,

grade road grade in *percentage*,

A_f vehicle frontal area in m^2,

C_d drag coefficient,

C_r rolling resistance coefficient,

F_{tr_max} maximum tractive force on the wheels in N,

ρ_{air} air density in kg/m^3.

Stopping Distance

Whether a vehicle can stop in time is an important criterion for safety. Stopping distance is composed of two parts, reaction distance and braking distance. The reaction distance is the vehicle displacement between the driver sees a danger and the driver hits the brake pedal. It depends on the driver reaction time and the vehicle speed. The braking distance, on the other hand, represents the distance traveled after the driver hits the brakes until the vehicle comes to a full stop. It is highly related with the conditions of the brakes, the tires, the weather and the road. The reaction distance (the linear term) and the braking distance (the quadratic term) with full braking on dry, level asphalt and an average perception-reaction time of 1.5 second are expressed in equation (3.4) [74]. The structure of this equation is based on empirical data.

$$\text{Stopping Distance} = 2.2 \times V + 0.048 \times V^2 \tag{3.4}$$

Where,

Stopping Distance stopping distance in *feet*,

V vehicle velocity in *mph*.

Gradeability

Gradeability limit is the maximum grade on which the test vehicle can just move forward. Gradeability at speed is the maximum vehicle speed which can be maintained on roads having different grades [75]. Sometimes, people define gradeability as the maximum grade a vehicle can maintain at a predetermined constant speed, e.g. 55 mph. Gradeability is expressed in percentage and it is equal to the tangent of the road gradient. The gradeability of a vehicle depends on vehicle tractive force, overall mass, rolling resistance and road/tire adhesion. Equations (3.5) and (3.6) provide gradeability estimates with and without considering road/tire adhesion [76].

$$Gradeability = 100 \times \left(\frac{F_{tr}}{g \cdot M} - C_r \right) \tag{3.5}$$

$$Gradeability = 100 \times \left(\frac{\mu \cdot F_{load}}{g \cdot M} - C_r \right) \tag{3.6}$$

Where,

F_{load} load force at the wheels in *N*,

μ coefficient of road/tire surface friction.

Towing Capability

Towing capability tells how much a vehicle can tow when it is operating under the same test conditions as for non-towing cases. It includes all driving scenarios we just mentioned. The towing capability can be estimated in simulations by changing the total vehicle mass, the frontal area and the drag coefficient to take into account the effects of the trailer.

Acceleration tests with grade, towing load or accessories on are sometimes considered as performance criteria as well.

3.3.2 Numerical References of Performance Metrics

Table 3.3 shows some numerical values of vehicle performance based on the majority vehicles on the road [87].

	Acceleration (s)			Top Speed (mph)	Towing Capability (lbs)	60~0 mph Braking Distance (ft)
	0~60 mph	30~50 mph	50~70 mph			
Two Seaters	5.6 ~11.6	1.6 ~ 5.2	3.1 ~ 7	109 ~ 168	N/A	118 ~ 149.6
Mini-compact	6.8 ~11.1	2.9 ~ 4.5	5.1 ~ 7.1	110 ~ 145	N/A	115 ~ 125
Sub-compact	5.8 ~ 8.2	2.5 ~ 3.6	2.9 ~ 5.4	103 ~ 156	~1000	112 ~ 120
Compact	6 ~ 9.3	2.6 ~ 3.9	3.5 ~ 5	119 ~ 150	~1000	142.7 ~ 183
Midsize	6.3 ~ 8	2.7 ~ 3.3	3 ~ 5	132 ~ 152	1000 ~ 2000	137.8 ~ 142.7
Large	5.8 ~ 6.9	2.1 ~ 2.7	3 ~ 3.8	131 ~ 153	1000 ~ 2000	140 ~ 150
Compact Pickups	8.7 ~ 9.5	3 ~ 4	5 ~ 6	100 ~ 120	3500 ~ 7500	140 ~ 150
Full-size Pickups	6 ~ 9.7	3.3 ~ 4.4	5.3 ~ 6	101 ~ 126	5250 ~ 15800	136 ~ 158
Compact SUVs	8.7 ~10.9	2.8 ~ 4.9	5.1 ~ 7.4	94 ~ 124	1500 ~ 3000	128 ~ 140
Midsize SUVs	8.0 ~9.0	3.6 ~ 4.3	5.3 ~ 5.7	111 ~ 116	3500 ~ 5000	132 ~ 140
Full-size SUVs	7.1 ~10.0	4.2~ 4.4	5.8 ~ 6	101 ~ 103	6500 ~ 8900	141 ~ 154
Minivans	9.6 ~10.1	4 ~ 4.1	5.5 ~ 5.6	110 ~ 114	2000 ~ 3800	128 ~ 145

Table 3.3 Vehicle Performance References

3.4 Objective Metrics for Driveability

3.4.1 Driveability Metrics

Driveability is a comprehensive terminology for vehicle responsiveness, operating smoothness and driving comfort. It evaluates the overall driver feeling under various driving conditions. The following issues due to improper design, control or operation are considered as driveability problems [89].

- Hesitation or delay: momentary lack of response as the accelerator pedal is pushed down especially when a vehicle starts from a stop.

- Sluggish: engine delivers less power than expected such that vehicle speed has little or no increase when the accelerator pedal is partially pressed.
- Hard start: engine does not start or may not continue to run.
- Surge: engine power varies under steady throttle. The vehicle speeds up or slows down with no change in the accelerator pedal.
- Idle roughness and instability: engine runs unevenly at idle or stalls, engine idle speed is incorrect or varying (i.e. hunting).
- Noise and oscillations: noise and vibrations from powertrain and/or road especially during idling, engine start/stop, hard acceleration/deceleration, shifting, steering, braking and running on bumpy roads.

These observations are evaluated by vehicle interior noise level, jerk amplitude and acceleration characteristics. Moreover, engine start/stop frequency and whether it is expected are often considered for HEVs.

Ideal shifting of a transmission is smooth, quiet, consistent, predictable and without hesitation. Shifting occurred too early, too late, too often or taking too long to complete are undesirable.

The discomfort caused by vibrations and accelerations depends on the vibration frequency and the direction, the point of contact with the body and the duration of vibration exposure [90]. Vibrations between 0.5 and 80 Hz are significant in exciting human body response. The most effective exciting frequency for horizontal vibrations lies between 1 and 2 Hz and that for vertical vibrations is from 4 to 8 Hz. Vibrations ranging from 2.5 to 30 Hz generate strong resonance with amplified magnitude of up to 200~350 %, which may cause permanent damage on human organs and body parts. [92]

Interior Noise Level

As a measure of the vehicle acoustic characteristics, interior noise level is defined as the sound pressure level inside a vehicle under normal vehicle operations. A number of noise sources contribute to the overall vehicle interior noise level, such as tire/road interaction, drivetrain, exhaust system, air turbulence, ventilation system and audio system. Sound insulation is effective in reducing the noise level. However, excessive insulation may decrease the detectability of outside warning and siren signals to penetrate the vehicle. Thus, it is more desirable to minimize noise generation and to impede noise propagation on the transmitting path other than taking efforts to prevent the external signals from coming in. [93]

Sound intensity I is the sound power per unit area in W/m^2 and is used to measure the noise level. Many measurements are made relative to the standard threshold of hearing intensity I_0 of 10^{-12} W/m^2 or the atmospheric sound pressure P_0 of 2×10^{-5} N/m^2 in decibel (dB) as shown in equation (3.7). [94]

$$I(dB) = 10\log_{10}\left(\frac{I}{I_0}\right) = 10\log_{10}\left(\frac{P^2}{P_0^2}\right) = 20\log_{10}\left(\frac{P}{P_0}\right) \tag{3.7}$$

Where,

I sound power per unit area in W/m^2,

I_0 standard threshold of hearing intensity of 10^{-12} W/m^2,

P_0 atmospheric sound pressure of 2×10^{-5} N/m^2.

<u>Acceleration Root Mean Square (RMS) Value</u>

Acceleration RMS value calculates the average acceleration during certain period of time. It is referred to as the A(8) method when this calculation is normalized to represent a 8-hour exposure [95]. The variable $\tilde{a}$ in equation (3.8) is the vehicle acceleration in m/s^2 filtered by a band-pass filter with the bandwidth of 1 to 32 Hz [96].

$$RMS = \sqrt{\int_{t_0}^{t_f} \tilde{a}^2 dt \Big/ \left(t_f - t_0\right)} \tag{3.8}$$

Where,

$\tilde{a}$ vehicle acceleration in m/s^2,

t_0 starting time in s,

t_f final time in s.

Vibration Dose Value (VDV) [48]

Vibration dose value is a mathematical concept which describes the total vibration dose received by being in contact with a vibrating surface over a specific period of time, taking account of the direction of the vibration, frequency characteristics and time history [90]. The VDV is more sensitive to acceleration peaks than the RMS value and hence is a better indicator of rides that contain shocks, jolts and jars [91]. This cumulative dosage is commonly calculated over a working day in $m/s^{1.75}$.

$$VDV = \left(\int_{t_0}^{t_f} \tilde{a}^4(t)dt \right)^{\frac{1}{4}} \tag{3.9}$$

Acceleration/Deceleration Jerk

Jerk is the first derivative of vehicle acceleration. It describes vehicle acceleration or deceleration changing rate in m/s^3. Vehicle jerk is highly related with driving comfort.

$$j = \frac{da}{dt} \tag{3.10}$$

Where,

a vehicle acceleration in m/s^2,

j vehicle jerk in m/s^3.

Maximum Transient Vibration Value (MTVV) / Maximum G-force

MVTT provides information on shock loads which are not revealed in the acceleration RMS value. It is particularly important to a vehicle which often runs on bumpy roads and has inadequate suspensions or poor seating [96]. Maximum G-force is the ratio of the maximum amplitude of acceleration or deceleration over the gravity acceleration in the unit of g. Both of them indicate the peak value of the acceleration and deceleration.

Tip-in/Tip-out Response

Besides the amplitude of acceleration, the shape of the acceleration profile is also critical to ride comfort. Figure 3.5 is an undesirable tip-in response at wide open throttle [97, 98]. Obviously, delay and sag in the acceleration should be minimized and oscillations need to be suppressed.

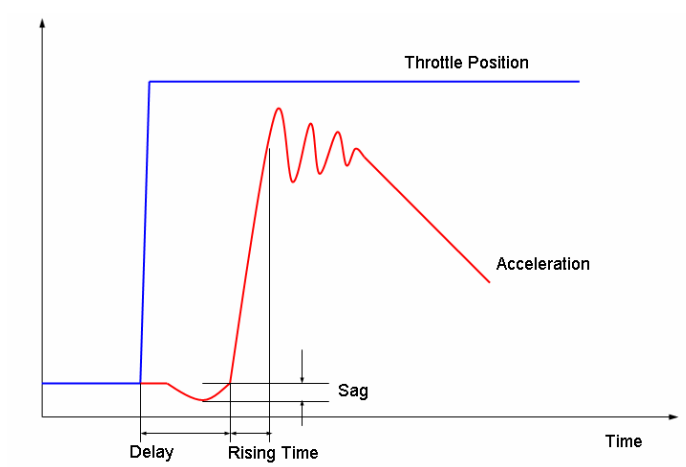

Figure 3.5 Tip-in response

Torque hole brings hesitation, sag and overshoot in vehicle speed and acceleration. Its effects are considered and measured in the vibration and acceleration related driveability metrics.

3.4.2 Numerical References of Driveability Metrics

The interior noise of vehicles at idle with all windows and doors closed, ventilation and audio systems off is ranging from 38 to 51 dB. That of the same vehicles at 70 mph is around 70 dB [92]. The threshold of pain is 130 dB [93].

According to ISO 2631-1 1985/1997 and British standard 6841-1987, vibration exposure limits in three dimensions and human comfort reaction based on 8-hour exposure are shown in Table 3.4 and Figure 3.6 to Figure 3.8 [90, 91]. A typical heavy transportation truck has approximately 0.42 to 2.0 m/s^2 A(8) value in the vertical axis [83] and small cars can reach 0.2 to 0.5 m/s^2 [95].

Acceleration RMS Value (m/s^2)	Comfort Reaction
≤ 0.315	not uncomfortable
0.315 ~ 0.63	a little uncomfortable
0.5 ~ 1	fairly uncomfortable
0.8 ~ 1.6	uncomfortable
1.25 ~ 2.5	very uncomfortable
≥ 2	extremely uncomfortable

Table 3.4 Comfort Reaction to Vibration Environments (ISO 2631-1 1997)

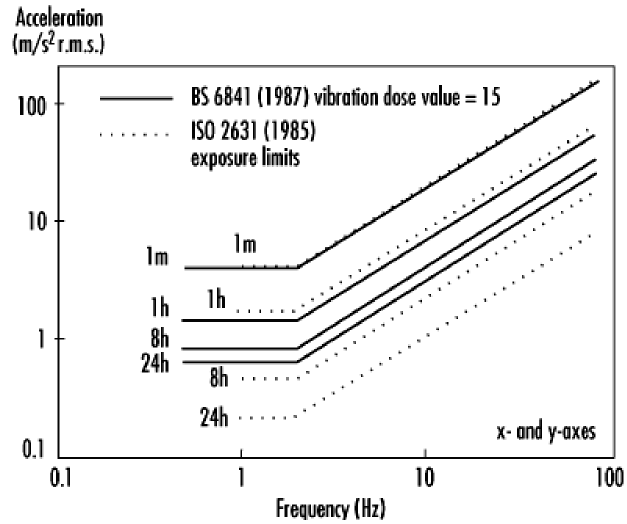

Figure 3.6 Horizontal Vibration Exposure Limit

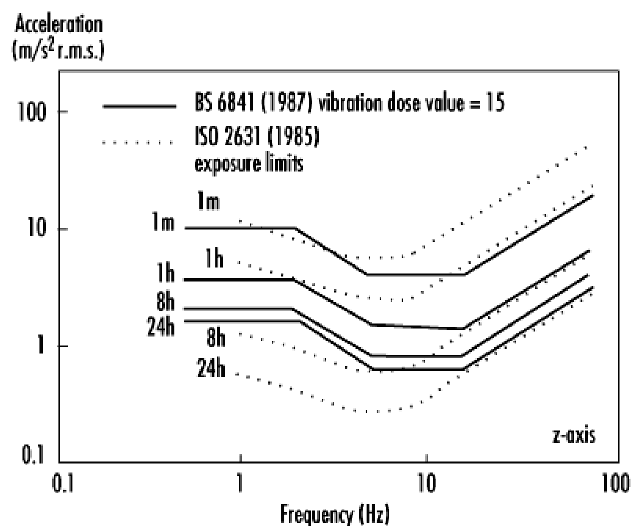

Figure 3.7 Vertical Vibration Exposure Limit

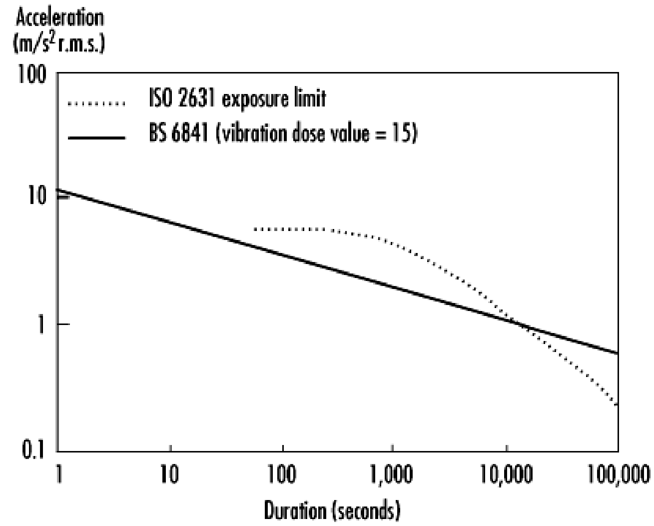

Figure 3.8 Time Dependency of Vibration Exposure Limit

The caution zone is reached when the VDV is 8.5 $m/s^{1.75}$ and the risk zone is at 15 $m/s^{1.75}$ for a working day [91].

The magnitude of jerk is highly related with driving comfort and safety. According to the literature [91, 99], an acceptable jerk is ±2 m/s^3 and a comfortable jerk is ±1 m/s^3. Jerk in emergency cases can be as high as ±10 m/s^3 [100].

The ratio of the MTVV over unweighted RMS (including vibrations with all frequencies) should be less than 1.5 to obtain good transient feel [96]. The maximum acceleration G-force of compact and midsize cars is about 0.8 to 0.9 g and that of SUVs can achieve 0.7 to 0.75 g [79]. The MTVV is as large as 1.0~1.2 g in emergency braking in some cars [101].

3.4.3 Relationship between Subjective and Objective Driveability Metrics

Sound loudness is a subjective term describing the strength of the ear's perception of a sound. It is not identical to sound intensity, but they are intimately related. Since increasing sound intensity or power by ten times is equivalent to doubling loudness, decibel scale is more convenient to be used to measure sound intensity. [94]

Wicke, Brace and Vaughan [102] investigated the correlation between subjective assessments and objective parameters on driveability and performance feel. Acceleration and delay time both exhibit fairly linear relationship with launch and performance feel. Higher acceleration value, lower delay time and medium jerk led to better driveability and performance feel. Launch tests conducted heavy pedal commands starting from standstill and performance tests were simulating merging and passing events with the maximum pedal position.

According to Dorey and Holmes [61], smaller overshoot and rise rate in the tip-in/tip-out response brought better driver assessments. Poor engine operating quality definitely degrades the vehicle overall rating. It is shown that the engine cranking time, the average speed variation and the post flare speed reduction all influenced engine operating smoothness, stability and hence the final scores in [64]. Moreover, speed overshoot and undershoot at idle determined engine idle response. Rating was reduced when the transients became severe.

3.5 Summary

Model-based control design requires building control oriented model and defining objective control criteria. The control criteria for this research include fuel economy, performance and driveability which have to be defined before one builds the model. This chapter reviews the existing measures and then introduces the objective metrics with numerical references for the three control criteria. In addition, it also shows the relationship between the subjective and objective driveability metrics. The objective metrics that are used in the model introduced in the next chapter include city/highway mileage for fuel economy; acceleration performance, top speed, braking distance, gradeability and towing capability for vehicle performance; and acceleration RMS, VDV, MTVV, jerk and tip-in response for driveability.

CHAPTER 4

MODEL DESCRIPTION

The control strategy which considers fuel economy, performance and driveability is developed hierarchically: finding the optimal solution for minimum fuel consumption first and then taking driveability into account. Good performance is always guaranteed since meeting power commands is set to be the first priority in optimization. The control strategy development consequently requires two models: one for fuel economy and performance optimization and the other for the case which considers driveability as well as fuel economy and performance. Due to the fact that vehicle fuel economy and performance is mainly determined by energy flows in the vehicle, a quasi-static model serves as the test-bed for fuel economy and performance optimization. Evaluating vehicle driveability requires a model which represents more vehicle dynamics and thus a low-frequency dynamic model is selected. This Chapter will introduce the two control-oriented models in details.

4.1 Drivetrain Model for Fuel Economy Optimization

The appropriate model for vehicle fuel economy and performance optimization is the static/quasi-static model which describes power input-output relationship of powertrain components with efficiency or power losses. The engine and the ISA use maps or the Willans line model to express the efficiency. This efficiency depends on both the operating speed and torque. While in the CVT and the final drive, constant efficiency and gear ratio are considered to describe the relation between the input and output speeds and torques. The CVT efficiency is sometimes expressed as a 3D map indexed by the gear ratio, speed and load torque. As the secondary energy source in the vehicle, the battery uses current integration to estimate the state of charge (SOC). The discharging and recharging power are both bounded as well as the battery SOC. Here, the SOC limits allow for operating the battery without being damaged. In this quasi-static model, the vehicle model is the only one that contains dynamics to calculate the vehicle speed from torque.

A 2.2 liter 4-cylinder SI engine and a 30 kW (peak) induction machine are selected as the energy converters for this parallel HEV. The engine has maximum torque of 209 N·m at 3000 rev/min and maximum power of 119 kW around 6000 rev/min. The ISA is connected directly to the engine to replace the flywheel. Its main functions include starting the engine, power assistance, regenerative braking and compensating torque fluctuations. A Sanyo NiMH battery (1.2 V, 45 W, 2.2 Ah and 56 g per cell) pack serves as the power source for the ISA. According to the nominal operating voltage of the ISA and the maximum power requirement, this HEV needs 180 cells in series and 5 strings in parallel. Therefore, the total capacity of this battery pack is 7.128 MJ and the total weight is 50.4 kg. The torque converter acts as a damper to connect the energy converters with the transmission. It has a minimum slip-type clutch which can be engaged to reduce power losses in the torque converter. The gear ratio of the CVT may vary from 0.42 to 2.15 continuously.

4.1.1 Internal Combustion Engine

Internal combustion engines (ICEs), as opposed to external combustion engines, breathe in air and fuel and release energy by burning the fuel inside the engine. Spark-ignition engines, such as Otto engines, mix the air and the fuel in the intake system prior to the entry of the engine cylinders using either a carburetor or a fuel injection system [103]. The appropriate engine models for fuel economy optimization include engine efficiency or fuel consumption maps and the Willans line model.

Engine Efficiency and Fuel Consumption Maps

The simplest engine model describes the engine as an energy converter that transforms chemical energy into mechanical energy with certain efficiency.

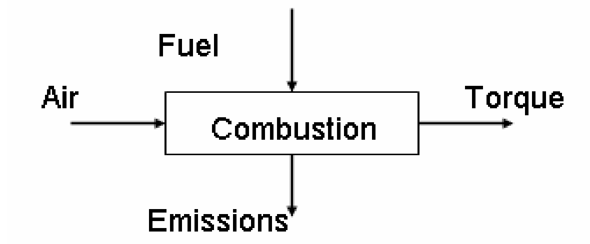

Figure 4.1 Schematic of engine basic functions

Figure 4.1 sketches the basic functions of the engine: taking air and fuel as inputs and producing torque and exhausts though combustion.

The engine efficiency map is a contour plot based on experimental engine efficiency data and is usually indexed by engine operating speed and torque. Figure 4.2 shows the efficiency map of a 2.2 L gasoline engine.

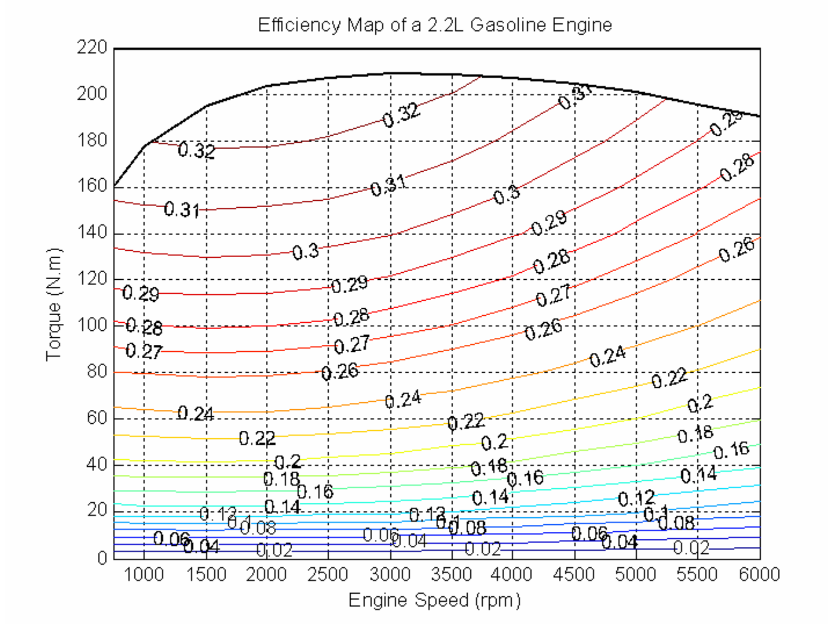

Figure 4.2 Engine efficiency map of a 2.2 L SI engine

Most of the engines have the highest efficiency, usually less than 35% for gasoline engines, at relative lower speed and higher torque. Efficiency data in the map are obtained at steady state and thus the engine efficiency maps do not represent engine dynamic behaviors.

The engine fuel consumption map (see Figure 4.3) is interchangeable with the engine efficiency map in the sense of describing engine losses.

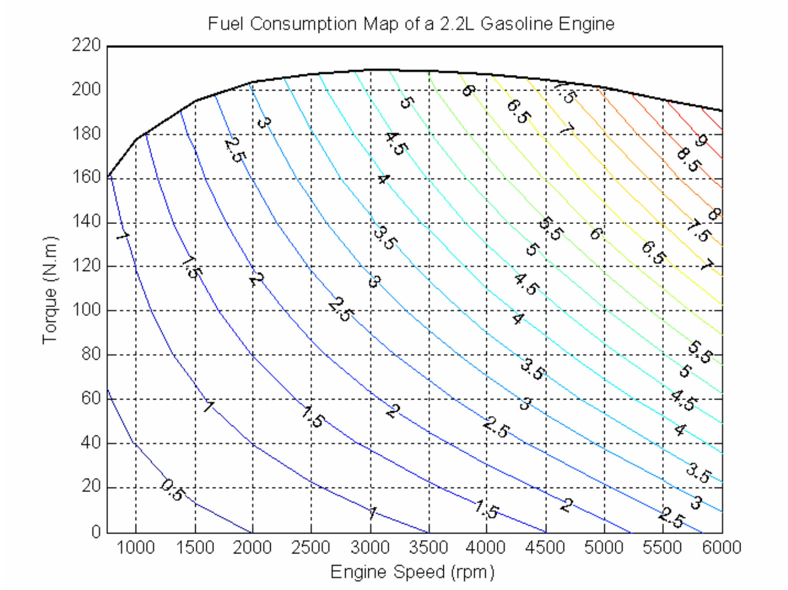

Figure 4.3 Engine fuel consumption map of a 2.2 L SI engine (g/s)

It is more convenient to use the fuel consumption map (static fuel mass flow rate $\dot{m}_f$) when calculating vehicle fuel economy. It is evident from the above map that engines consume more fuel under higher load, i.e., higher speed or higher torque or both. According to equations (4.1) to (4.3), these two maps can be easily converted to each other as long as the gasoline lower heating value H_v is known.

$$P_{in\_ice} = H_v \times \dot{m}_f \tag{4.1}$$

$$P_{out\_ice} = T_{ice} \times \omega_{ice} \tag{4.2}$$

$$\eta_{ice} = \frac{P_{out\_ice}}{P_{in\_ice}} \times 100\% \tag{4.3}$$

Where

P_{in_ice}	engine input power in *W*,
P_{out_ice}	engine output power in *W*,
H_v	gasoline lower heating value in *J/kg*,
T_{ice}	engine torque in *N·m*,
$\dot{m}_f$	engine mass flow rate of fuel in *kg/s*,
η_{ice}	engine efficiency in *percentage*,
ω_{ice}	engine speed in *rad/s*.

Willans Line Model

The Willans line model was originally used to describe an approximate linear relationship between the brake mean effective pressure and the fuel consumption of engines [103]. Rizzoni, Guzzella and Baumann [104] extended this model to describe generalized energy converters, i.e., the engines and the electric machines. Based on known steady state efficiency data of the reference machine, the efficiency of a new machine in the same category can be estimated using this scaling approach. Furthermore, it permits an automated exploration in the design space which considers some candidate machines even though the machine itself and/or its efficiency data do not exist in reality.

In the Willans line model, the energy conversion efficiency of an energy converter is defined as the ratio between the output and input powers. The resulting affine representation is described by two coefficients: the slope, or intrinsic energy conversion efficiency *e*; and the vertical axis intercept P_{loss}, describing losses due to air pumping, mechanical friction, magnetic phenomena, etc., as shown in Figure 4.4.

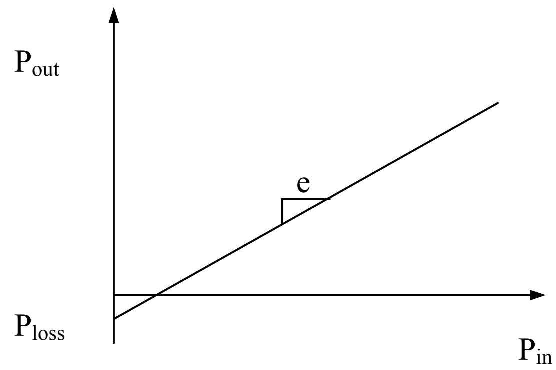

Figure 4.4 input-output relationship of an energy converter

The energy conversion efficiency and the affine relationship between the input power and output power are expressed in equations (4.1) to (4.4):

$$P_{out\_ice} = e_{ice} \times P_{in\_ice} - P_{loss\_ice} \tag{4.4}$$

In order to eliminate sizing effects, the engine speed and the torque are substituted by the normalized variables including the mean piston speed and the mean effective pressures as shown below:

$$C_{m\_ice} = \frac{S\omega_{ice}}{\pi} \tag{4.5}$$

$$P_{ma\_ice} = \frac{4\pi H_v \dot{m}_f}{V_d \omega_{ice}} \tag{4.6}$$

$$P_{me\_ice} = \frac{4\pi T_{ice}}{V_d} \tag{4.7}$$

Hence, the energy conversion efficiency becomes

$$\eta_{ice} = \frac{P_{me\_ice}}{P_{ma\_ice}} \tag{4.8}$$

and the input-output relationship can be written in a corresponding format as

$$P_{me\_ice} = e_{ice} \times P_{ma\_ice} - P_{ml\_ice} \tag{4.9}$$

After P_{ma_ice} and P_{me_ice} are calculated at each operating speed, the intrinsic efficiency e_{ice} and the mean friction pressure P_{ml_ice} are approximated to be functions of C_{m_ice} and P_{ma_ice}:

$$\begin{aligned} e_{ice} = &(e_{00\_ice} + e_{01\_ice} C_{m\_ice} + e_{02\_ice} C_{m\_ice}{}^2) \\ &- (e_{10\_ice} + e_{11\_ice} C_{m\_ice}) \times P_{ma\_ice} \end{aligned} \tag{4.10}$$

$$P_{ml\_ice} = P_{ml0\_ice} + P_{ml2\_ice} C_{m\_ice}{}^2 \tag{4.11}$$

e_{10_ice} and e_{11_ice} in equation (4.10) are often close to zero, reducing e_{ice} to a function of C_{m_ice} alone.

The wide-open throttle mean effective pressure curve of engines is identified as

$$P_{\max\_ice} = \sum_{i=0}^{3} P_{\max i\_ice} C_{m\_ice}{}^i \tag{4.12}$$

Where

C_{m_ice} engine mean piston speed in *m/s*,

P_{loss_ice} engine power losses in *W*,

P_{ma_ice} engine theoretically available mean effective pressure in P_a,

P_{max_ice} engine wide-open throttle mean effective pressure in P_a,

P_{maxi_ice} scaling coefficients of wide-open throttle mean effective pressure P_{max_ice},

P_{me_ice} engine actual mean effective pressure in P_a,

P_{ml_ice} engine mean friction pressure in P_a,

P_{mli_ice} scaling coefficients of engine mean friction pressure P_{ml_ice},

S engine stroke in m,

V_d engine displacement in m^3,

e_{ice} engine intrinsic energy conversion efficiency excluding transferring losses in *percentage*,

e_{ij_ice} scaling coefficients of engine intrinsic energy conversion efficiency $e_{\_ice}$.

The most commonly used engines in automotive applications are the spark-ignition (SI) gasoline-fueled and the compression-ignition (CI) diesel-fueled engines. A set of coefficients of the engine in each category can be calculated through curve fitting and stored for later scaling applications. In the scaling process, the mean piston speed is computed with the dimensional parameters of the scaled machine. The intrinsic efficiency and the frictional losses are then calculated for each operating speed using the stored scaling coefficients of the same class. Therefore, the Willans line model can assist in quickly constructing a design space suitable to a search for the optimal vehicle configuration and sizing of powertrain components. In addition, it also permits the generation of scalable optimal control algorithms for HEVs if it is based on the efficiency maps.

Two important things need to be noticed when applying the Willans line model. First, the scaled machine and the scaling machine should be from the same class of engines, e.g. SI or CI engines. Further, when generating the scaling coefficients, one should curve fit over a wide range of the scaling variable of C_{m_ice} so that during the subsequent use of the model, the efficiency is not obtained by doing extrapolation.

Figure 4.5 shows the Willans line model of the 2.2 L gasoline engine scaled from a 1.9 L engine. The efficiency data of the 2.2 L engine is very linear and it matches the scaled Willans line.

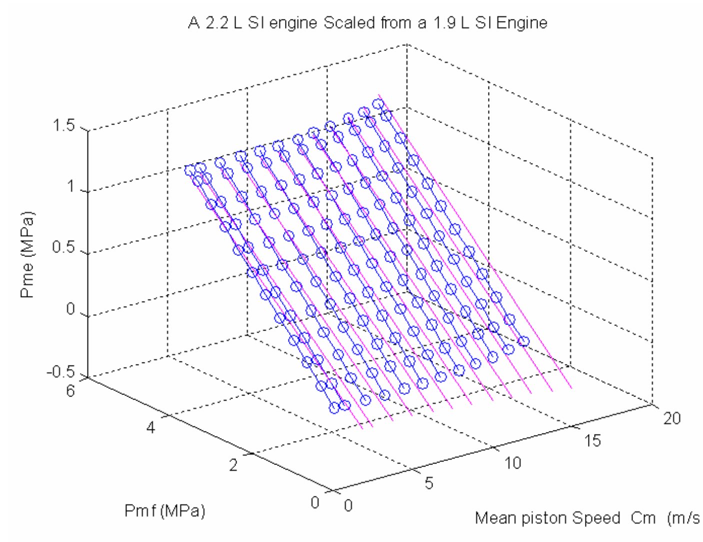

Figure 4.5 Scaled Willans line model of a gasoline engine (2.2 L)

4.1.2 Electric Machine

The AC induction machine is selected as the ISA in our hybrid drivetrain due to its wide torque-speed range, high performance, ruggedness, better failure mode and low cost [105]. The electric machine model suitable for energy flow calculation is the efficiency map and the Willans line model.

Electric Machine Efficiency Map

The efficiency map which is not restricted to the machine type finds extensive applications in solving automotive design and control problems. Similar to the engine efficiency map, the EM efficiency map also represents static empirical efficiency data as contours on a torque-speed plot. Figure 4.6 shows the efficiency map of a 30 kW (peak rated power) induction machine.

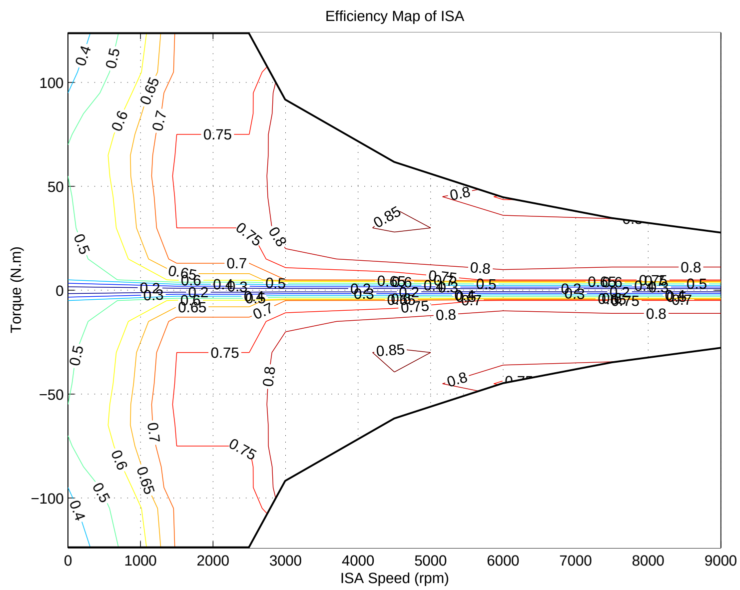

Figure 4.6 Efficiency map of a 30 kW (peak) induction machine

The flat segment in the maximum torque curve is the so-called constant torque region and the hyperbolic decaying segment reflects the flux weakening region. The EM behaviors in the generating mode (negative EM torque region) is usually different from those in the motoring mode (positive EM torque region), but engineers may consider they are the same, i.e., symmetric about the zero torque line for simplicity. In general, the highest efficiency of an EM is located at the higher power region.

Willans line model

As it is mentioned earlier, the Willans line model is also applicable in describing electric machines. The input-output powers and the efficiency of an EM in the motoring mode are

$$P_{in\_em} = U \times I \tag{4.13}$$

$$P_{out\_em} = T_{em} \times \omega_{em} \tag{4.14}$$

$$\eta_{em} = \frac{P_{out\_em}}{P_{in\_em}} \times 100\% \tag{4.15}$$

Where

I electric machine input current in *A*,
P_{in_em} electric machine input power in *W*,
P_{out_em} electric machine output power in *W*,
T_{em} electric machine torque in *N·m*,
U electric machine input voltage in *V*,
η_{em} electric machine efficiency in *percentage*,
ω_{em} electric machine speed in *rad/s*.

Then, using the Willans line concept, the EM input-output relationship can be converted into

$$P_{out\_em} = e_{em} \times P_{in\_em} - P_{loss\_em} \tag{4.16}$$

Applying the normalized variables of the mean rotor speed and the air gap shear stresses, we obtain

$$C_{m\_em} = r_r \omega_{em} \tag{4.17}$$

$$P_{ma\_em} = \frac{UI}{2V_r \omega_{em}} \tag{4.18}$$

$$P_{me\_em} = \frac{T_{em}}{2V_r} \tag{4.19}$$

$$\eta_{em} = \frac{P_{me\_em}}{P_{ma\_em}} \tag{4.20}$$

$$P_{me\_ice} = e_{ice} \times P_{ma\_ice} - P_{ml\_ice} \tag{4.21}$$

Noting the success of the polynomial models for the engine, polynomials in C_{m_em} were initially selected to model e_{em} and P_{ml_em} of the EM. The simulation result has shown that fourth order polynomials capture the behavior of e_{em} and P_{ml_em} with sufficient accuracy and without excessive coefficients

$$e_{em} = \sum_{i=0}^{4} e_{0i\_em} C_m^i \tag{4.22}$$

$$P_{ml\_em} = \sum_{i=0}^{4} P_{mli\_em} C_m^i \tag{4.23}$$

Where

C_{m_em}	electric machine mean rotor speed in *m/s*,
P_{loss_em}	electric machine power losses in *W*,
P_{ma_em}	electric machine theoretically available air gap shear stress in P_a,
P_{me_em}	electric machine actual air gap shear stress in P_a,
P_{ml_em}	electric machine mean friction pressure in P_a,
P_{mli_em}	scaling coefficients of electric machine mean friction pressure P_{ml_ice},
V_r	electric machine rotor volume in m^3,

e_{em} electric machine intrinsic energy conversion efficiency in *percentage*,

e_{ij_em} scaling coefficients of electric machine intrinsic energy conversion efficiency $e_{\_ice}$,

r_r electric machine rotor radius in *m*.

The Willans line model for the electric machines also allows building the scalable models within the same category, such as induction EM, permanent magnet synchronous EM and switched reluctance EM. One may refer to engine's Willans line model for detailed description of model application and restrictions.

The figure below shows the Willans line model of the 30 kW induction machine scaled from an 83 kW machine. The real efficiency data matches the scaled Willans line very well except for the high pressure region.

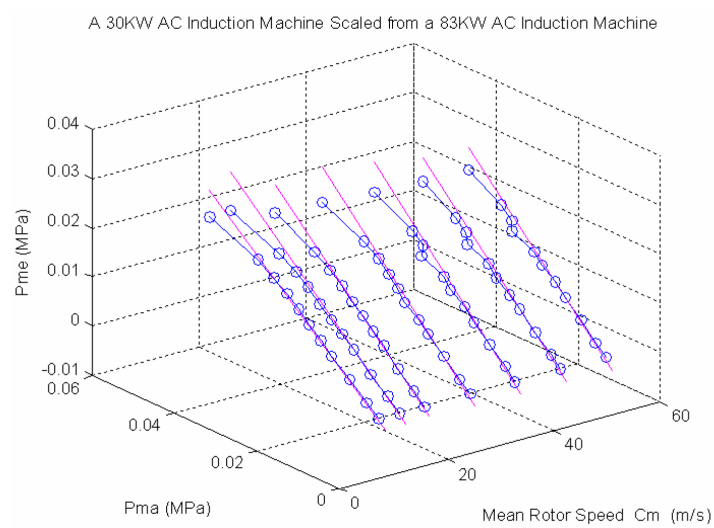

Figure 4.7 Scaled Willans line model of an electric machine (30 kW induction)

4.1.3 Battery

Batteries typically used in HEVs are the lead acid and the Nickel Metal Hydride (NiMH) batteries. Lithium polymer, lithium ion, nickel cadmium, nickel iron, nickel zinc, sodium sulfur, zinc air and zinc bromide, etc. are also under investigation for future massive applications. In the HEV, the nonlinear nature of the electrochemical processes in the battery is magnified due to dramatic current flowing in and out of the battery and larger range of the temperature variation. The simplest battery model uses constant discharging and recharging efficiencies neglecting the fact that the power losses are related to the battery current.

A simple battery model which considers the open circuit voltage U_o and the internal resistance R_i is shown in Figure 4.8.

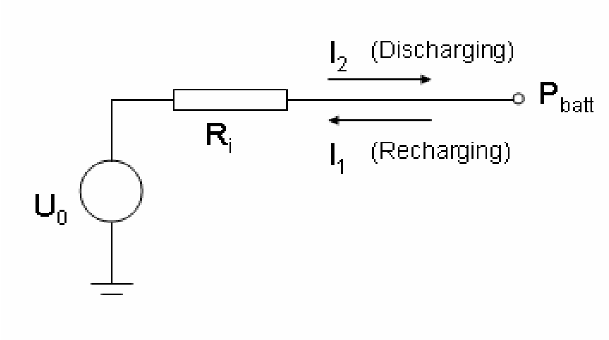

Figure 4.8 Battery Model Schematic

The battery current is then derived from power balancing equation in (4.24).

$$P_{batt} = \left(U_o - R_i \times I\right) \times I \tag{4.24}$$

$$I = \frac{U_o - \sqrt{U_o^2 - 4R_i P_{batt}}}{2R_i} \tag{4.25}$$

$$U_o = U_{o0} - U_{o1}(1 - SOC) \tag{4.26}$$

$$R_i = R_{i0} + R_{i1}(1 - SOC) \tag{4.27}$$

Where,

I	battery current in A,
P_{batt}	battery power in W,
R_i	battery internal resistance in Ω,
$R_{i0,1}$	battery internal resistance coefficients,
U_o	battery open circuit voltage in V,
$U_{o0,1}$	battery open circuit voltage coefficients.

The open circuit voltage U_o and the internal resistance R_i are functions of battery SOC. At higher SOC, the battery has larger open circuit voltage and smaller resistance. These two parameters of NiMH battery are sometimes regarded as constants since they do not change much over the full battery operating range, e.g. 50% to 80%.

4.1.4 Torque Converter (TC)

Interest in hydraulic torque converters (TCs) began in the early 1930's [106]. The primary functions of the TC include torque multiplication to provide sufficient torque during vehicle lunch and fluid damping to smooth torque fluctuations in the drivetrain. A fluid-filled three-element TC has two phases: torque multiplication phase and fluid coupling phase. The TC impeller (also referred as the TC pump) is driven by the engine and the turbine is attached to the transmission input shaft. The turbine and the stator that is connected to the TC housing via a one-way clutch are initially at rest during vehicle lunch. The turbine speed begins to increase under the angular momentum of the impeller that is transmitted through circulating fluid inside the TC. When the ratio of the turbine speed to the pump speed is low, the stator remains at rest and it redirects the fluid flowing in the same direction as the pump torque such that the resulting output torque of the TC is amplified (see Figure 4.9, the lower part). This is called the torque multiplication or torque amplification phase. At higher turbine speed, the stator rotates freely in the same direction of the pump and it is considered to consume no torque (see Figure 4.9, the upper part). Therefore, the turbine torque in this torque coupling phase is the same as the pump torque. [107]

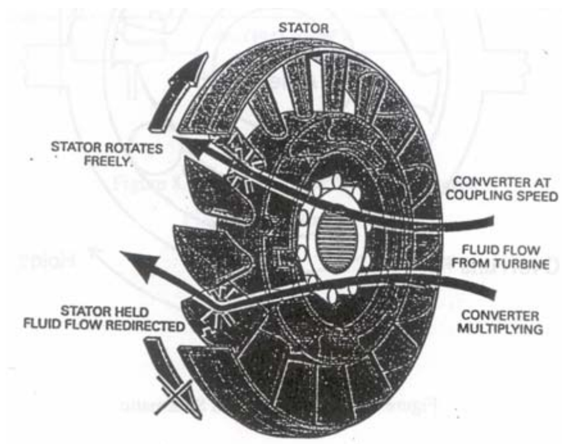

Figure 4.9 Torque converter stator operation

The TC speed ratio, torque ratio and K factor are useful to describe TC pump and turbine speeds and torques:

$$SR = \frac{\omega_t}{\omega_p} \tag{4.28}$$

$$TR = \frac{T_t}{T_p} = f_1(SR) \tag{4.29}$$

$$K = \frac{\omega_p}{\sqrt{T_p}} = f_2(SR) \tag{4.30}$$

Where

SR TC speed ratio,

TR TC torque ratio,

K TC K factor,

T_p TC pump torque in $N{\cdot}m$,

T_t TC turbine torque in $N{\cdot}m$,

ω_p TC pump speed in rad/s,

ω_t TC turbine speed in rad/s.

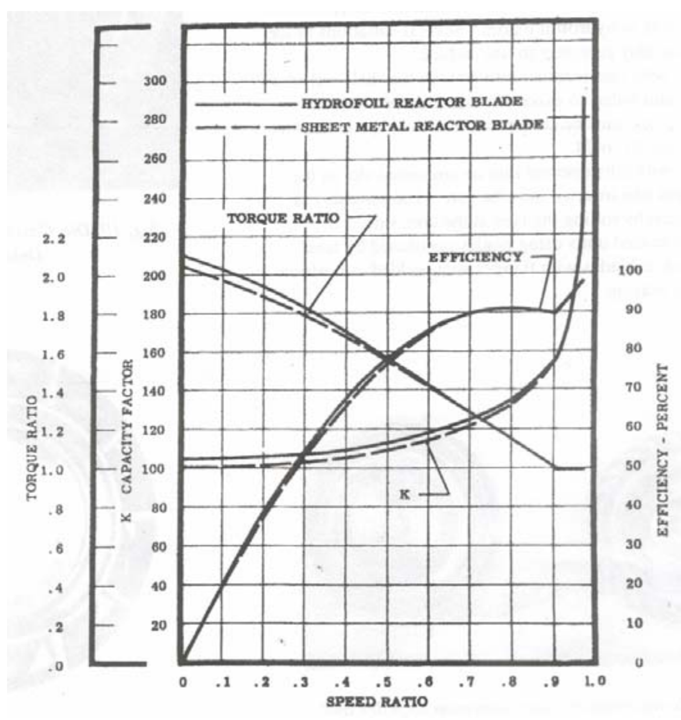

Figure 4.10 Torque converter performance curves [107]

Steady state characteristic curves of a typical TC are plotted in Figure 4.10. The non-smooth point in the torque ratio curve is the coupling point which indicts that before the speed ratio reaches this point (around 0.9), the TC is in the torque multiplication mode and after the speed ratio exceeds 0.9, the TC enters the torque coupling mode. The efficiency in the torque multiplication mode is usually less than 0.92% and that in the coupling mode is proportional to the speed ratio since the torque ratio now is 1.

The TR and the K factor curves can be used to calculate the pump torque, the turbine torque and the turbine speed by setting the pump speed equal to the engine speed.

4.1.5 Continuously Variable Transmission (CVT)

A continuously variable transmission is a stepless speed reduction device with infinite number of transmission ratios between two limits. Comparing the three types of the CVTs used in automobiles, i.e., mechanical, hydraulic and electrical, the mechanical CVT is more attractive due to its better performance on efficiency, noise level, size, weight and cost [108]. Among the mechanical CVTs, the variable pulley CVT is most commercialized than the variable stroke CVT and the traction drive CVT. The variable pulley could be rubber belt, chain or push-belt (see Figure 4.11) and the push-belt CVT accounts for the largest share of the market.

Figure 4.11 A push-belt CVT [108]

Both the V belt and the trapezoidal belt CVTs use a variator which has a primary pulley to connect the engine side and a secondary pulley attached to the downstream such as the differential. The CVT ratio can be varied by changing the radii of these two pulleys with a hydraulic control system as it is illustrated in Figure 4.12.

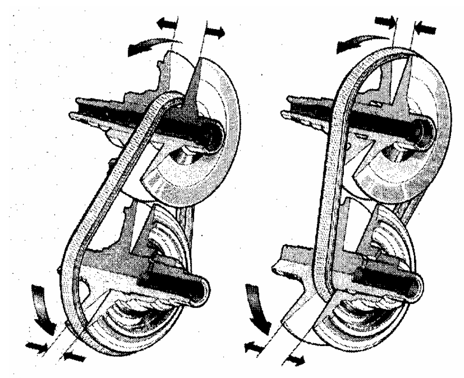

Figure 4.12 Shifting of a push-belt CVT [109]

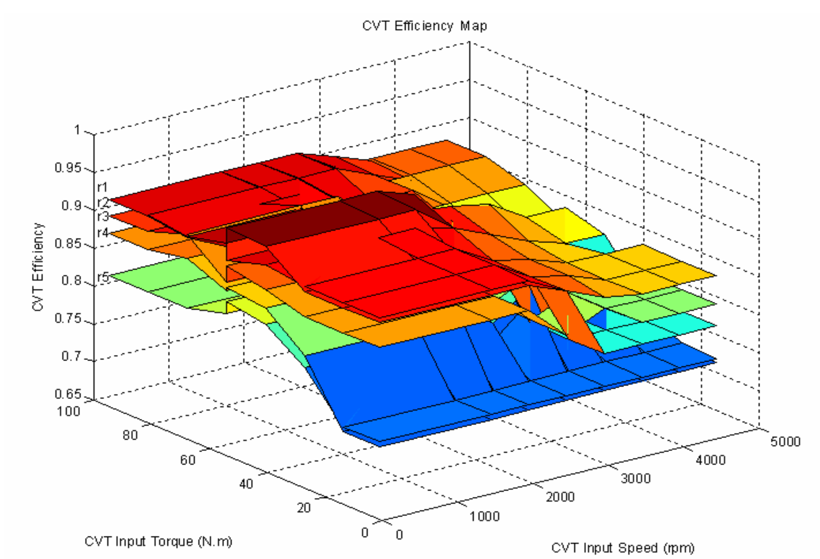

Figure 4.13 CVT efficiency map

Neglecting the dynamics, the CVT is modeled with an efficiency map with speed, torque and transmission ratio as the arguments. In Figure 4.13, the CVT has higher efficiency at lower speed, lower CVT ratio and medium torque. *r1* to *r5* represent evenly distributed CVT ratios of 0.5 to 2.5. The efficiency at any ratio in between is obtained by using linear interpolation. The efficiency of a steel-belt CVT with special oil containing rubber molecules to lock the belt with the pulley can reach 97%, similar to that of a manual transmission [110].

Compared to a drivetrain equipped with a stepped-gear transmission, the one with a CVT has better overall efficiency and driveability. A variable pulley type CVT with a metal V belt is introduced here. The input-output speed and torque are expressed as functions of the efficiency and the CVT ratio:

$$r_{cvt} = \frac{\omega_{cvt\_p}}{\omega_{cvt\_s}} \tag{4.31}$$

$$T_{cvt\_s} = \eta_{cvt} r_{cvt} T_{cvt\_p} \tag{4.32}$$

$$r_{cvt\_min} \leq r_{cvt} \leq r_{cvt\_max} \tag{4.33}$$

Where

$T_{cvt\_p,s}$ CVT primary, secondary pulley torque in $N{\cdot}m$,

r_{cvt} CVT speed ratio,

r_{cvt_max} maximum CVT speed ratio,

r_{cvt_min} minimum CVT speed ratio,

η_{cvt} CVT efficiency,

$\omega_{cvt\_p,s}$ CVT primary, secondary pulley speed in *rad/s*.

4.1.6 Final Drive (Differential)

A final drive is represented as a gear set. The ratio is defined as the final drive speed over the driveshaft speed. Efficiency of the final drive is simplified by taking a constant value:

$$r_{fd} = \frac{\omega_{cvt\_s}}{\omega_{ds}} \tag{4.34}$$

$$T_{fd} = \eta_{fd} r_{fd} T_{cvt\_s} \tag{4.35}$$

Where

T_{fd} FD torque in $N{\cdot}m$,

r_{fd} FD speed ratio,

η_{fd} FD efficiency.

ω_{ds} driveshaft speed in *rad/s*.

More accurate efficiency model of the final drive considers its efficiency as a function of operating condition, i.e., efficiency map indexed with speed and load.

4.1.7 Vehicle Longitudinal Dynamics

Vehicle dynamics are captured with Newton's second law for a longitudinal moving object. Resistance forces including aerodynamic, rolling resistance and gravity forces are expressed as follows:

$$M \cdot \frac{dV}{dt} = F_{tr} - F_a - F_r - F_g \tag{4.36}$$

$$F_a = \frac{1}{2} \rho_{air} C_d A_f V^2 \tag{4.37}$$

$$F_r = MgC_r \cos(grade) \tag{4.38}$$

$$F_g = Mg \sin(grade) \tag{4.39}$$

Where,

M	vehicle mass in *kg*,
V	vehicle velocity in *m/s*,
g	gravity acceleration in m/s^2,
$grade$	road grade,
A_f	vehicle frontal area in m^2,
C_d	drag coefficient,
C_r	rolling resistance coefficient,
F_a	aerodynamic force in *N*,
F_g	gravity force in *N*,
F_r	rolling resistance force in *N*,
ρ_{air}	air density in kg/m^3.

4.1.8 Controller

A rule-based control strategy containing five states (see Figure 4.14), i.e., stop, start, hard acceleration, hard deceleration and cruise, is used in this model. This controller sends out engine, ISA and brake torque requests together with engine ON/OFF, TC lockup and CVT ratio commands according to accelerator (α) and brake (β) pedal position, vehicle velocity and battery state of charge (SOC). The control strategy does not perform optimizations and the rules are based on simple heuristics. The model containing this simple control strategy is called the baseline vehicle and it is used as the reference for future control algorithm comparisons.

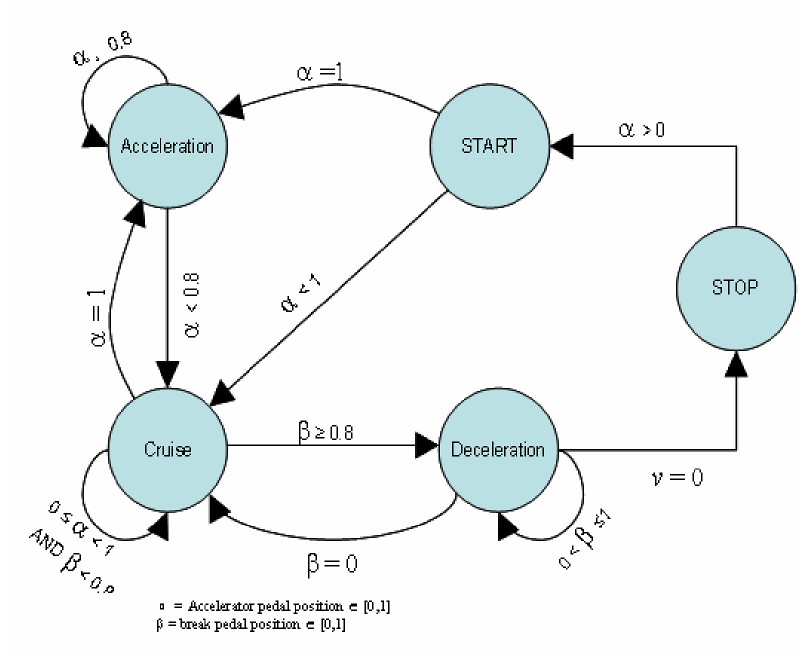

Figure 4.14 Control strategy for the baseline vehicle

4.1.9 Driver

A "Forward" simulator needs a "Driver" block to imitate a human driver generating accelerator and brake pedal commands. This is accomplished by feeding vehicle speed difference between the desired and the actual into a PID controller [18].

4.2 Drivetrain Model for Fuel Economy, Performance and Driveability Optimization

When driveability becomes one of the control criteria, the quasi-static model is obviously not sufficient to evaluate it. Dynamics of driveability are in the frequency of a few hertz in a real vehicle and thus a low-frequency dynamic model is built since it has the proper time scale. Most of the powertrain components are modeled as actuators with first or second order dynamics plus saturations and some nonlinearity. The models for the battery, the final drive, the vehicle, the controller and the driver remain the same as those used in the fuel economy optimization problem except for one of the controller output is changed from engine torque request to commanded air mass flow rate.

4.2.1 Engine

The mean-value model of an engine describes the engine behaviors in a cycle-averaged sense. Though it does not contain transient individual cylinder dynamics, the average of the engine dynamics over several cycles provides adequate low-frequency dynamic information and it is suitable for many control problems. Figure 4.15 depicts a schematic of the mean-value engine model including throttle airflow dynamics, intake manifold dynamics, fuel film dynamics, engine torque production and crankshaft dynamics. A diagram of the entire powertrain with control is shown in Figure 4.16.

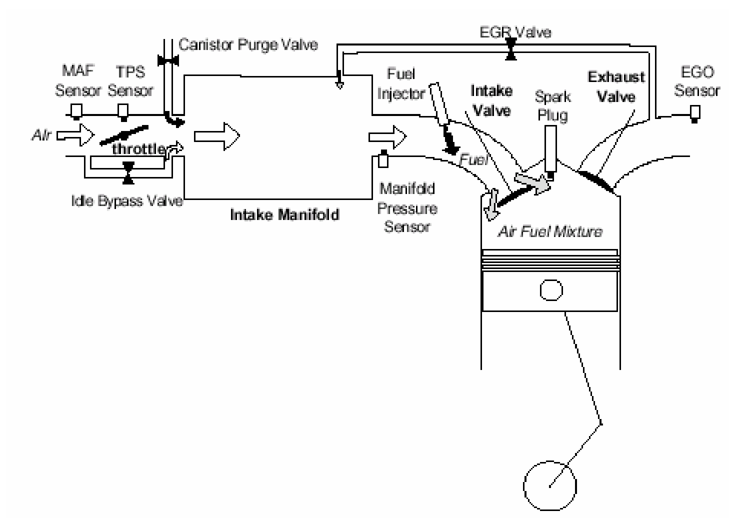

Figure 4.15 Schematic of a SI gasoline engine (after Kim [107])

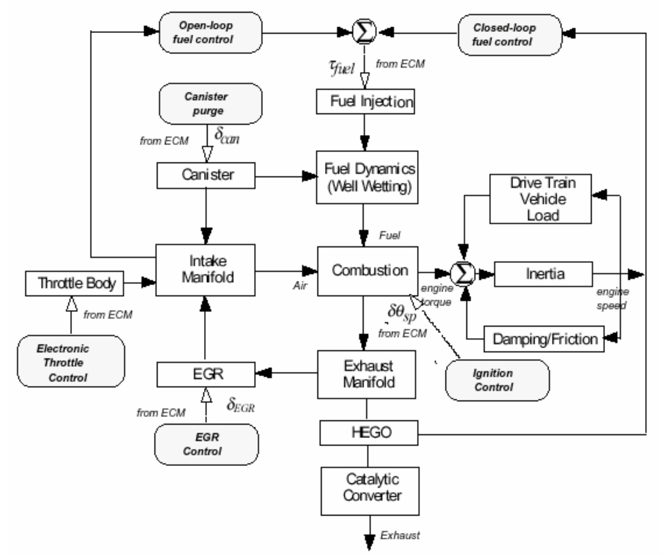

Figure 4.16 Block diagram of automotive powertrain dynamics (after Rizzoni [107])

The time domain mean-value engine model introduced in the next section assumes exhaust gas recirculation (EGR) is realized internally by variable valve timing (VVT) and spark advance (SA) remains constant in certain operating conditions (hard acceleration/deceleration and other driving conditions). Air fuel ratio (AFR) is also well maintained at stoichiometric. Therefore, this engine model is broken down into four subsystems: electronically controlled throttle body, intake manifold, combustion and crank shaft dynamics neglecting fuel dynamics.

Electronically Controlled Throttle Body (ETB)

Unlike a conventional mechanically driven throttle which has a fixed relation between accelerator pedal position and throttle valve position, an electronically controlled throttle body (ETB) has these two positions decoupled with programmable control. The ETB contains a DC motor with reduction gears and return-springs [111]. Electronic throttle control (ETC) initially found its applications in traction control and cruise control. Recent research shows that it is also useful in reducing torque oscillations and emissions, which in turn provides good fuel economy and driveability [111, 112].

Wit, Kolmanovsky and Sun have created a second order nonlinear electronic throttle model by applying dynamic LuGre model for friction torque [112]. This model is rather complicated for our purpose. Therefore, the ETB is identified as a first order system, i.e., the output air mass flow rate follows the requested input with a lag:

$$\tau_{etb} \frac{d\dot{m}_{th}}{dt} = -\dot{m}_{th} + \dot{m}_{th\_req} \tag{4.40}$$

Where,

$\dot{m}_{th}$ air mass flow rate entering the ETB in *kg/s*,

$\dot{m}_{th\_req}$ ETB air mass flow rate request in *kg/s*,

τ_{etb} ETB time constant in *s*.

The actual mass flow rate of air entering the intake manifold decreases with lower throttle and higher manifold pressure especially when the flow becomes subsonic. This is considered by setting a limit, which is apparently a function of throttle and manifold pressure (see Figure 4.17) represented by:

$$\dot{m}_{th} \le \dot{m}_{th\_limit} \tag{4.41}$$

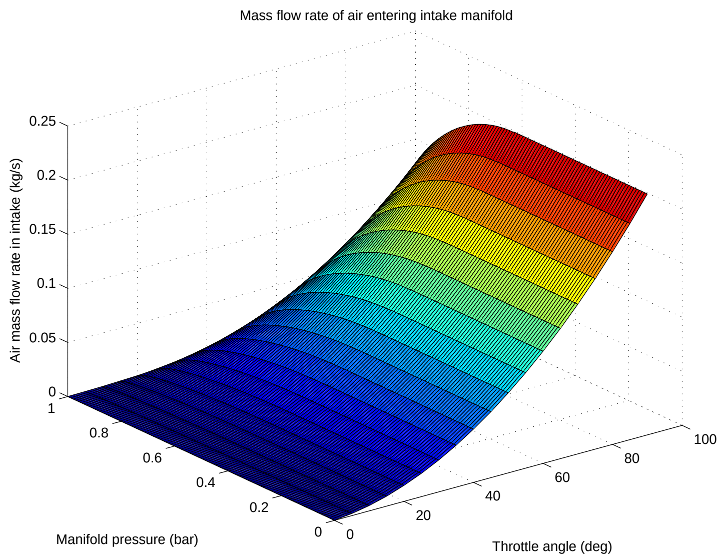

Figure 4.17 Effect of manifold pressure on intake air mass flow rate

Using the air flow instead of the throttle position makes characterizing the ETB easier, but the controller needs to know how to translate the pedal positions to the air flow command.

<u>Intake Manifold</u>

The intake manifold is the plenum between the ETB and the engine cylinders. Equation (4.42) describes a mean-value filling-and-emptying intake model based on the continuity principle and the ideal gas law [107]. The total air that goes into the cylinders is expressed in an empirical equation (4.43).

Fuel dynamics are not modeled here since engine air fuel ratio (AFR) is always well maintained at stoichiometric operating conditions. Fuel consumption is thus calculated as the total air mass flow rate entering the cylinders divided by 14.7.

$$\frac{dp_m}{dt} + \frac{R_m T_m}{V_m} \dot{m}_{cyl} = \dot{m}_{th} \frac{R_m T_m}{V_m} \tag{4.42}$$

$$\dot{m}_{cyl} = M_1 \omega_e + M_2 p_m + M_3 \omega_e p_m + M_4 \omega_e p_m^2 \tag{4.43}$$

Where,

M_1~M_4	cylinder air mass flow rate coefficients,
R_m	ideal gas constant of air in *J/(kg·k)*,
T_m	manifold temperature in *k*,
V_m	intake manifold volume in m^3,
$\dot{m}_{cyl}$	mass flow rate of air entering the cylinders in *kg/s*,
p_m	intake manifold pressure in P_a.

Combustion

Engine combustion takes air and fuel as inputs and produces torque and exhausts with losses. Torque production from combustion is usually estimated by a regression model that takes air flow, SA, AFR and engine speed into account. Since AFR is assumed to be constant in this model, its effect on produced torque is combined into T_0 term. The engine torque therefore becomes

$$T_e = T_0 + T_1 \dot{m}_{cyl}(t - t_d) / \omega_e + T_2 SA + T_3 SA^2 + T_4 \omega_e + T_5 SA\, \omega_e + T_6 \omega_e^2 \tag{4.44}$$

Where,

SA	spark advance in *deg*,
T_e	engine torque in *N·m*,
T_0 ~T_6	engine torque production coefficients,
t_d	engine torque production delay in *s*,

ω_e engine speed in *rad/s*.

T_e in equation (4.44) is the engine brake torque which considers both engine production and friction torques. Air in this equation is delayed by t_d which varies in the time domain due to varying engine speed. The engine torque is bounded by wide open throttle and minimum throttle torques according to

$$t_d = \frac{2\pi}{\omega_e} \tag{4.45}$$

$$T_{e\_\min} \le T_e \le T_{e\_\max} \tag{4.46}$$

Where,

T_{e_max} WOT engine torque in $N \cdot m$,

T_{e_min} minimum throttle engine torque in $N \cdot m$.

Crank Shaft

Crank shaft speed dynamics are intrinsically based on Newton's second law for a rotational object. The ISA torque is added into the ICE torque as the total traction torque on the engine side. T_p in equation (4.47) represents the load torque from the torque converter pump. Idle and redline are the physical speed constraints for the engine. These relationships are represented as

$$J_1 \frac{d\omega_e}{dt} = T_e + T_{isa} - T_p - B_{eng}\omega_e \tag{4.47}$$

$$idle \le \omega_e \le redline \tag{4.48}$$

Where,

idle	engine idle speed in *rad/s*,
redline	engine redline speed in *rad/s*,
B_{eng}	engine damping coefficient,
J_1	lumped inertia of engine, ISA and TC pump in $N{\cdot}m{\cdot}s^2/rad$,
T_{isa}	ISA torque in $N{\cdot}m$,
T_p	TC pump toque in $N{\cdot}m$.

4.2.2 Integrated Starter/Alternator (ISA)

High-order electric machine model [4] is excessively complex for describing driveability. Therefore, simplified models of ISA and power electronics are lumped together as one single model. The ISA is described as a first-order system. Equations (4.49) to (4.51) characterize the ISA dynamics and its physical limitations:

$$\tau_{isa} \frac{dT_{isa}}{dt} = -T_{isa} + T_{isa\_req} \tag{4.49}$$

$$T_{isa\_\min} \le T_{isa} \le T_{isa\_\max} \tag{4.50}$$

$$\omega_{isa\_\min} \le \omega_{isa} \le \omega_{isa\_\max} \tag{4.51}$$

Where,

T_{isa_max}	maximum ISA torque in $N{\cdot}m$,
T_{isa_max}	minimum ISA torque in $N{\cdot}m$,
T_{isa_req}	ISA torque request in $N{\cdot}m$,
η	lumped ISA, power electronics and battery efficiency,
τ_{isa}	ISA time constant in *s*,
ω_{isa}	ISA speed in *rad/s*,
ω_{isa_max}	maximum ISA speed in *rad/s*,

ω_{isa_max} minimum ISA speed in *rad/s*.

4.2.3 Torque Converter

Torque converters (TCs) act as hydraulic dampers to interrupt vibration propagation originated from either engines or road bumps and to provide torque multiplication during vehicle launch [12]. Since the TC is essentially a damper, losses are not negligible. However, these losses can be reduced by employing a TC bypass clutch, which mechanically connects the TC pump and the turbine when the clutch is engaged. This connection improves TC efficiency at the price of losing the capability to absorb oscillations in the drivetrain. A compromising solution is proposed by Hiramatsu et al., allowing 1 to 2 % of clutch slip to achieve similar results as the TC is working as a damper [112, 113]. Obviously, people desire to minimize this slip for efficiency consideration. This type of bypass clutch is a so-called minimal slip-type TC clutch.

The torque converter is expressed with a regression model based on Kotwicki's research of more than twenty years ago [12]. In this model, there are three modes in the forward drive case (power is flowing from the engine to the wheels) and two modes in the backward drive case (overrun case), shown in equations (4.52) to (4.57).

***FORWARD*:** ($\omega_p > \omega_t$)

Torque multiplication mode: ($T_t > T_p$)

$$T_p = b_1\omega_p^2 + b_2\omega_p\omega_t + b_3\omega_t^2 \tag{4.52}$$

$$T_t = c_1\omega_p^2 + c_2\omega_p\omega_t + c_3\omega_t^2 \tag{4.53}$$

Torque coupling mode: ($T_t = T_p$)

$$T_p = T_t = a_1\omega_p^2 + a_2\omega_p\omega_t + a_3\omega_t^2 \tag{4.54}$$

Lockup mode:

$$\omega_p \approx \omega_t \tag{4.55}$$

$$T_p = T_t \leq T_{clutch\_\max} \tag{4.56}$$

***BACKWARD (overrun)*:** ($\omega_t > \omega_p$)

Torque coupling mode: ($T_t = T_p$)

$$T_t = T_p = d_1\omega_p^2 + d_2\omega_p\omega_t + d_3\omega_t^2 \tag{4.57}$$

Lockup mode: the same as in the forward drive case.

Where,

T_{clutch_max}	maximum torque converter clutch torque in *N·m*,
T_t	TC turbine toque in *N·m*,
$a_1 \sim d_3$	TC pump/turbine torque coefficients,
ω_p	TC pump speed in *rad/s*,
ω_t	TC turbine speed in *rad/s*.

As shown in Figure 4.18, this TC has the maximum torque ratio (turbine torque over pump torque) of about 1.65 and the coupling point at the speed ratio (turbine speed over pump speed) of 0.88. Its efficiency before the coupling point is lower than 90 % and that in the lockup mode is around 99 %.

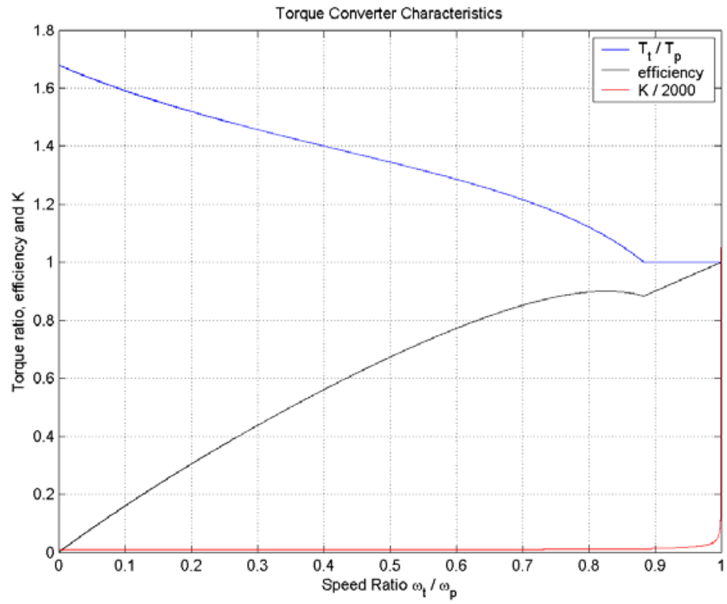

Figure 4.18 Torque converter characteristics

4.2.4 Continuously Variable Transmission (CVT)

The CVT ratio is controlled by changing the radii of the primary and the secondary pulleys with a hydraulic control system and it behaves close to a first order system. In addition to equations (4.58) to (4.60), the following equations summarized the dynamic CVT model:

$$\tau_{cvt}\frac{dr_{cvt}}{dt}+r_{cvt}=r_{cvt\_req} \tag{4.58}$$

$$J_2\frac{d\omega_t}{dt}=T_t-T_{cvt\_p} \tag{4.59}$$

$$J_3\frac{d\omega_{cvt\_s}}{dt}=T_{cvt\_s}-T_{fd} \tag{4.60}$$

Where

J_2 lumped inertia of TC turbine and CVT primary pulley in $N{\cdot}m{\cdot}s^2/rad$,

J_3 lumped inertia of CVT secondary pulley, final drive and wheels in $N{\cdot}m{\cdot}s^2/rad$,

T_{cvt_p} CVT primary pulley torque in $N{\cdot}m$,

T_{cvt_s} CVT secondary pulley torque in $N{\cdot}m$,

T_{fd} final drive torque in $N{\cdot}m$,

r_{cvt} CVT speed ratio,

r_{cvt_req} CVT speed ratio request,

τ_{cvt} CVT time constant in s,

ω_{cvt_s} CVT secondary pulley speed in rad/s,

ω_t torque converter turbine speed in rad/s.

4.2.5 Driveshaft

Shaft flexibility is modeled as lumped compliance, which is helpful in absorbing oscillations in the drivetrain. The nonlinear damper is characterized as a function of driveshaft speed and its square:

$$\frac{dT_{wh}}{dt} = K_{ds}\left(\omega_{ds} - \omega_{wh}\right) \tag{4.61}$$

$$T_{fd} = T_{wh} + D_1\omega_{ds} + D_2\omega_{ds}^{\ 2} \tag{4.62}$$

Where,

D_1 linear coefficient of driveshaft nonlinear damper,

D_2 quadratic coefficient of driveshaft nonlinear damper,

K_{ds} lumped driveshaft compliance in $N{\cdot}m/rad$,

T_{wh} wheel torque in $N{\cdot}m$,

ω_{wh} wheel speed in rad/s.

4.2.6 Brake-By-Wire (BBW)

Brake-by-wire (BBW) systems were initially designed for aircrafts and now are in many production vehicles on the market, such as Mercedes-Benz SL500 cars [114]. In a vehicle incorporating a BBW, a driver's braking intention is transmitted electronically from the brake pedal to electro-hydraulic or electro-mechanic brake actuators located at each wheel [114, 115]. Simple structure and cheap realization with easy adaptation to other systems like anti-lock brake system (ABS) via software will enable BBWs to be utilized into more and more mass production vehicles.

Equation (4.63) describes the first order behavior of a BBW driven by a motor:

$$\tau_{brk}\frac{dT_{brk}}{dt} = -T_{brk} + T_{brk\_req} \tag{4.63}$$

$$F_{tr} = \frac{T_{wh} - T_{brk}}{R_{wh}} \tag{4.64}$$

Where,

F_{tr} total traction force in N,

R_{wh} wheel radius in m,

T_{brk}: brake torque in $N \cdot m$,

T_{brk_req} brake torque request in $N \cdot m$,

τ_{brk} BBW time constant in s.

4.3 Summary

This chapter introduces a quasi-static model and a low-frequency dynamic model to be used for optimal control strategy development. The quasi-static model focuses on describing power losses of each component in the HEV drivetrain to estimate fuel economy. Therefore, this model does not contain dynamics except for the vehicle subsystem. In contrast to the quasi-static model, the low-frequency dynamic model has ten states and six inputs, modeling powertrain components as low-order actuators with saturations and nonlinearity.

Both models are implemented in MATLAB®/SIMULINK® and tested with various driving cycles. The simulation results in Appendix B demonstrate that the quasi-static model is adequate to estimate fuel economy and performance, and the low-frequency dynamic model is sufficient to evaluate vehicle driveability.

CHAPTER 5

CONTROL STRATEGY DEVELOPMENT

The supervisory control strategy in a parallel HEV contains energy management rules to split power requirements between the engine and the electric machine as well as to determine the transmission gear ratio. As shown in Figure 5.1, the optimal control strategy is developed in two steps: optimizing fuel economy and performance first and then taking vehicle driveability into consideration.

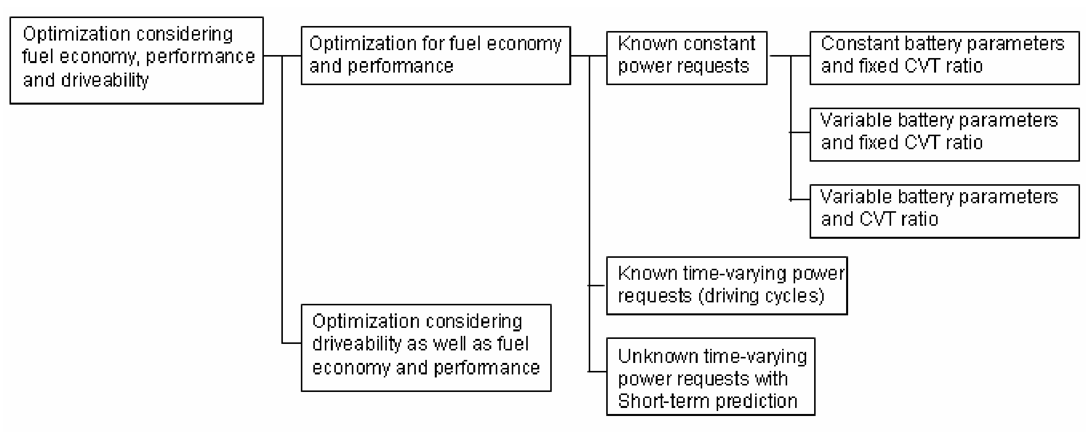

Figure 5.1 Optimal control solving procedure

There exist three steps in finding optimal control strategy for best fuel economy. First, defining the battery state of charge as the state variable and the engine torque as the control variable, optimal control is found for constant power requests. The solution is then extended for known time-varying power requirements, such as official driving cycles and user-defined maneuvers. Finally, optimal control is found for the case with predicted driving conditions of a few minutes ahead. Except for the case with constant power requests where solutions for both constant and variable battery parameter are found, other cases with time-varying and unknown driving conditions only consider variable battery parameters. The CVT ratio is fixed only in the first two cases for constant power requests. In all other cases, the CVT ratio is one of the control variables to be found to achieve the optimal fuel economy.

The optimal control strategy is developed using Pontryagin's minimum principle based on the control oriented models introduced in Chapter 4. Since the minimum principle only provides necessary condition for finding finite number of (or unique) optimal control solutions, the control candidates obtained by setting the derivative of the Hamiltonian with respect to the control variable to zero need to be compared with the control boundary values when the control variable is bounded. The control which leads to the minimum Hamiltonian is the actual solution. If the Hamiltonian is not a smooth function, all the non-smooth points must also be considered as control candidates as well. If none of the control candidates satisfies the state boundary conditions, the solution could result from switching between two candidates such that the equivalent control satisfies the boundary conditions, as the equivalent Hamiltonian would still remain at the minimum. The optimal control that switches between two values is referred to as sliding optimal control. Two motivating examples introduced below illustrate the existence of the sliding optimal control and the significance of the switching frequency.

Example #1: Time Optimal Control Problem

The system contains two states x_1, x_2 and one control variable u:

$$\begin{cases} \dot{x}_1 = -u^2 + x_2^2 \\ \dot{x}_2 = -u \end{cases} \tag{5.1}$$

The control constraint and the state boundary conditions are

$$|u| \leq 1 \tag{5.2}$$

$$x_1(t_0) \geq x_2(t_0) > 0 \tag{5.3}$$

$$x_1(t_f) = 0, x_2(t_f) = 0 \tag{5.4}$$

A time optimal control is defined with the cost function of

$$J = \int_{t_0}^{t_f} 1 \cdot dt \tag{5.5}$$

Where,

J	cost function,
t	time in s,
u	control variable,
t_0	initial time,
t_f	final time,
$x_{1,2}$	system states.

Intuitively, the cost function is minimized when both x_1 and x_2 decrease at the maximum speed, i.e., $\dot{x}_1$ and $\dot{x}_2$ are as negative as possible. If the control variable u is 1,

x_2 will decrease at the maximum rate and so will x_1 since both $(-\,u^2)$ and (x_2^2) are minimized. After x_2 reaches zero, one still wishes to keep $-\,u^2+x_2^2$ at the minimum in order to decrease x_1 as fast as possible. Thus the optimal control should maximize the absolute value of u and minimize the absolute value of x_2. To maintain x_2 at zero the control u should take values of 1 and -1 alternatively, as if it is dynamically equivalent to zero. This control is called sliding optimal control. The control and state trajectories of this system are shown in Figure 5.2 and Figure 5.3 respectively.

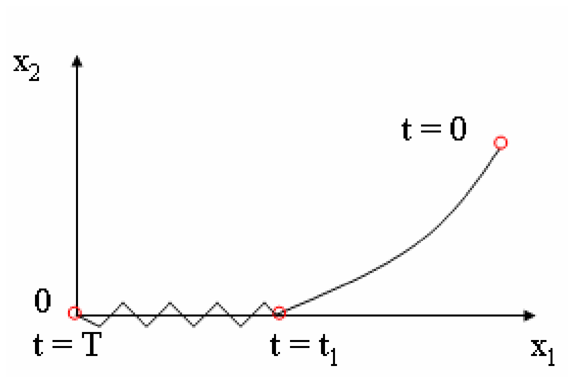

Figure 5.2 Example #1: state trajectory under sliding optimal control

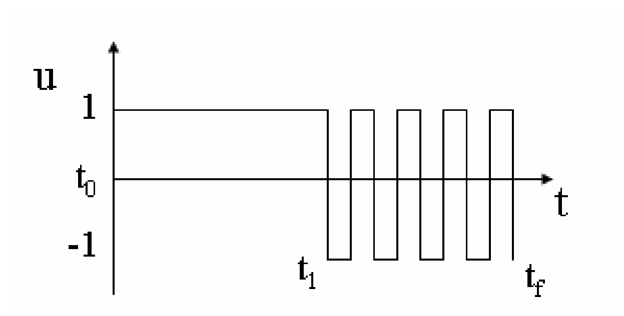

Figure 5.3 Example #1: sliding optimal control trajectory

Switching frequency in this sliding optimal control system is critical. The maximum rate of decrease of x_1 can be maintained only if the value of x_2 is strictly held to zero. Keeping x_2 very near to zero requires the control, u, to spend a very small amount of time at each of its two levels (1 and -1) before switching to the other level. When in switching mode, asymptotically decreasing the maximum absolute value of x_2 to zero requires the asymptotically decrease the time spent at each control level. As this time asymptotically approaches zero, the switching frequency approaches infinity. Practically, the switching frequency of a real system will be bounded at some maximum value and thus the optimal control does not exist for the real system.

Example #2: Control Effort Optimization

System equation in state space format is

$$\dot{x} = u \tag{5.6}$$

The boundary conditions of the state are

$$x(0) = 0, x(2) = 1 \tag{5.7}$$

The cost function is given as

$$J = \int_0^2 u^2 \cdot (1-u)^2 \, dt \tag{5.8}$$

According to Pontryagin's minimum principle, the Hamiltonian and the differential equation of the co-state variable λ are

$$H = u^2 \cdot (1-u)^2 + \lambda \cdot u = u^4 - 2u^3 + u^2 + \lambda \cdot u \tag{5.9}$$

$$\dot{\lambda} = -\frac{\partial H}{\partial x} = 0 \tag{5.10}$$

Where,

H Hamiltonian,

λ Lagrange multiplier, the co-state variable.

Since the co-state variable λ is constant and the Hamiltonian only depends on u and λ, the optimal control is constant as well and it can be calculated by using state boundary conditions as follows:

$$u = \frac{x(2) - x(0)}{2 - 0} = \frac{1}{2} \tag{5.11}$$

The cost with this constant control is then calculated using equation (5.8):

$$J = \int_0^2 u^2 \cdot (1-u)^2 \, dt = \int_0^2 \frac{1}{4} \cdot \frac{1}{4} dt = \frac{1}{8} \tag{5.12}$$

If the control variable switches between 0 and 1 such that the state boundary conditions are still satisfied, the cost will be reduced to the minimum value, i.e., zero. This result does not violate Pontryagin's minimum principle even though it does not match the conventional solution. Selecting $\lambda = 0$ in equation (5.9) results in equation (5.13) which has 3 roots: 0, 0.5 and 1.

$$\frac{\partial H}{\partial u} = 4u^3 - 6u^2 + 2u = 0 \tag{5.13}$$

Figure 5.4 shows a plot of $H(u)|_{\lambda=0}$ where 0 and 1 correspond to local minima and 0.5 is a local maximum.

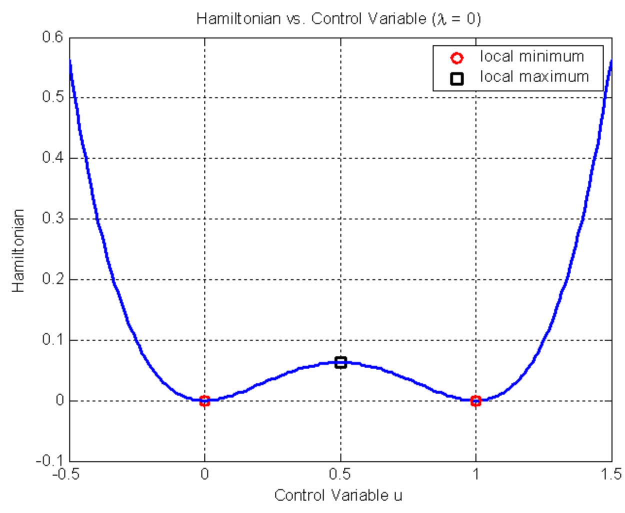

Figure 5.4 Example #2: Hamiltonian versus control variable

(sliding optimal control exists: $u_1 = 0$, $u_2 = 1$ when $\lambda = 0$)

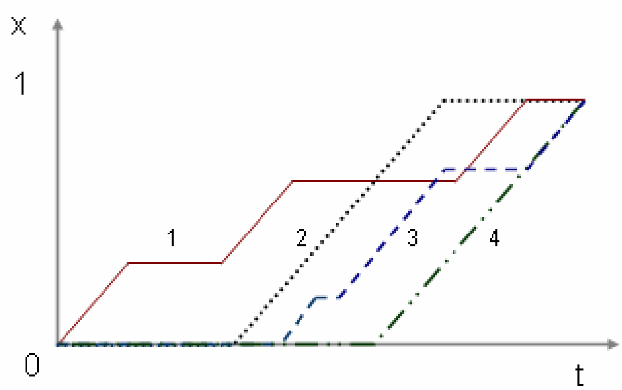

Figure 5.5 Example #2: state trajectories under sliding optimal control

In contrast to the conventional solution that takes one root, the sliding optimal control takes two alternatively because when acting alone neither one can satisfy the state boundary conditions. It is evident that the switching frequency in this system has no effect on the cost function since either 0 or 1 result in zero-cost. State trajectories shown in Figure 5.5 all have the same cost. In this case, there are an infinite number of optimal control solutions. The control which switches finite times is also referred to as the sliding optimal control.

5.1 Optimal Control for Best Fuel Economy

There exist operating conditions for which a proper optimization problem cannot be formulated. For instance, when the speed requirement at the engine shaft is outside the ICE operating region, the ICE has to shut down and the ISA (and the BBW) is used to meet the positive (or negative) torque requirement. Another example says if the torque requirement exceeds the sum of the ICE and the ISA torque limits, both of them need to produce the maximum torques since meeting the torque command has the highest priority. Therefore, optimization in splitting the ICE and the ISA torques is needed only if the speed and the torque requests are both within their physical limitations. When the torque requirement is negative, the ICE is ON only when shutting down the engine will result in restarting the engine immediately, i.e., the engine remaining in the stop mode is too short such that the benefits of fuel saving is less than the driveability degradation due to engine start-stop. The brake is activated only when the ICE and the ISA cannot meet the negative torque requests. All of these comments are valid only if the battery SOC is within its preferred operating region. The actual ISA torque command needs to be adjusted according to the actual battery SOC.

Torque and Speed Requirements	Control Strategy
ω_{req} < idle or ω_{req} > redline $T_{req} \geq 0$	ICE is OFF; ISA is ON $T_{em\_com} = \min(T_{req} - T_{ice\_friction}, T_{em\_max})$
ω_{req} < idle or ω_{req} > redline $T_{req} < 0$	ICE is OFF; ISA (and BBW) is ON $T_{em\_com} = \max(T_{req} - T_{ice\_friction}, T_{em\_min})$; $T_{BBW\_com} = T_{req} - T_{em\_com}$
idle $\leq \omega_{req} \leq$ redline $0 < T_{ice\_max} + T_{em\_max} \leq T_{req}$	ICE and ISA are ON $T_{ice\_com} = T_{ice\_max}$; $T_{em\_com} = T_{em\_max}$
idle $\leq \omega_{req} \leq$ redline $0 < T_{req} < T_{ice\_max} + T_{em\_max}$	ICE or ISA or both are ON Optimal torque splitting between the ICE and the ISA $T_{ice\_com} + T_{em\_com} = T_{req}$
idle $\leq \omega_{req} \leq$ redline $T_{ice\_min} < T_{req} \leq 0$	If ICE is ON: $T_{ice\_com} = T_{req} - T_{ice\_friction}$ If ICE is OFF, ISA is ON: $T_{em\_com} = T_{req} - T_{ice\_friction}$
idle $\leq \omega_{req} \leq$ redline $T_{ice\_min} + T_{em\_min} \leq T_{req} < T_{ice\_min}$	If ICE is ON: $T_{ice\_com} = T_{ice\_friction}$; $T_{em\_com} = \max(T_{req} - T_{ice\_com}, T_{em\_min})$ If ICE is OFF, ISA or BBW is ON: $T_{em\_com} = \max(T_{req} - T_{ice\_friction}, T_{em\_min})$; $T_{BBW\_com} = T_{req} - T_{em\_com}$
idle $\leq \omega_{req} \leq$ redline $T_{req} < T_{ice\_min} + T_{em\_min}$	ICE is OFF, ISA and BBW is ON: $T_{em\_com} = \max(T_{req} - T_{ice\_friction}, T_{em\_min})$; $T_{BBW\_com} = T_{req} - T_{em\_com}$

Table 5.1 Control Strategies for Different Torque and Speed Requirements

Table 5.1 lists the supervisory control rules for all commanded speed and torque cases at the engine shaft. The general rules are as follows:

- The vehicle needs to meet the power request whenever possible and optimality is sacrificed if the power request is not met
- The supervisory control strategy optimizes the power split between two energy sources to achieve minimum fuel consumption
- The BBW is used only if the engine and the ISA cannot provide all the commanded negative torque

The rest of this chapter focuses on the optimal control strategy development, i.e., the 4th case in the above table. In all other driving conditions except for the 4th case, the control strategy listed in Table 5.1 is taken.

The optimal control solution found for minimum fuel consumption is based on the HEV fuel economy optimization model introduced in Chapter 4.1. The solution considers the battery model with constant open circuit voltage and internal resistance first and then uses the model with variable battery parameters.

5.1.1 Control Problem Formulation

Problem Statement

Torques from the engine and the electric machine must be allocated so as to minimize fuel consumption while meeting the power demand for some finite period of time. The vehicle must be charge sustaining over the cycle and the battery state of charge (SOC) must remain within a predefined operating range.

Problem Formulation

The cost function is then defined as the total fuel consumption of the trip:

$$J = \int_{t_0}^{t_f} \dot{m}_f \, dt \tag{5.14}$$

Since the vehicle is charge sustaining, the battery SOC before and after the trip should be equal. This requirement is necessary to maintain the vehicle charge sustaining. However, it never happens in practice. The battery SOC also needs to stay within a predefined operating range to avoid any damage to the battery.

$$S(t_f) = S(t_0) \tag{5.15}$$

$$S_{min} \le S \le S_{max} \tag{5.16}$$

Where,

J	cost function or criteria,
S	battery state of charge,
S_{max}	battery state of charge upper limit,
S_{max}	battery state of charge lower limit,
$\dot{m}_f$	mass flow rate of fuel in *kg/s*,
t_0	initial time in *s*,
t_f	final time in *s*.

5.1.2 Optimal Control for Constant Power Requirement

In addition to enabling regenerative braking and coordinating the engine and the electric machine to operate efficiently, some control strategies use engine start-stop to further reduce fuel consumption and emissions. Typically, control strategies propose to stop the engine at low speeds or during decelerations. New investigations have shown that engine start-stop can improve fuel economy even when the vehicle speed remains constant. This engine start-stop strategy is called sliding optimal control. Theoretical proof of the optimality of the sliding optimal control in hybrid electric vehicle with constant battery parameters (the open circuit voltage and internal resistance) is introduced with Pontryagin's minimum principle. The optimal control solution becomes step-wise continuous when battery parameters depend on battery SOC. The CVT ratio is first considered as fixed to find the optimal solution for the cases with constant and variable battery parameters and then it is considered as one of the free selected control variables in the optimization.

<u>Solution Existence</u>

There exist at least two control trajectories which lead the battery SOC to change from its initial value to its desired final value, so that the optimal control solution exists.

However, this does not guarantee the solution will be found by using the minimum principle.

Solution for HEV with Constant Battery Parameters

The control solution found in this section considers the battery open circuit voltage and internal resistance as constants as shown below:

$$U_o = U_{o0} \tag{5.17}$$

$$R_i = R_{i0} \tag{5.18}$$

Where,

R_i	battery internal resistance in Ω,
R_{i0}	battery internal resistance constant coefficient,
U_o	battery open circuit voltage in V,
U_{o0}	battery open circuit voltage constant coefficient.

Conventional Solution

Defining the engine power, P_{ice}, as the control variable and the battery SOC as the system state, the time trajectories of the engine and the electric machine torques must be determined for this bounded-state, bounded-control system. Due to the fact that the speed request is constant, the optimal engine torque is obtained by dividing the optimal engine power with the constant desired speed as

$$T_{ice} = \frac{P_{ice}}{\omega_{req}} \tag{5.19}$$

Meeting the power/torque requirement has the highest priority, so the sum of the engine power and the electric machine power should be equal to the power request whenever possible.

$$P_{ice} + P_{em} = P_{req}, \quad (0 \le P_{ice} \le P_{ice\_max}) \tag{5.20}$$

When P_{req} is negative or ω_{req} at the engine shaft is lower than engine idle speed, there is no optimization problem and the electric machine should work alone. The solution introduced in this section is only for positive P_{req} and ω_{req} greater than idle.

The cost function in equation (5.14) is modified to take the battery SOC constraint into consideration:

$$J = \int_{t_0}^{t_f} \left[\dot{m}_f + \gamma_1 (S - S_{max}) sg(S - S_{max}) + \gamma_2 (S_{min} - S) sg(S_{min} - S) \right] dt \tag{5.21}$$

$$sg(\alpha) = \begin{cases} 1, & \alpha > 0 \\ 0, & \alpha < 0 \end{cases} \tag{5.22}$$

Where,

S battery state of charge,
P_{em} electric machine power in W,
P_{ice} engine power in W,
P_{ice_max} maximum engine power in W,
P_{req} total power request at the engine shaft in W,
T_{ice} engine torque in $N{\cdot}m$,
$\gamma_{1,2}$ weighting coefficients,
ω_{req} speed request at the engine shaft in rad/s,
$\dot{m}_f$ engine mass flow rate of fuel in kg/s.

The penalty function of the SOC in equation (5.21) is only activated when the SOC runs outside of its limits and the penalty is proportional to how much the actual SOC exceeds the limits. The parameters γ_1 and γ_2 are selected to be very high such that the duration of the state staying in its prohibited regions is very short. Since there is no penalty if the SOC remains between its upper and lower limits, the vehicle can make full use of the battery over the allowable range.

The Hamiltonian of this optimization problem is rewritten as

$$H = \dot{m}_f + \gamma_1 (S - S_{max}) sg(S - S_{max}) + \gamma_2 (S_{min} - S) sg(S_{min} - S) - \lambda \frac{I}{Q_{batt}} \tag{5.23}$$

According to Pontryagin's minimum principle,

$$\dot{S} = \frac{\partial H}{\partial \lambda} = -\frac{I}{Q_{batt}} = -\frac{1}{2R_i \cdot Q_{batt}} \cdot \begin{cases} \left(U_o - \sqrt{U_o^2 - 4R_i \cdot (P_{req} - P_{ice}) / \eta_{em}}\right), & \textit{(discharging)} \\ \left(U_o - \sqrt{U_o^2 - 4R_i \cdot (P_{req} - P_{ice}) \cdot \eta_{em}}\right), & (\textit{recharging}) \end{cases} \tag{5.24}$$

$$\dot{\lambda} = -\frac{\partial H}{\partial S} = \begin{cases} \gamma_2, & S < S_{min} \\ 0, & S_{min} < S < S_{max} \\ -\gamma_1, & S > S_{max} \end{cases} \tag{5.25}$$

Where,

I	electric machine current in A,
Q_{batt}	battery capacity in C,
R_i	battery internal resistance in Ω,
U_o	battery open circuit voltage in V,
η_{em}	electric machine efficiency.

When the battery SOC stays within the limits, the co-state variable λ is constant. The optimal control should be constant as well because the Hamiltonian only depends on λ and the control variable P_{ice} as represented below:

$$H = \frac{\left(P_{ice} + P_{ml}\right)}{e \cdot H_v} - \frac{\lambda}{2R_i \cdot Q_{batt}} \cdot \begin{cases} \left(U_o - \sqrt{U_o^2 - 4R_i \cdot (P_{req} - P_{ice}) / \eta_{\mathrm{em}}}\right), & \text{(discharging)} \\ \left(U_o - \sqrt{U_o^2 - 4R_i \cdot (P_{req} - P_{ice}) \cdot \eta_{\mathrm{em}}}\right), & \text{(recharging)} \end{cases} \tag{5.26}$$

Where,

e	intrinsic engine energy conversion efficiency excluding transferring losses,
H_v	lower heating value of fuel in J,
P_{ml}	mean friction pressure in P_a.

The mean friction pressure P_{ml} in equation (5.26) is zero at zero engine power P_{ice}, indicating there is no friction when the engine is shut down and the clutch is disengaged.

Therefore, the optimal control is found by using the state boundary conditions.

$$P_{ice} = P_{req} = constant \tag{5.27}$$

The battery SOC constraint is obviously satisfied under this constant control since the electric machine has never been used. The fuel consumption in this case is

$$m_f = \frac{\left(P_{req} + P_{ml}\right) \cdot t_f}{e \cdot H_v} \tag{5.28}$$

Sliding Optimal Control

Since Pontryagin's minimum principle only provides necessary condition, the above solution may not be the optimal one. The two examples shown in the beginning of this chapter suggest checks for the existence of the sliding optimal control in this problem. The Hamiltonian in equation (5.26) is not smooth; it contains three segments corresponding to $P_{ice} = 0$, $0 < P_{ice} \le P_{req}$ and $P_{req} < P_{ice} \le P_{ice\_max}$.

When $P_{ice} = 0$, the fuel consumption is zero and the Hamiltonian is

$$H = -\frac{\lambda}{2R_i \cdot Q_{batt}} \cdot \left(U_o - \sqrt{U_o^2 - 4R_i \cdot P_{req} / \eta_{\mathrm{em}}} \right) \tag{5.29}$$

When $0 < P_{ice} \leq P_{req}$, the EM is in discharging mode and the Hamiltonian is

$$H = \frac{\left(P_{ice} + P_{ml0}\right)}{e \cdot H_v} - \frac{\lambda}{2R_i \cdot Q_{batt}} \cdot \left(U_o - \sqrt{U_o^2 - 4R_i \cdot (P_{req} - P_{ice}) / \eta_{\mathrm{em}}} \right) \tag{5.30}$$

When $P_{req} < P_{ice} \leq P_{ice\_max}$, the EM is in recharging mode and the Hamiltonian is

$$H = \frac{\left(P_{ice} + P_{ml0}\right)}{e \cdot H_v} - \frac{\lambda}{2R_i \cdot Q_{batt}} \cdot \left(U_o - \sqrt{U_o^2 - 4R_i \cdot (P_{req} - P_{ice}) \cdot \eta_{\mathrm{em}}} \right) \tag{5.31}$$

In order to analyze the characteristics of the Hamiltonian function, the first and the second derivatives of the Hamiltonian are calculated as follows:

$$\frac{\partial H}{\partial P_{ice}} = \frac{1}{e \cdot H_v} + \frac{\lambda}{Q_{batt}} \cdot \begin{cases} \dfrac{1/\eta_{\mathrm{em}}}{\sqrt{U_o^2 - 4R_i \cdot (P_{req} - P_{ice}) / \eta_{\mathrm{em}}}}, & \textit{(discharging)} \\[2ex] \dfrac{\eta_{\mathrm{em}}}{\sqrt{U_o^2 - 4R_i \cdot (P_{req} - P_{ice}) \cdot \eta_{\mathrm{em}}}}, & \textit{(recharging)} \end{cases} \tag{5.32}$$

$$\frac{\partial^2 H}{\partial P_{ice}{}^2} = -\frac{2\lambda \cdot R_i}{Q_{batt}} \cdot \begin{cases} \dfrac{1/\eta_{\mathrm{em}}{}^2}{\left(U_o^2 - 4R_i \cdot (P_{req} - P_{ice}) / \eta_{\mathrm{em}}\right)^{\frac{3}{2}}}, & \textit{(discharging)} \\[2ex] \dfrac{\eta_{\mathrm{em}}{}^2}{\left(U_o^2 - 4R_i \cdot (P_{req} - P_{ice}) \cdot \eta_{\mathrm{em}}\right)^{\frac{3}{2}}}, & \textit{(recharging)} \end{cases} \tag{5.33}$$

The first derivative of Hamiltonian $\partial H / \partial P_{ice}$ in equation (5.32) has two terms: the first one is always positive and the second one has the same sign as the co-state variable λ for both discharging and recharging cases. If λ is negative, there exists the possibility of having $\partial H / \partial P_{ice}$ to change from negative to positive when P_{ice} increases from 0 to P_{ice_max}. The second derivative $\partial^2 H / \partial P_{ice}^2$ is positive for any negative λ, implying that the Hamiltonian is concave except for the point where $P_{ice} = 0$. With a negative λ, the Hamiltonian starts at a positive value for $P_{ice} = 0$ (since P_{req} is non-negative) and then jumps up when P_{ice} is slightly increased from zero. Subsequently, the Hamiltonian first decreases and then increases with increasing P_{ice} if $\partial H / \partial P_{ice}$ changes from negative to positive. Therefore, finding sliding optimal control becomes solving for a negative λ such that there exist two P_{ice} which have the same minimum Hamiltonian. One is at $P_{ice1} = 0$ and the other one is found from below:

$$\frac{\partial H}{\partial P_{ice}} = \frac{1}{e \cdot H_v} + \frac{\lambda}{Q_{batt}} \cdot \frac{\eta_{\mathrm{em}}}{\sqrt{U_o^2 - 4R_i \cdot (P_{req} - P_{ice}) \cdot \eta_{\mathrm{em}}}} = 0 \tag{5.34}$$

For any positive and some negative λ that gives only positive or negative $\partial H / \partial P_{ice}$, it is obviously impossible to find two minimum Hamiltonian points and thus sliding optimal control does not exist.

The reason that only the recharging mode is considered in equation (5.34) is because the battery is discharged when $P_{ice1} = 0$ and it has to be recharged if the vehicle is charge sustaining. The second switching point P_{ice2} is then solved from the above equation:

$$P_{ice2} = P_{req} - \frac{U_0^2}{4R_i \cdot \eta_{em}} + \frac{\lambda^2 \cdot e^2 \cdot H_v^2 \cdot \eta_{em}}{4R_i \cdot Q_{batt}{}^2} \tag{5.35}$$

The co-state variable λ at which there exist two equal minimum Hamiltonian points is obtained by substituting P_{ice2} found in equation (5.36) into equation (5.31) and setting the resulting Hamiltonian equal to that given in equation (5.29).

$$\lambda = -\frac{\left(\pi\sqrt{\frac{U^2\eta_{em} - 4R_i P_{req}}{\eta_{em}}} + \sqrt{\frac{\pi R_i\left(-4\pi P_{req} + 4\pi\eta_{em}^2 P_{req} + \eta_{em}^2 P_{ml0}\omega_e V_d\right)}{\eta_{em}}}\right)Q_{batt}}{\pi \cdot H_v \cdot e \cdot \eta_{em}} \qquad (5.36)$$

Where,

P_{ice1} engine power in discharging in W,
P_{ice2} engine power in recharging in W,
V_d engine displacement in m^3.

Figure 5.6 illustrates the existence of the sliding optimal control when P_{req} is 5.35 kW and λ is -0.693. As a necessary condition for finding optimal control, Pontryagin's minimum principle provides control candidates including the optimal one. The sliding optimal control is considered as one solution which takes two candidates among them while the conventional solution takes only one candidate. Since both P_{ice1} and P_{ice2} are the solutions of the Hamiltonian reaching its minimum, this sliding solution does not violate Pontryagin's minimum principle.

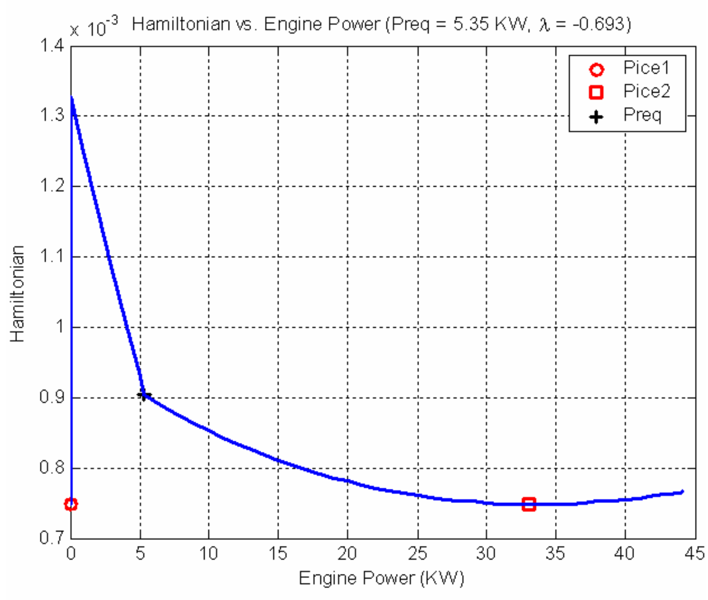

Figure 5.6 Hamiltonian versus engine power

(sliding optimal control exists: $P_{ice1} = 0$ and $P_{ice2} > P_{req}$ when $P_{req} = 5.35$ kW and $\lambda = -0.693$)

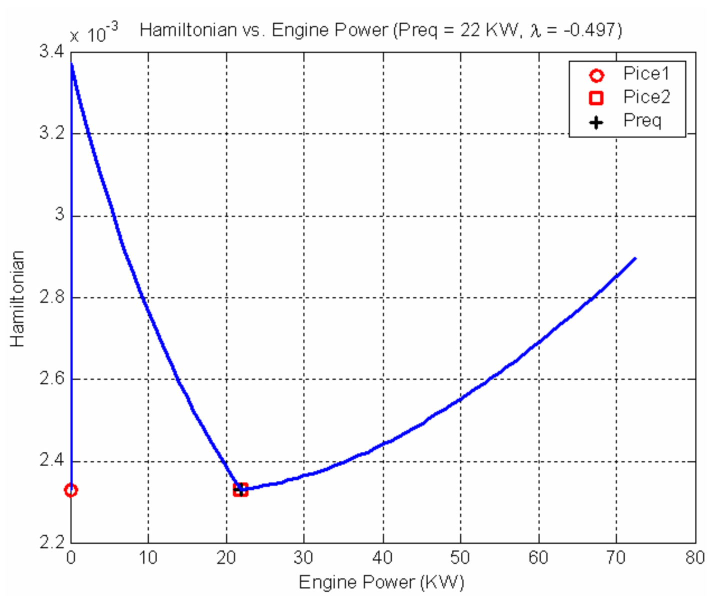

Figure 5.7 Hamiltonian versus engine power

(sliding optimal control does not exist: $P_{ice} = P_{req}$ when $P_{req} = 22$ kW and $\lambda = -0.497$)

The variable μ is defined as the recharging time fraction in the trip, i.e., when P_{ice} is equal to P_{ice2}, and it is calculated by using the battery SOC boundary conditions:

$$\mu = \frac{I_1}{I_1 - I_2} \tag{5.37}$$

$$I_1 = \frac{U_o - \sqrt{U_o^2 - 4R_i \cdot P_{req} / \eta_{em}}}{2R_i} \tag{5.38}$$

$$I_2 = \frac{U_o - \sqrt{U_o^2 - 4R_i \cdot \left(P_{req} - P_{ice2}\right) \cdot \eta_{em}}}{2R_i} \tag{5.39}$$

Where,

μ time fraction of recharging in the trip,

I_1 electric machine discharging current in A,

I_2 electric machine recharging current in A.

The variables I_1 and I_2 in equation (5.38) and (5.39) are the discharging and recharging current corresponding to P_{ice1} and P_{ice2}. Then the total fuel consumption of the trip is expressed as

$$m_f = \frac{\mu \cdot \left(P_{ice2} + P_{ml}\right) \cdot t_f}{e \cdot H_v} + \frac{\left(1 - \mu\right) \cdot \left(P_{ice1} + P_{ml}\right) \cdot t_f}{e \cdot H_v} = \frac{\mu \cdot \left(P_{ice2} + P_{ml}\right) \cdot t_f}{e \cdot H_v} \tag{5.40}$$

The fuel consumption under the sliding optimal control is compared with that under the constant control ($P_{ice} = P_{req}$ as shown in equation (5.28)), both satisfying the battery SOC boundary conditions, to find the final optimal solution.

When P_{req} is smaller than a specific value P_{req}^*, the sliding optimal control consumes less fuel. Otherwise, using the engine alone is better. In the second case, even though one can find two minimum Hamiltonian points as shown in Figure 5.7, one of them is at P_{req}, implying the control may switch between 0 and P_{req}. This violates the battery SOC constraint and thus $P_{ice} = P_{req}$ is the solution.

$$P_{req}^* = \frac{2\pi U_o^2\left(\eta_{em}^2 - 1\right) - \eta_{em}^3 R_i P_{ml0}\omega_e V_d + 2U_o\sqrt{\pi^2 U_o^2\left(\eta_{em}^4 - 2\eta_{em}^2 + 1\right) + \pi\eta_{em}^3 R_i P_{ml0}\omega_e V_d}}{4R_i \cdot \pi \cdot \eta_{em}^3} \tag{5.41}$$

When $P_{req} < P_{req}^*$ (but $\omega_e \geq$ idle, otherwise only the electric machine will be used), the system saves fuel by shutting down the engine while discharging the battery and then restarting the engine to recharge the battery at the maximum total efficiency. Here, the total efficiency considers the engine efficiency, the electric machine efficiency and the battery heat losses. When $P_{req} \geq P_{req}^*$, the gain of fuel saving from engine start-stop is no longer larger than the additional losses in the battery and the electric machine. Therefore, using the engine alone to meet the power requirement is a better choice.

The optimal control solutions for vehicles with batteries of different capacity, Q_{batt}, and internal resistance, R_i, running from 0 to 45 m/s (0-100 mph) are shown in Figure 5.8. When the vehicle is running slower than 6.7 m/s (15 mph), the engine is off and the HEV uses the motor alone to propel the vehicle. Hence, the vehicle is not strictly charge sustaining. However, the electricity consumed by the battery at such low speeds for a 100-second long trip is negligible. When the capacity increases and the resistance decreases, the region for the sliding optimal control being the optimal solution moves slightly to the higher power region. P_{req}^* is about 22 kW at vehicle speed of 36 m/s (80 mph) when R_i is 0.3 or 0.25 Ω. It increases to 26 kW at 38 m/s (85 mph) when R_i decreases to 0.2 Ω. In the vehicle with batteries of lower resistance, the losses due to discharging and recharging are smaller, and thus the sliding optimal control tends to be more fuel efficient than the constant control even at higher power levels. Moreover, as the battery resistance decreases, the engine tends to run at higher power levels. The higher power levels result in greater engine efficiency and larger energy draws from the battery. The increased battery efficiency helps to reduce the net losses even at the higher energy draws.

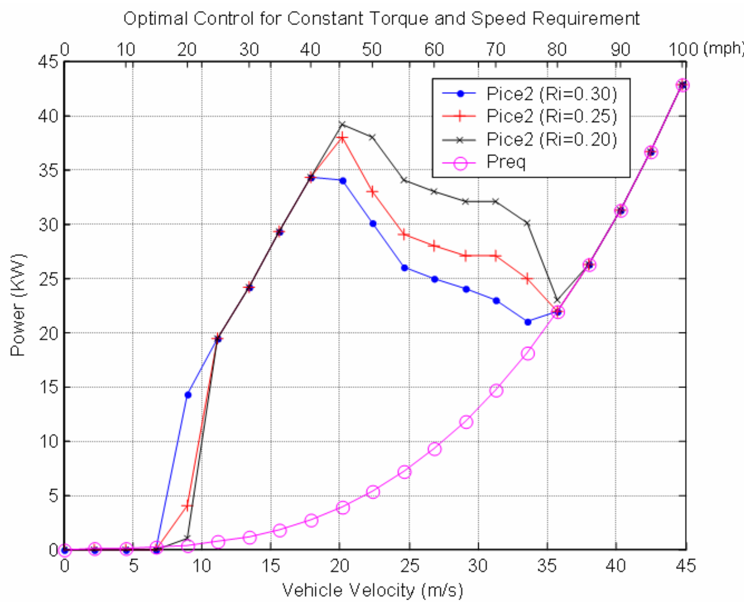

Figure 5.8 Optimal control for vehicles with batteries of different internal resistance

Figure 5.9 depicts fuel consumption savings comparing a mild HEV with a 2.2 L engine and a 30 kW (peak) motor to a conventional vehicle with a 3.2 L engine and also that for the two control candidates in the HEV. At higher vehicle speeds, hybridization saves about 5~20% of fuel and using the sliding optimal control saves an additional up to 45% of fuel. Therefore, the total fuel consumption saving of the HEV with the sliding optimal control over the conventional vehicle is around 5 to 55%. Highway cruising speed in the United States is around 25 to 30 m/s (60~70 mph), the HEV with the sliding optimal control reduces fuel consumption for roughly 8~15%. Fuel saving becomes larger (28~50%) when the vehicle cruises in rural areas (17~22 m/s or 40~50 mph). The optimal energy management strategy in the HEV depends on both the vehicle configuration and its parameters. The fuel economy improvement could be larger for other HEVs.

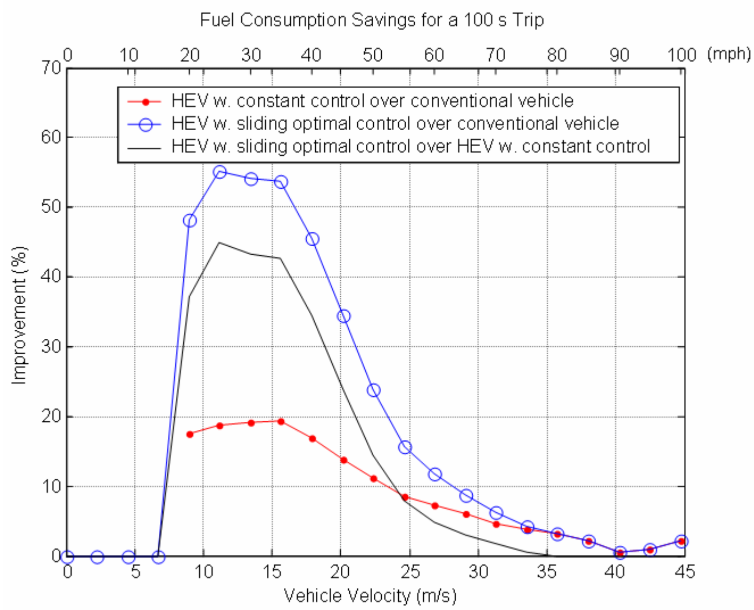

Figure 5.9 Fuel consumption savings comparing HEV, conventional vehicle and HEV with different controls

The switching frequency in this problem has no effect on the total fuel consumption since the state equation does not depend on the state variable itself. Consequently, the Hamiltonian does not depend on the state and there exist infinite number of optimal solutions. Figure 5.10 shows state trajectories under some possible optimal controls when the vehicle is cruising at 29 m/s (65 mph).

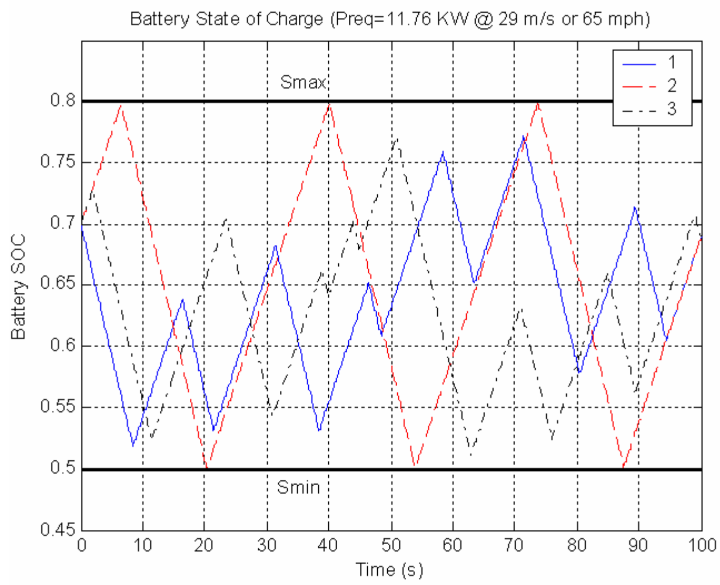

Figure 5.10 State trajectories under sliding optimal control
when vehicle is cruising at 29 m/s (65 mph)

When the two control values P_{ice1} and P_{ice2} are fixed, the variable μ is fixed and hence the total fuel consumption remains the same because it only depends on μ, P_{ml0} and P_{ice2}. Therefore, the minimum number of switchings should be used to take into account the effect of the unavoidable engine start-stop losses. This number is determined by the selected battery SOC boundaries, which depend on the battery size and type.

Solution for HEV with Variable Battery Parameters

When the battery open circuit voltage and internal resistance are functions of the battery SOC as shown in equations (4.26) and (4.27), the Hamiltonian in equation (5.23) also depends on the battery SOC even when the SOC stays between S_{min} and S_{max} (see equation (5.42)).

$$H = \dot{m}_f + \gamma_1 (S - S_{max}) sg(S - S_{max}) + \gamma_2 (S_{min} - S) sg(S_{min} - S)$$
$$- \lambda \frac{U_{o0} - U_{o1}(1-S) - \sqrt{(U_{o0} - U_{o1}(1-S))^2 - 4P_{batt}(R_{i0} + R_{i1}(1-S))}}{2Q_{batt}(R_{i0} + R_{i1}(1-S))} \tag{5.42}$$

$$sg(\alpha) = \begin{cases} 1, & \alpha > 0 \\ 0, & \alpha < 0 \end{cases} \tag{5.43}$$

According to Pontryagin's minimum principle, the co-state variable λ now is no longer a constant regardless of the value of the battery SOC. Therefore, the optimal control is found numerically by adjusting the initial value of the co-state variable λ_0 until the SOC at the final time coincides with the desired value. If the optimal solution is outside of the control boundaries, one of the boundary values which has smaller *H* is taken as the solution. The flow chart in Figure 5.11 also describes this procedure in details.

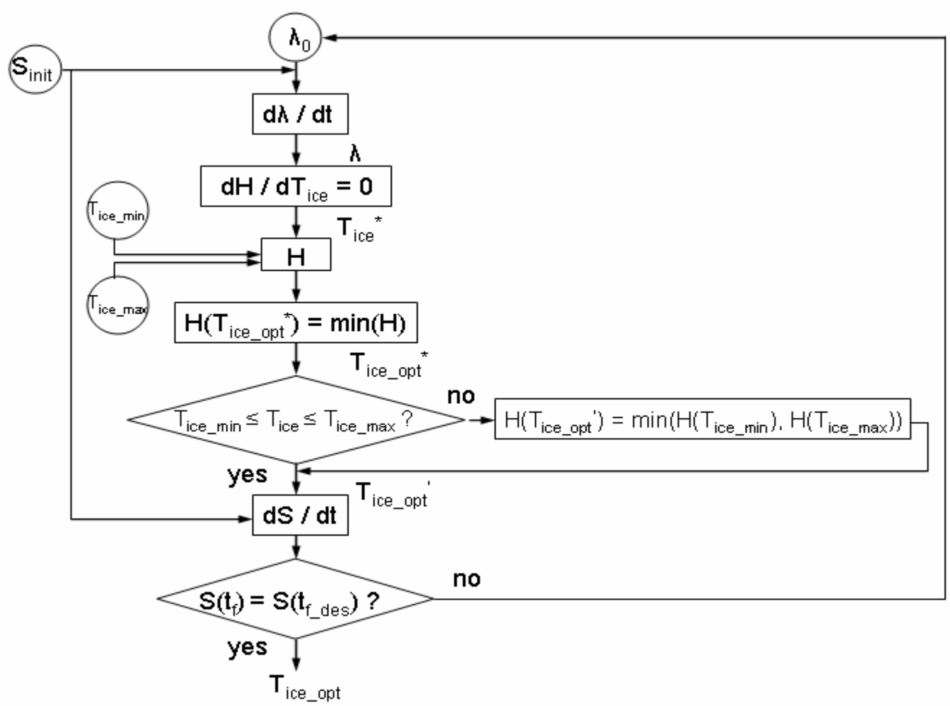

Figure 5.11 Flow chart of solving optimal control for constant power requests with variable battery parameters

Figure 5.12 shows the optimal control solution for 120-second long constant speed and torque requirement trips using the battery model with non-constant open circuit voltage and internal resistance.

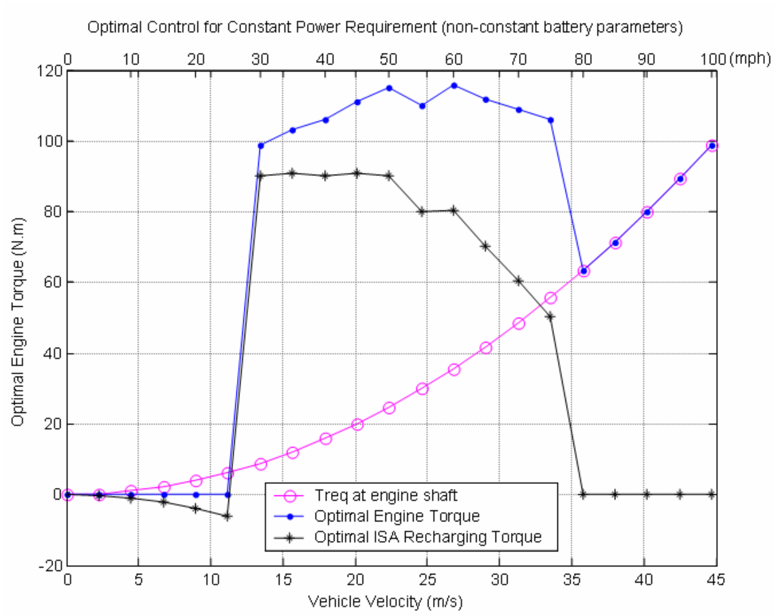

Figure 5.12 Optimal control for constant speed and torque requirement

(non-constant battery parameters)

The optimal engine torque takes a large positive value and then switches to zero when the torque requirement at the engine shaft is lower than 63.34 N·m (80 mph). The ISA correspondingly recharges the battery and then discharges it to maintain the final SOC. When the vehicle speed becomes larger than 80 mph (35.7 m/s) the engine works alone to propel the vehicle. Figure 5.13 depicts the optimal engine torque, battery SOC and co-state variable when the torque request is about 30 N·m.

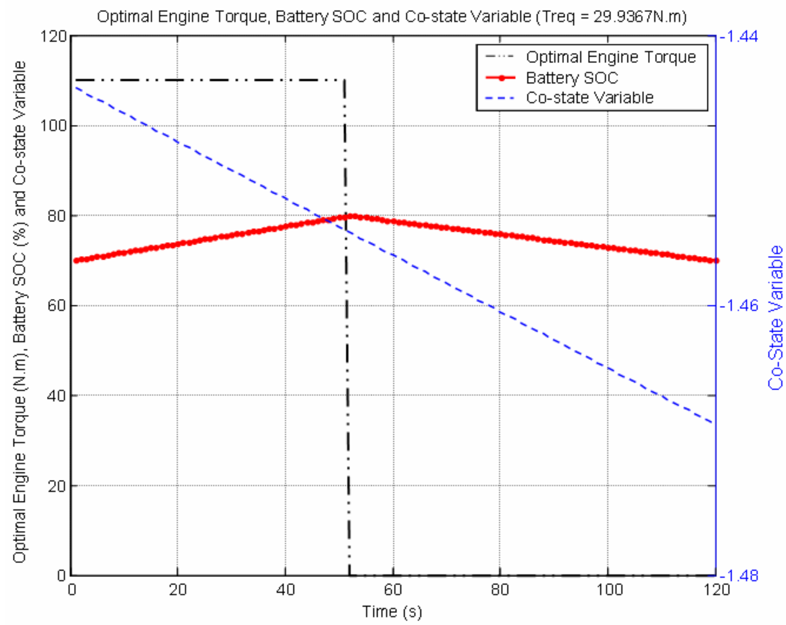

Figure 5.13 Optimal engine torque, battery SOC and co-state variable for a 120-second long constant torque request trip (T_{req} = 29.94 N·m)

Noticing the co-state variable changes versus time, one may expect that the Hamiltonian may have its minimum at different engine torque while time passes by. Before 51 s, the Hamiltonian has its minimum at the engine torque of 110 N·m, and then it moves to zero engine torque with the decreases of the co-state variable (see Figure 5.14 and Figure 5.15).

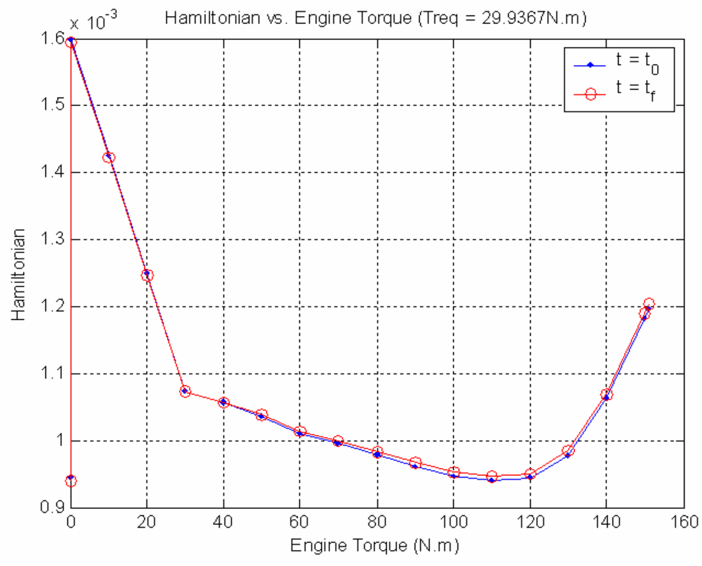

Figure 5.14 Hamiltonian versus engine torque (T_{req} = 29.94 N·m)

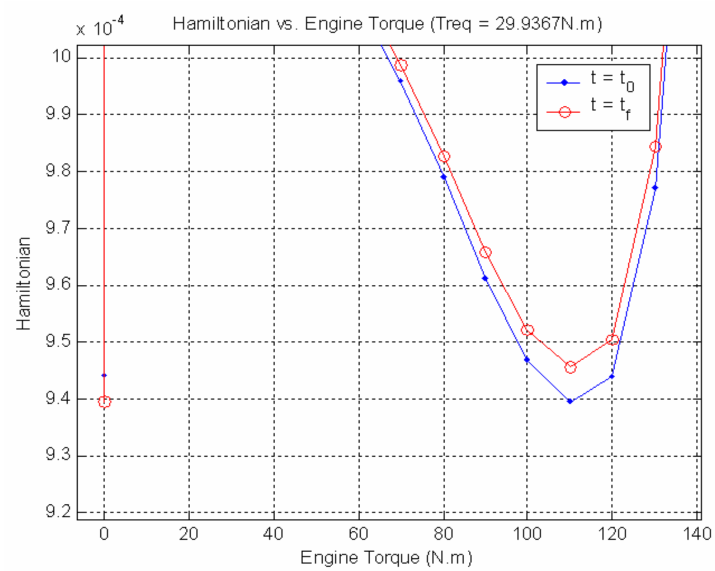

Figure 5.15 Zoom-in Hamiltonian versus engine torque (T_{req} = 29.94 N·m)

Unlike in the previous case with constant battery parameters where the optimal control (the sliding optimal control) switches passively using the extended minimum principle, the control solution in this case (the "switching" type control) switches automatically as the co-state variable varies. In addition, the solutions for any two trips with the same power request but different trip lengths are completely different. In particular, the solution for the longer trip is not a repetition of the shorter trip solution, unlike in the case where the battery parameters are fixed. One has to solve for the optimal control for the new trip entirely. The problem formulation does not change except for the trip length.

Solution for HEV with Optimal CVT Ratio

The solutions for the two cases introduced above for constant power requests assume that the CVT ratio is fixed at direct drive, i.e., the ratio is one, implying that the CVT ratio is not one of the control variables in the optimization. This is intuitively not true for all power requests. Therefore, this section introduces fuel economy optimization taking the CVT ratio as one of the control variables. The battery parameters in this case also depend on the SOC as it is in the last case.

Figure 5.16 depicts the optimal engine and ISA torques at the optimal CVT ratio for constant power requests with variable battery parameters and CVT ratio. Except that at the second speed of around 2 m/s where the electric machine propels the vehicle due to engine speed constraints, the engine always works alone to provide all the power at all other speeds. For each desired vehicle speed, this result is most fuel efficient only at the optimal CVT ratio shown in Figure 5.17.

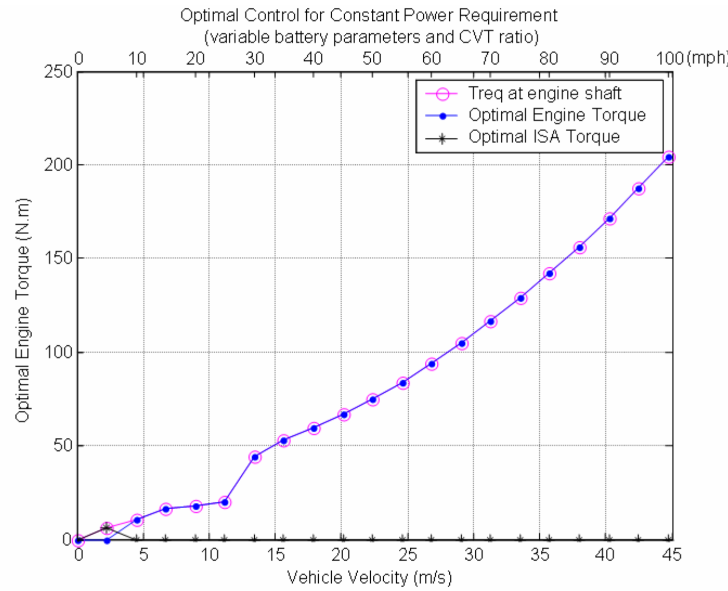

Figure 5.16 Optimal engine and ISA torques for constant power requests with optimal CVT ratio (variable battery parameters)

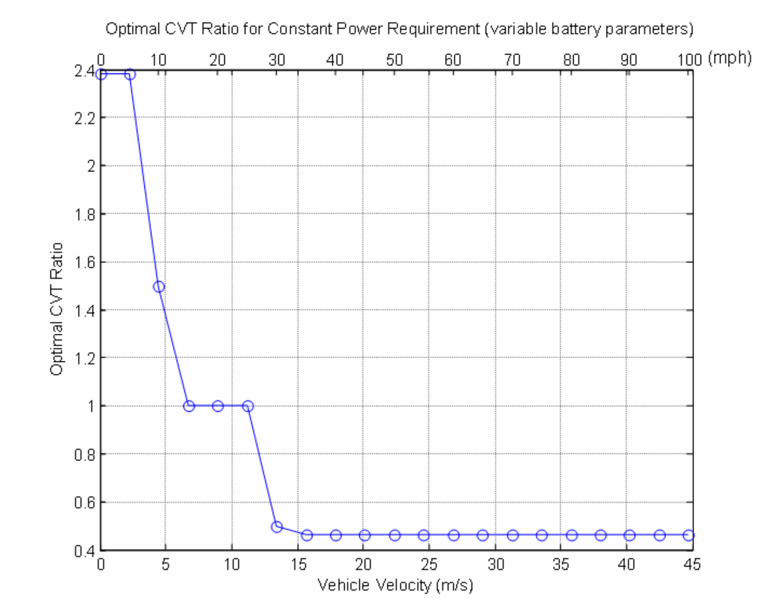

Figure 5.17 Optimal CVT ratio for constant power requests (variable battery parameters)

This vehicle apparently operates at the lowest gear when the desired speed is very low. When the vehicle speed is above 15 m/s (around 35 mph), the vehicle tends to stay at the highest gear. This strategy places the engine to operate at low-speed, high-torque region (i.e., the highest efficiency region) at almost all given desired vehicle speed. The "switching" type engine operations, not the sliding optimal control, in the variable battery parameters without CVT ratio optimization case do not appear in this case. This is because the optimal CVT ratio at direct drive only happens at the speeds which require a zero engine torque instead of a "switching" type torque trace. If the optimal CVT ratio is at one for moderate vehicle speeds, the "switching" type torque operation will be the optimal solution.

Figure 5.18 shows the fuel improvement of the HEV with the optimal control strategies found in the above three cases over the conventional vehicle which has a 3.2 L engine.

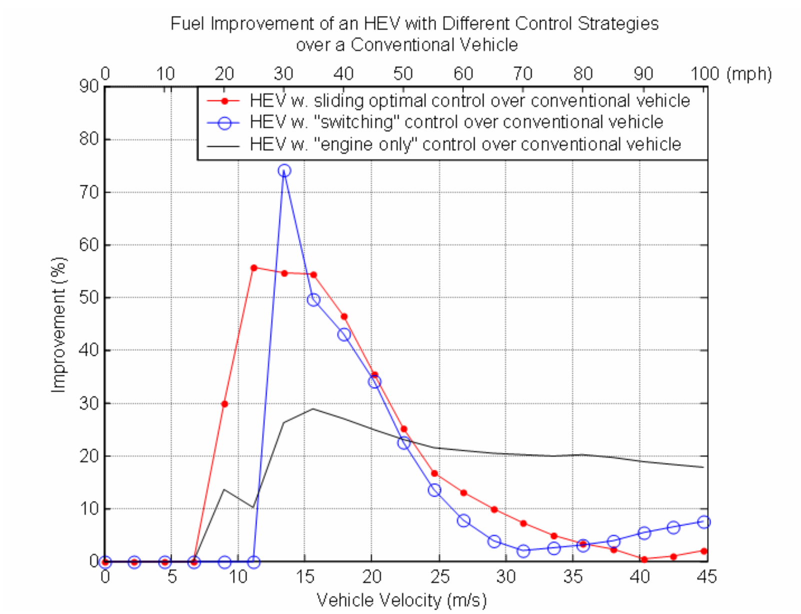

Figure 5.18 Fuel Improvement of an HEV with Different Control Strategies over a Conventional Vehicle for Constant Power Requests

(line w. dot: constant battery parameters with no CVT ratio optimization; line w. circle: variable battery parameters with no CVT ratio optimization; solid line: variable battery parameters with CVT ratio optimization)

Without optimizing the CVT ratio, the optimal solution for the case with variable battery parameters is generally less fuel efficient than the one where battery parameters are fixed. The fuel economy improvement is lower at low speed and higher at high speed when comparing the case with CVT ratio optimization over the one without. This demonstrates that running the engine alone in the most fuel efficient region during the whole trip without bothering to recharge and discharge the battery achieves better fuel economy. Converting energy between chemical and electrical costs extra fuel and therefore it is only desirable when fuel economy improvement by moving the engine to the most efficient region gains more than the losses from energy conversions. If the engine is already operating in the most efficient region, there is clearly no need to ask for energy conversions.

5.1.3 Optimal Control for Time-Varying Power Requirement

Solution from Pontryagin's Minimum Principle

The optimal control problem needs to be reformulated for a vehicle running under realistic driving cycles, i.e., with time-varying speed and torque requirements. This problem now contains two control variables, the optimal engine torque T_{ice_opt} and the optimal transmission ratio r_{cvt_opt}. They are both time-varying in general. The Hamiltonian in equation (5.42) then becomes a function of the engine torque, the transmission ratio, the battery SOC and the co-state variable. As in the case of constant power request with variable battery parameters, the solution for time-varying power requests with variable battery parameters needs to be found numerically as well. The detailed procedure is shown in Figure 5.19.

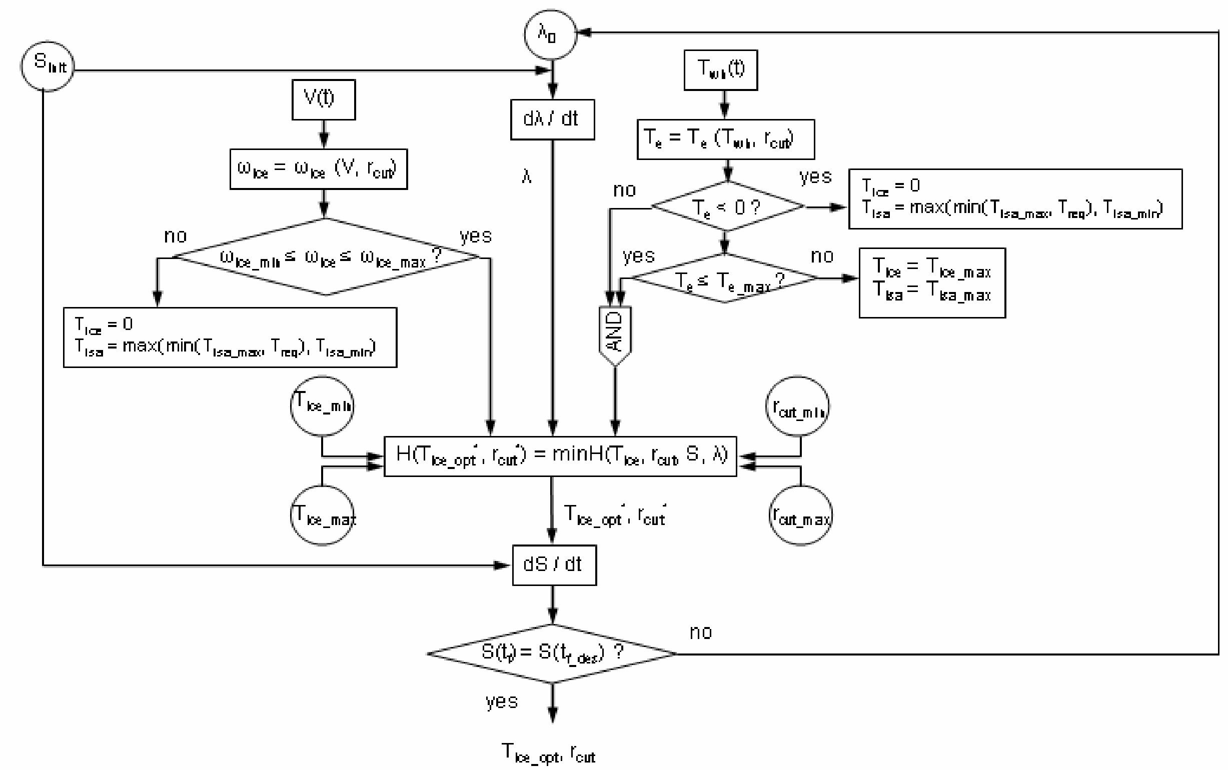

Figure 5.19 Flow chart of solution method for optimal control for variable power requests

The left part of the flow chart determines whether the engine should be involved in the propulsion according to the required vehicle speed and engine speed constraints. Only for the cases where there exists at least one CVT ratio which results in the operating speed at the engine shaft lies between idle and redline, optimal splitting power requests between the engine and the electric machine is possible. The right part of the figure describes how the optimal splitting solution is found numerically. The key issue here is to find the right initial value of the co-state variable λ such that the Hamiltonian is minimized and the final value of the battery SOC coincides with the desired value. When the torque requests are negative, the engine is shut down and the electric machine recharges the battery.

Figure 5.20 and Figure 5.21 depict the optimal engine and ISA operating points for the FUDS (city) cycle on the engine fuel consumption and the ISA efficiency maps.

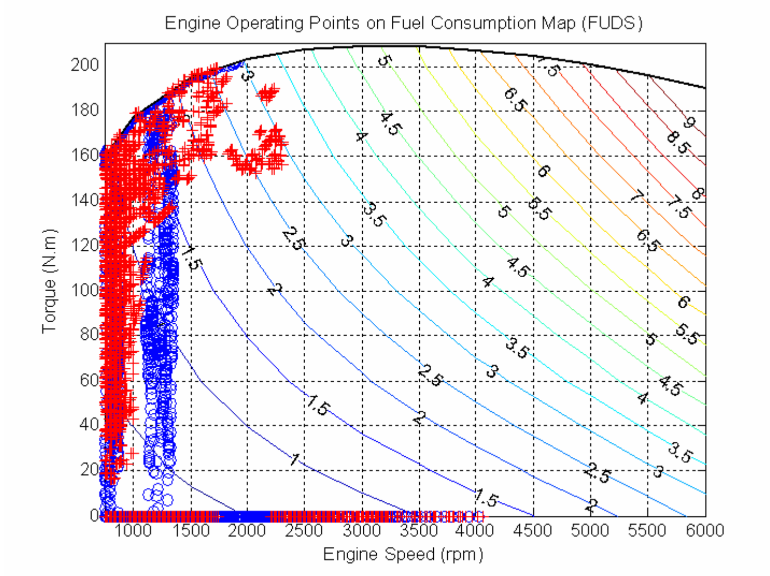

Figure 5.20 Optimal engine operating points on fuel consumption map (FUDS)
(blue circle: baseline controller; red plus: optimal controller)

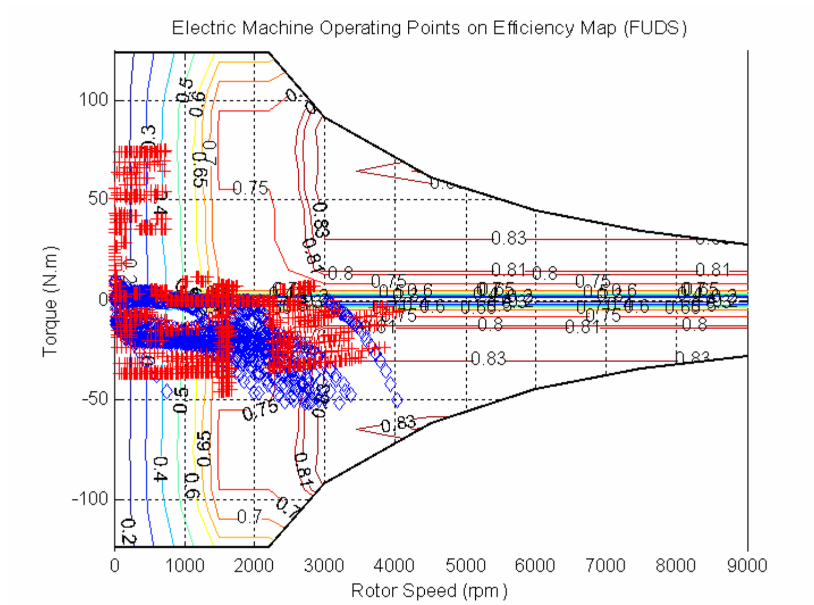

Figure 5.21 Optimal electric machine operating points on efficiency map (FUDS)
(blue circle: baseline controller; red plus: optimal controller)

The blue circle represents the operating points of the vehicle with the baseline controller (the heuristic controller introduced in Chapter 4) and the red plus represents the ones of the vehicle with the optimal controller. With the optimal controller, the engine operates at low fuel consumption region and the ISA functions as a motor mainly in the region which has higher efficiency than the engine does. The ISA sometimes works in the low efficiency region and this is due to the engine speed constraint. In a frequent start-stop cycle as the FUDS, the advantage of the ISA recharging the battery whenever the vehicle slows down is relatively large. When the vehicle is controlled under the baseline controller, the engine and the electric machine operate at relatively low speed and low speed/medium torque regions respectively. Comparing the operating points with the optimal controller and those with the heuristic controller, the engine tends to operate in the medium fuel consumption region. However, the total effect of having the engine always running in the medium fuel consumption region consumes more fuel than the case that the engine spends most of its time in the low consumption region and only spends short period of time in the slightly higher fuel consumption region. The vehicle fuel economy consequently improves when the optimal control strategy is applied, from 35.09 mile/gal to 42.88 mile/gal.

Figure 5.22 and Figure 5.23 show the optimal CVT ratio and the battery state of charge for the FUDS cycle.

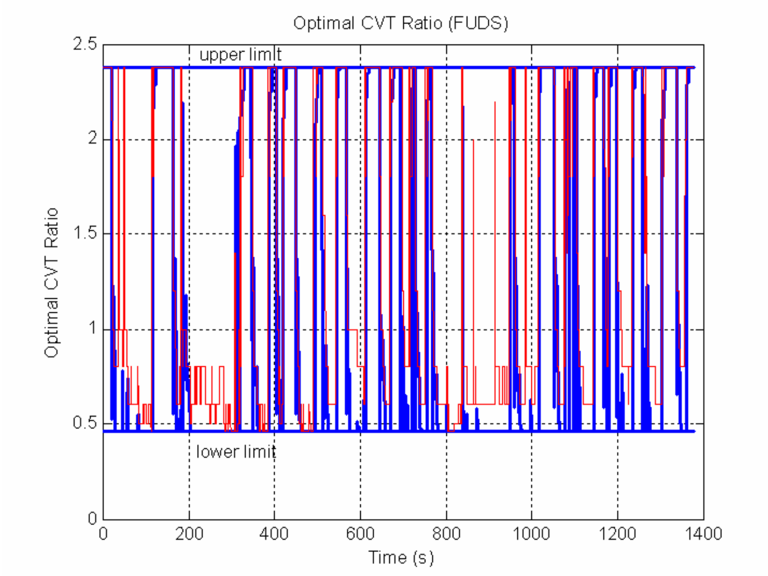

Figure 5.22 Optimal transmission ratio (FUDS)
(blue thicker line: baseline controller; red thinner line: optimal controller)

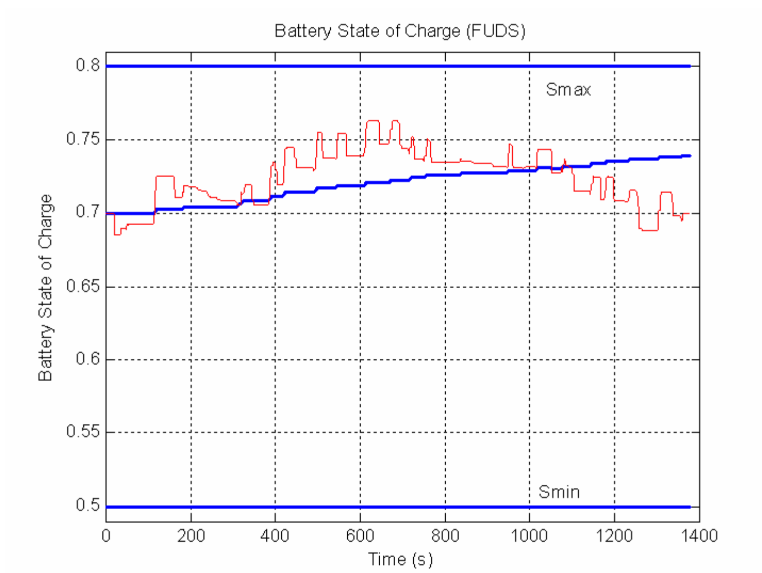

Figure 5.23 Battery state of charge under optimal control (FUDS)
(blue thicker line: baseline controller; red thinner line: optimal controller)

The optimal CVT ratio is found together with the optimal engine torque and it is one of the inputs to the vehicle controller. The battery SOC goes up and down along the driving cycle but always stays within its operating limits (0.5 ~ 0.8). The SOC constraint is satisfied for the vehicle with the optimal controller which is ensured by the optimal principle. However, it is not easy to tune the heuristic controller to meet this constraint. The SOC constraint here refers to that the final SOC value needs to be equal to a desired value, usually its initial value.

Figure 5.24 to Figure 5.27 compare the optimal solution and the battery SOC of the vehicles with the baseline and the optimal controllers when the vehicle is running under the FHDS (highway) cycle.

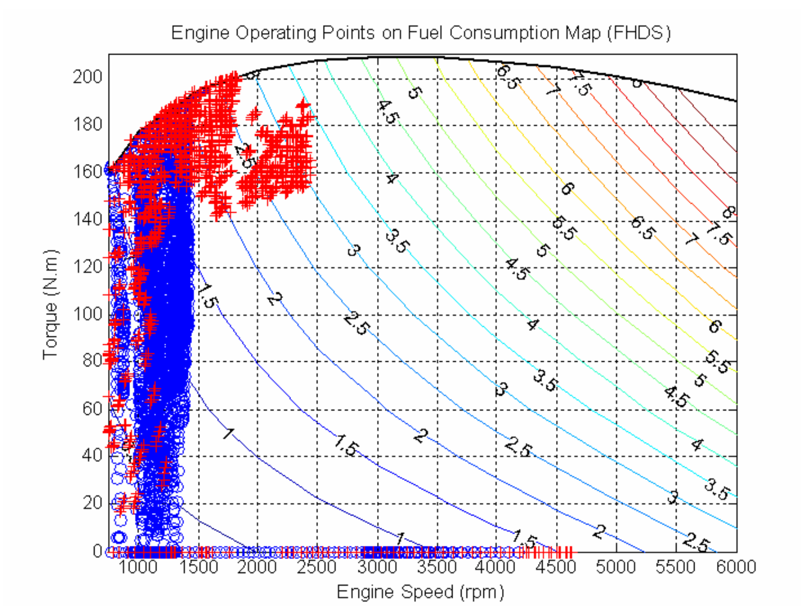

Figure 5.24 Optimal engine operating points on fuel consumption map (FHDS)
(blue circle: baseline controller; red plus: optimal controller)

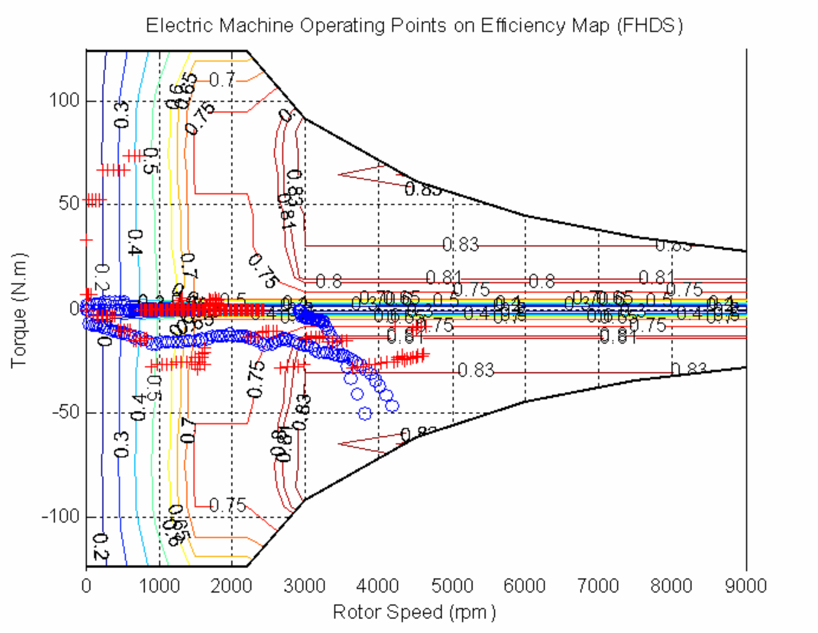

Figure 5.25 Optimal electric machine operating points on efficiency map (FHDS)
(blue circle: baseline controller; red plus: optimal controller)

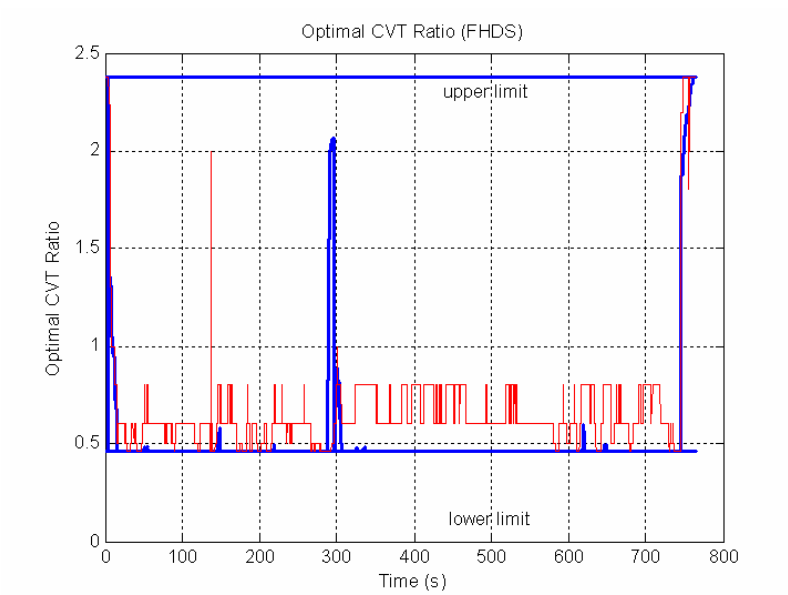

Figure 5.26 Optimal transmission ratio (FHDS)
(blue thicker line: baseline controller; red thinner line: optimal controller)

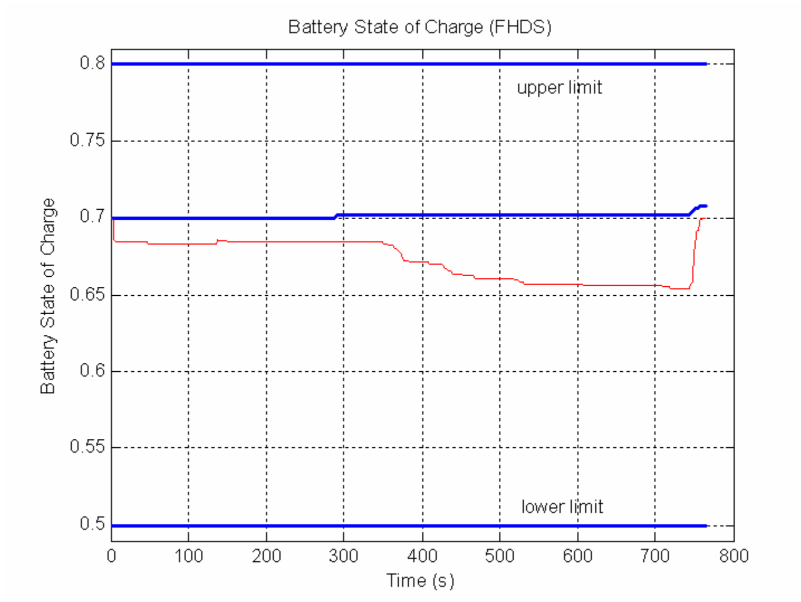

Figure 5.27 Battery state of charge under optimal control (FHDS)
(blue thicker line: baseline controller; red thinner line: optimal controller)

Similar as for the FUDS cycle, the engine operating points concentrate at the medium fuel consumption region. However, the engine consumes more fuel than it does for the city cycle due to higher power requirements for the highway cycle. The ISA recharges the battery much less than for the city cycle since the vehicle does not decelerate much under the highway cycle. The fuel economy for the FHDS cycle is improved from 36.53 to 40.01 mile/gal, less than that for the city cycle. The main reason for this is because that the HEV has less potential for fuel economy improvement for non-frequent start-stop driving conditions with high power requests. In Figure 5.26, the CVT for the optimal controller case remains at lower gear, i.e., higher ratio for most of the time. The final battery SOC for the baseline controller again is not equal to its initial value, but it is much closer than that for the FUDS cycle.

5.1.4 Optimal Control with Predicted Driving Conditions

The strategy shown in Figure 5.19 has been modified to find the optimal control for predicted driving conditions. For each prediction window depicted in Figure 5.28, i.e., w_1 to w_n, finding the optimal engine torque, the CVT ratio and the initial value of the co-state variable such that the fuel consumption of each short trip (for each prediction window) is minimized, the battery SOC operates between two limits and the SOC is equal to the initial value of the entire trip $S(t_0)$ at the end of each prediction window (S with stars in the figure below should be equal to $S(t_0)$).

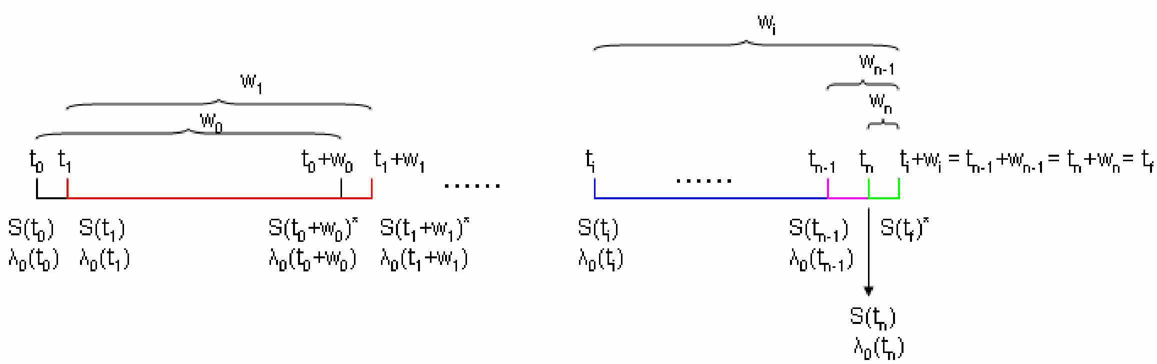

Figure 5.28 Schematic of the prediction window in the optimal control problem

Prediction windows may have different length even before the vehicle approaches the end of the entire journey. For simplicity, this research only considers the prediction window with fixed length, i.e., 300-second long for the FUDS and the FHDS cycles. The prediction window becomes shorter and shorter when the vehicle gets closer to the final destination. Only when the equation (5.44) holds the prediction window has the full length of 300 seconds.

$$t_i + w_i \le t_f \qquad (i = 0,1,2,\cdots,n) \tag{5.44}$$

Where,

t_i starting time of the i[th] window in s,

t_f final time of the entire trip in s,

w_i length of the i[th] window in s.

Figure 5.29 to Figure 5.36 depict the operating conditions of the key powertrain components for the FUDS and the FHDS cycles. With the optimal controller, the engine and the electric machine operating points scatter in a wider region including the higher fuel consumption and the lower efficiency regions when the vehicle is running with limited known driving conditions. The fuel economy in this case is about 38.33 mile/gal for the FUDS and 38.41 mile/gal for the FHDS, both are lower than the cases with fully known driving conditions shown in Figure 5.20 to Figure 5.23 and Figure 5.24 to Figure 5.27. According to Figure 5.29 and Figure 5.33, it seems that the vehicle with the optimal controller should have worse fuel economy. Actually, even though the engine operates in the higher fuel consumption region than it does with the heuristic controller, the engine stays longer at "OFF" mode. The power request at the wheel is satisfied by the ISA when the engine is at the "OFF" mode. The ISA operating points shown in Figure 5.30 and Figure 5.34 depict that the ISA in the optimal controller case runs longer in the motoring mode resulting in more operating points with positive torque. The overall efficiency of running the engine at higher loads for shorter period of time and then shutting it down is higher than that in the heuristic controller case.

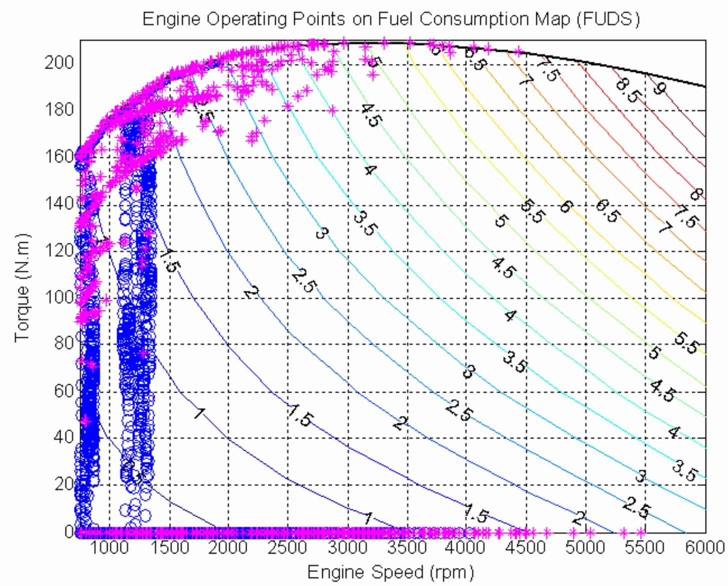

Figure 5.29 Optimal engine operating points on fuel consumption map (FUDS) **(prediction window)** (blue circle: baseline controller; magenta star: optimal controller)

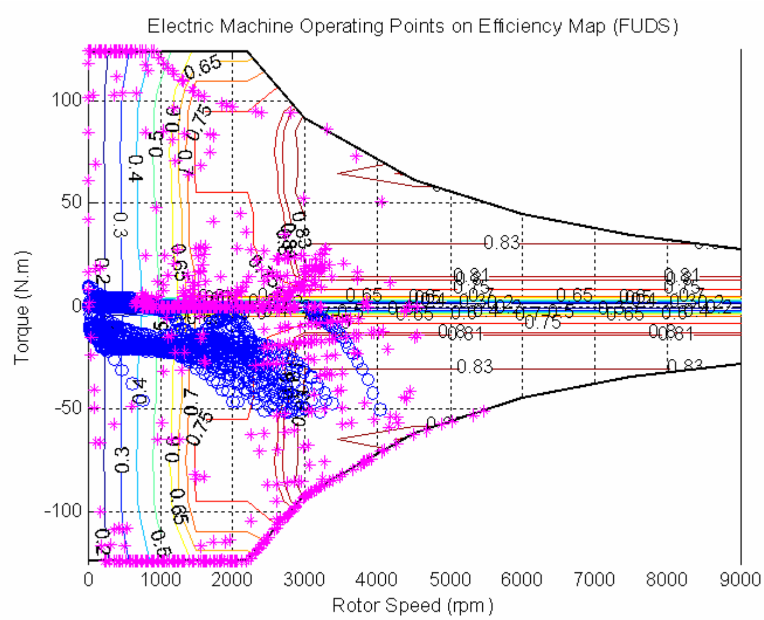

Figure 5.30 Optimal electric machine operating points on efficiency map (FUDS) **(prediction window)** (blue circle: baseline controller; magenta star: optimal controller)

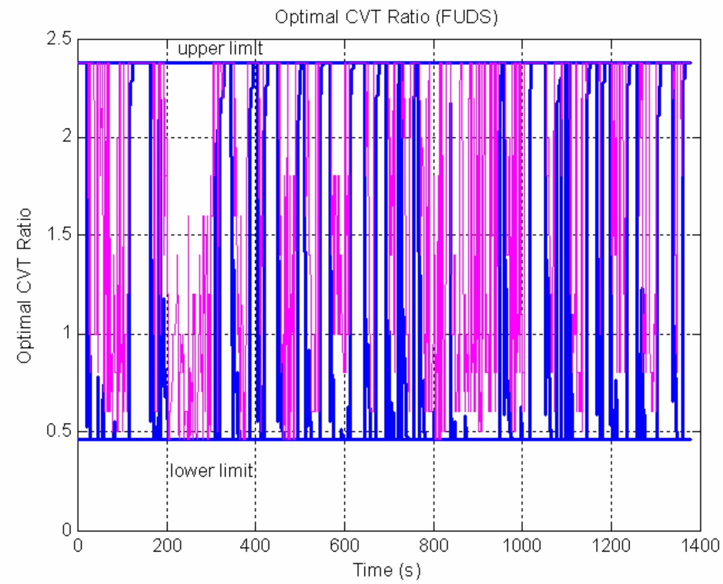

Figure 5.31 Optimal transmission ratio (FUDS) **(prediction window)**
(blue thicker line: baseline controller; magenta thinner line: optimal controller)

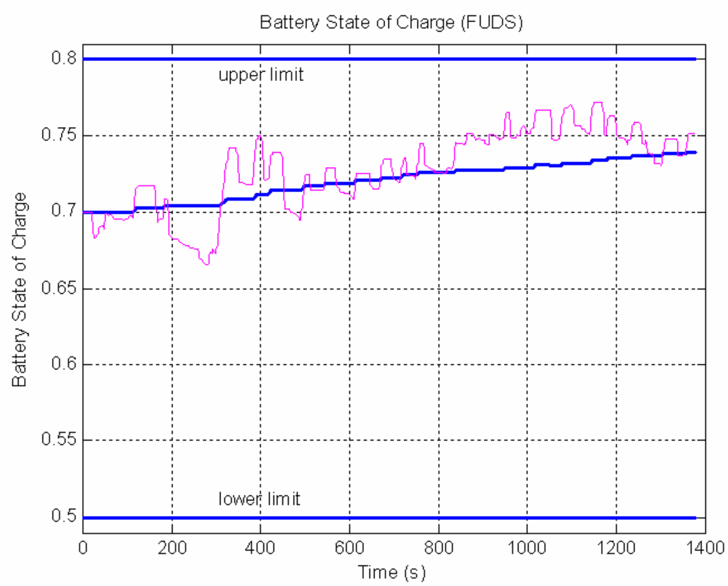

Figure 5.32 Battery state of charge under optimal control (FUDS) **(prediction window)**
(blue thicker line: baseline controller; magenta thinner line: optimal controller)

It is also harder to keep the vehicle charge sustaining if the entire driving condition is not known in prior, especially in the city driving scenario where frequent start-stop occurs. For either the FUDS or the FHDS cycle, the engine for the vehicle with the optimal controller tends to operate at near wide open throttle region while that for the vehicle with the baseline controller tends to run in lower speed region. This is mainly because different controllers choose the optimal CVT ratio differently. The baseline controller chooses higher gear (lower gear ratio) and thus the engine in this case runs at lower speed. The lower gear selection for the optimal controller case consequently results in higher engine operating speed.

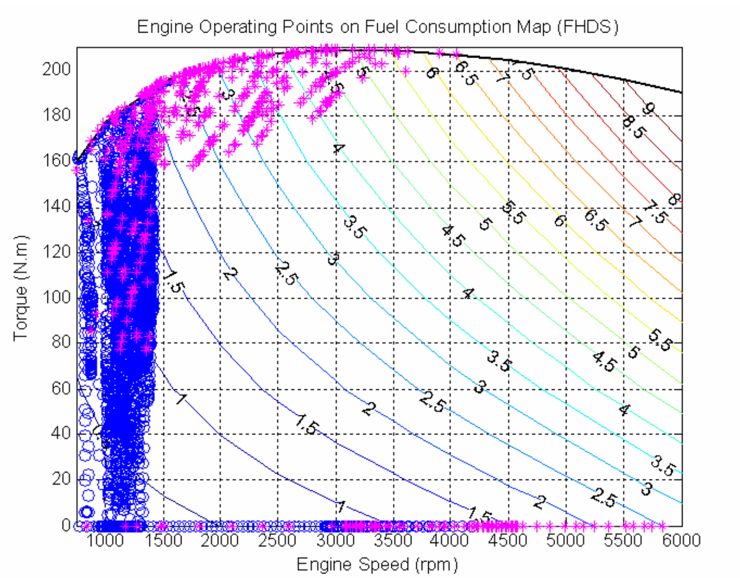

Figure 5.33 Optimal engine operating points on fuel consumption map (FHDS) **(prediction window)** (blue circle: baseline controller; magenta star: optimal controller)

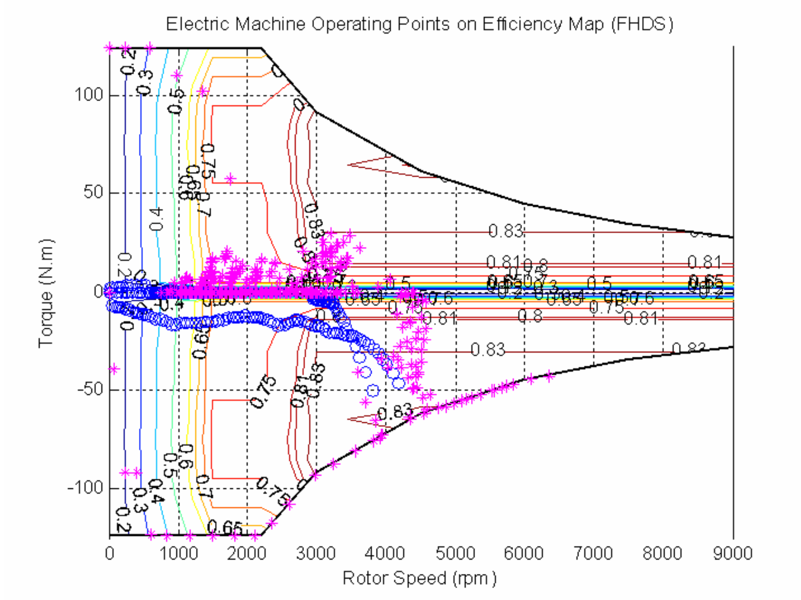

Figure 5.34 Optimal electric machine operating points on efficiency map (FHDS) **(prediction window)** (blue circle: baseline controller; magenta star: optimal controller)

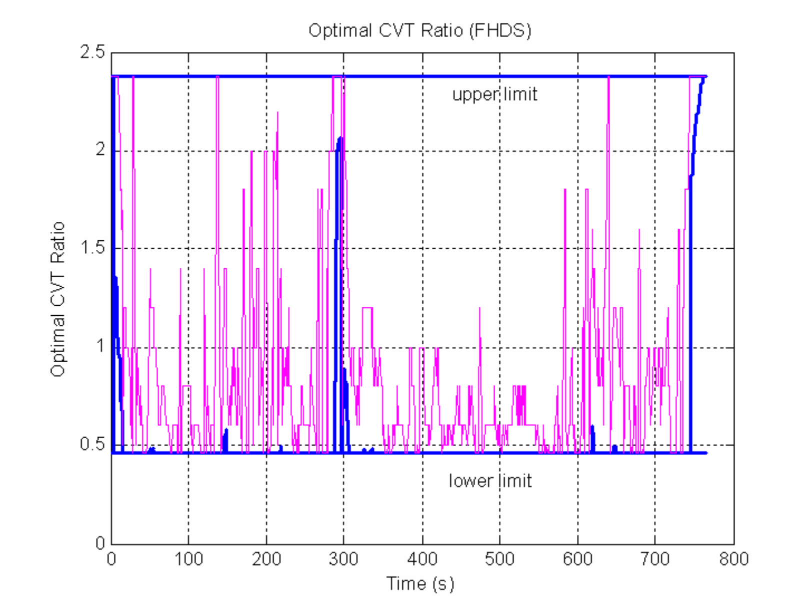

Figure 5.35 Optimal transmission ratio (FHDS) **(prediction window)**

(blue thicker line: baseline controller; magenta thinner line: optimal controller)

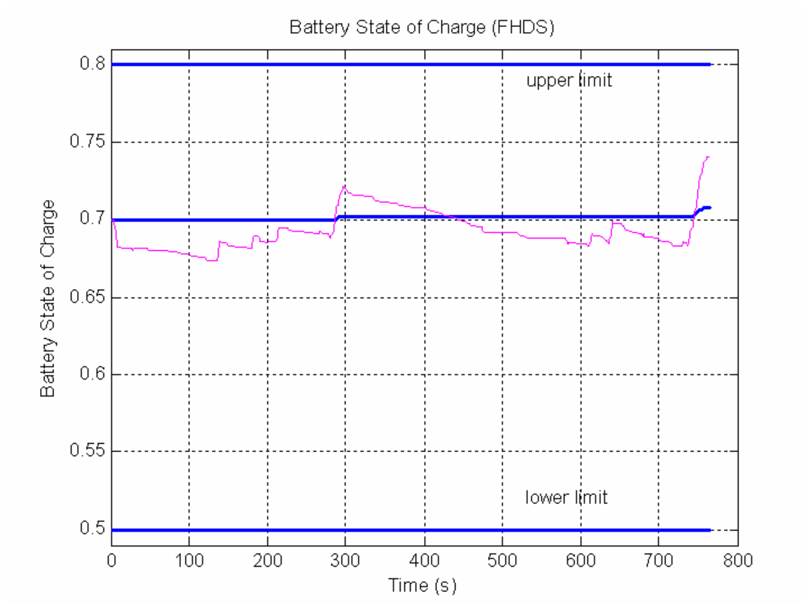

Figure 5.36 Battery state of charge under optimal control (FHDS) **(prediction window)**
(blue thicker line: baseline controller; magenta thinner line: optimal controller)

When there exist prediction errors, the optimal solution for the current state needs to be recalculated to reflect the actual driving conditions. This requires a fast real-time computer and sensors with shorter delays to be equipped in the vehicle. The investigation on the relationship between the vehicle fuel economy and the prediction window length with and without prediction errors provides an interesting research topic to extend the research covered by this dissertation.

5.2 Optimal Control Considering Fuel Economy, Performance and Driveability

This section introduces one way to formulate the cost function for fuel economy, performance and driveability optimization problem. Alternatively, the optimal solution considering these three criteria may be found hierarchically: finding the solution for best fuel economy and performance first and then taking driveability into consideration. The second part of this section provides some qualitative explanations about how the three control criteria are affected by limiting the derivative of the control variables.

5.2.1 Problem Formulation

When the vehicle tracks a driving cycle perfectly, there is no freedom to optimize performance and driveability since their criteria (acceleration time, RMS value, VDV, MTVV, jerk, etc.) are all related with vehicle acceleration. They are thus determined by the desired vehicle velocity profile. However, any deviation from this desired profile may change the value of the performance and driveability measures. Minimizing the tracking error will bring these values close to those for the driving cycle. The cost function formulated below considers weighted fuel economy, performance and driveability for a given cycle:

$$J = \int_{t_0}^{t_f} \Big[\underbrace{w_1' \dot{m}_f(T_{ice}, r_{cvt}, t)}_{\text{Fuel consumption}} + \underbrace{\gamma_1 (S - S_{max}) sg(S - S_{max}) + \gamma_2 (S_{min} - S) sg(S_{min} - S)}_{\text{SOC penalty}} + \underbrace{w_2' \big(V(T_{ice}, r_{cvt}, t) - V_{des}(t)\big)^2}_{\text{Velocity tracking error}} \Big] dt \tag{5.45}$$

Where,

J	cost function,
S	battery state of charge (SOC),
V	actual vehicle velocity in *m/s*,
t	time in *s*,
S_{max}	battery SOC upper limit,
S_{min}	battery SOC lower limit,
T_{ice}	engine torque in *N·m*,
V_{des}	desired vehicle velocity in *m/s*,

r_{cvt} CVT ratio,

t_0 initial time in s,

t_f final time in s,

$w_{1,2}$' weighting coefficients for fuel economy and speed tracking error,

$\gamma_{1,2}$ weighting coefficients for battery SOC penalty functions.

$\dot{m}_f$ engine mass fuel flow rate in kg/s.

Since the vehicle tractive force can be easily converted into the torque requirements at the wheels, the desired vehicle velocity profile is translated into the desired tractive force profile and the cost function becomes

$$J = \int_{t_0}^{t_f} \Big[\underbrace{w_1 \dot{m}_f (T_{ice}, r_{cvt}, t)}_{\text{Fuel consumption}} + \underbrace{\gamma_1 (S - S_{max}) sg(S - S_{max}) + \gamma_2 (S_{min} - S) sg(S_{min} - S)}_{\text{SOC penalty}} + \underbrace{w_2 \big(F_{tr}(T_{ice}, r_{cvt}, t) - F_{tr\_des}(t)\big)^2}_{\text{Tractive force tracking error}} \Big] dt \tag{5.46}$$

Where,

F_{tr} actual vehicle tractive force at the wheels in N,

F_{tr_des} desired vehicle tractive force at the wheels in N,

$w_{1,2}$ weighting coefficients for fuel economy and tractive force tracking error.

The desired tractive force here is the desired force from the driver pedal command.

In general, the cost function for all driving conditions, not just driving cycles should contain the penalty functions for fuel consumption, acceleration time and jerk as shown below:

$$J = \int_{t_0}^{t_f} [\underbrace{w_1 \dot{m}_f (F_{tr}, t)}_{\text{Fuel consumption}} + \underbrace{\gamma_1 (S - S_{max}) sg(S - S_{max}) + \gamma_2 (S_{min} - S) sg(S_{min} - S)}_{\text{SOC penalty}} + \underbrace{w_2 \left(F_{tr}(T_{ice}, r_{cvt}, t) - F_{tr\_des}(t)\right)^2}_{\text{Tractive force tracking error}}$$

$$+ \underbrace{\frac{w_3}{a^2 (F_{tr}, t) + w_0}}_{\text{Performance}} + \underbrace{w_4 j^2 (F_{tr}, t)}_{\text{Driveability}}] dt \qquad (5.47)$$

Where,

a vehicle acceleration in m/s^2,

j vehicle jerk in m/s^3,

$w_{0,3,4}$ weighting coefficients for vehicle performance and driveability.

The vehicle acceleration shown in equation (5.47) is in the denominator, implying that the acceleration needs to be maximized to achieve good performance. The total tractive force at the wheels is to be optimized to achieve the best fuel economy, performance and driveability. More weights are on performance and driveability during vehicle hard acceleration and braking and more weights are on fuel economy during vehicle coasting.

For the performance (top speed, stopping distance, gradeability and towing capability) and the driveability (the acceleration RMS value and the VDV) criteria which are set to be greater or less than certain values should not be written into the cost function, but they are checked after the optimal solution is found. Minimizing jerk will minimize the oscillations in the acceleration profile and may reduce the acceleration RMS and the VDV values simultaneously.

An analytical optimal solution is realistic only when every term in equation (5.47) can be expressed as an explicit algebraic equation of the control variables. In practice, even if these expressions are available, the complexity of the cost function generally prevents an analytical solution to be found. Hence, it is more realistic to solve complex cost function numerically. The focus of this dissertation is not to provide the solution for equation (5.47), but to find the optimal solution for best fuel economy, to formulate the optimization considering all three aspects and to introduce some preliminary results about how fuel economy, performance and driveability could be affected.

5.2.2 Relationship of Control Variables with Performance and Driveability Measures

The performance and driveability measures are related with the control variables such as mass flow rate of air, ISA torque, brake torque and CVT ratio. Table 5.2 shows the effects of these control variables on performance and driveability measures. When setting upper or lower limits for the derivative of these control variables, i.e., limiting the changing rate of these control variables, vehicle fuel economy, performance metrics of acceleration time, top speed and top speed-to-0 braking distance, and driveability metrics of VDV, RMS, MTVV and jerk are all affected.

Metrics / Control Variable		Fuel Economy (mile/gal)	Acceleration Time (s)	Top Speed (mph)	Braking Distance (m)	MTVV (m/s^2)	VDV (m/s$^{1.75}$)	RMS (m/s^2)	Jerk (m/s^3)
Baseline		9.80	8.64	100.88	183.35	7.70 -6.37	1.97	0.144	See Figure 5.37
Air Mass Flow Rate	Upper Limit (0.01)	↑↑	**12.20**	**100.85**	183.35	**3.35** -6.37	1.31	0.098	1↓↓, 2↓↓
	Lower Limit (-0.01)	↓↓↓	8.64	100.88	339.55	7.70 -3.77	1.99	0.160	6↓↓, 7↓↓ 8↑↑
ISA Torque	Upper Limit (50)	↓	9.60	100.88	183.35	5.85 -6.37	1.58	0.121	1↓↓, 2↓↓ 8↑
	Lower Limit (-50)	↑↑	8.64	100.88	186.11	7.70 -6.37	1.94	0.140	3↓↓↓, 4↓↓↓ 8↑
Brake Torque	Upper Limit (50)	↑↑↑	8.64	100.88	**398.11**	7.70 **-3.75**	1.88	0.121	8↓↓, 5↑↑, 7↑↑
	Lower Limit (-50)	Same as baseline	8.64	100.88	183.35	7.70 -6.37	1.96	0.139	8↑↑
CVT Ratio	Upper Limit (0.025)	↓	8.64	100.88	183.35	7.70 -6.37	1.97	0.144	Same as baseline
	Lower Limit (-0.025)	↓	8.64	100.88	206.10	7.70 -5.61	1.97	0.144	6↓, 7↑, 8↑
Promising Control		↑↑↑	9.57	100.88	283.57	5.32 -6.09	**0.90**	**0.07**	1↓↓↓, 2↓↓↓ 3↓↓↓, 4↓↓↓ 5↑↑, 8↑

(Bold: maximum or minimum values in each column.)

Table 5.2 Effects of the Derivative of the Control Variables on Fuel Economy, Performance and Driveability Measures

Figure 5.37 shows vehicle jerk profile under the baseline controller. All positive and negative spikes are labeled with numbers. Triple arrows in Table 5.2 indicate significant changes, double arrows are for big changes and single arrows represent small changes. Arrows pointing up imply an increase in the length of the spike regardless of its sign and vice versa.

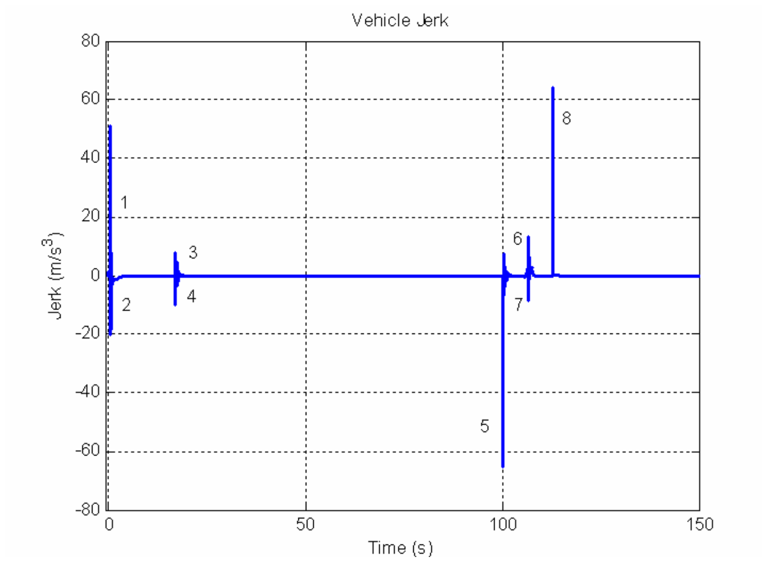

Figure 5.37 Vehicle jerk for the baseline vehicle under hard-acceleration/deceleration test

Limiting the derivative of the control variables has significant influence on vehicle fuel economy, performance and driveability. For instance, vehicle fuel economy is significantly affected by the increasing rate of the brake torque and the decreasing rate of the air mass flow rate since either to use more brake or to delay fuel cutting down will increase vehicle fuel consumption. The restrictions on the maximum air mass flow rate and minimum ISA torque improve fuel economy. The former technique cuts down the fuel usage while the latter one helps to have more ISA torque involved in the deceleration to save fuel in the future.

Limiting the increasing rate of the air mass flow rate and the ISA torque dramatically changes vehicle 0-60 mph acceleration time since the vehicle could not use the full power. The top speed would be affected in both cases if the ISA was used during the full acceleration process (The ISA was actually shut down when the vehicle reached a quarter miles). The upper boundary of the brake torque is the most important factor for the stopping distance. In addition, this distance would be lengthened if the engine torque cannot quit fast enough during hard deceleration. Introducing or removing a torque in the drivetrain suddenly would increase the VDV, RMS value and the jerk. The spike 1 and 2 in Figure 5.37 are related with initial acceleration, so limiting the total tractive force would reduce them. Shutting down the ISA abruptly during acceleration causes spikes 3 and 4 and thus they almost disappear when the ISA torque decreasing rate is bounded. If the brake cannot be pushed hard enough, the spike 5 would increase. Spike 8 is related with the removal of all torques in the drivetrain when the vehicle approaches a full stop. Therefore, setting lower limits for all the control variables would increase it. The CVT ratio has minor influence on fuel economy, performance and driveability. This is due to the fact that the ratio in the baseline controller only makes slow and smooth changes.

In summary, any technique encouraging less energy waste improves vehicle fuel economy. Holding the engine to work while unnecessary will consume more fuel. Any limitation on the total tractive power reduces vehicle top speed, delays acceleration and hence results in longer acceleration time. The vehicle takes longer to stop when the total braking torque is saturated. All driveability measures are related with the vehicle acceleration. Introducing and removing torques slowly from the powertrain improves driveability. It is evident that vehicle performance and driveability are contradictory. Good vehicle performance asks for quickly kicking in or out tractive or braking torques while good driveability requires these torques to be established or eliminated as gently as possible.

A solution considering vehicle fuel economy, performance and driveability for the hard-acceleration-deceleration test is proposed based on the simulation results shown in Table 5.2. Setting the upper limit for the air mass flow rate and the brake torque together with both limits for the ISA torque (see Table 5.3) significantly improves vehicle fuel economy and driveability, but brings in acceptable degradations in vehicle acceleration time and stopping distance.

Air Mass Flow Rate Derivative	ISA Torque Derivative		Brake Torque Derivative
Upper Limit	Upper Limit	Lower Limit	Upper Limit
0.05	100	-50	500

Table 5.3 Limits of the Control Variable Derivatives for the Controller Considering Fuel Economy, Performance and Driveability

In Figure 5.38, limitations on air mass flow rate and ISA torque derivatives significantly reduce spikes 1, 2, 3 and 4. However, spikes 5 and 8 are slightly increased due to the limited ISA and brake torque derivatives.

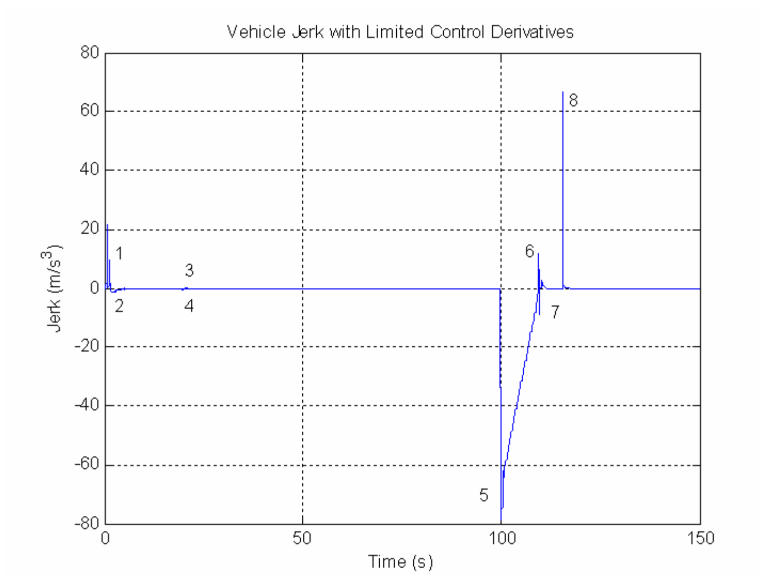

Figure 5.38 Vehicle jerk with limited control derivatives under hard-acceleration/deceleration test

5.3 Summary

This Chapter introduces the control strategy which considers fuel economy, performance and driveability. The optimal control solution for best fuel economy and performance is found in three steps before driveability is taken into account: for known constant power requests, for known time-varying power requests and for unknown time-varying power requests with short-term predictions. In the step of optimizing fuel economy with constant power requests, the solutions for both constant and variable battery parameters are found. Fixed CVT ratio is only considered in the constant power requests with constant battery parameter case. In all the other cases, the CVT ratio is free to select and thus it becomes one of the control variables. Except for the case with constant battery parameter for constant power requests where finding an analytical solution is possible, the solutions for other cases are all found numerically. The sliding optimal control which switches between two best control values has been theoretically proven to be the optimal solution for constant power requests with constant battery parameter and fixed CVT ratio. Simulation results demonstrate that the optimal solutions found with Pontryagin's minimum principle have an improvement over the heuristic controller. The fuel economy improvement is slightly decreased when the future driving condition is not known in prior.

This Chapter also introduces one way to formulate the optimization problem which has fuel economy, performance and driveability in the cost function without giving the solution. Some simulation results indicate that limiting the derivative of the control variables can effectively change vehicle fuel economy, performance and driveability. Taking tradeoffs among these limits results in an overall better fuel economy, performance and driveability.

CHAPTER 6

CONCLUSIONS AND FUTUREWORK

6.1 Conclusions

The objective of this research is to design an optimal supervisory control strategy for a parallel hybrid electric vehicle with fuel economy, performance and driveability as the control criteria. Due to the fact that the control strategy is designed based on models and tested in simulations, this research also includes building the appropriate models and simulators for control design and defining the objective measures for the control criteria. The control and the model here are called model based control and control oriented model. The model based control design applies optimal control theories and develops the strategy based on the control oriented model. The control oriented model needs to be appropriate for control strategy design, i.e., adequate to evaluate control criteria but not too complex to develop the control strategy.

Since the control strategy is found for the minimum fuel consumption first and then takes the driveability into consideration, two models, the quasi-static and the low-frequency dynamic models are established correspondingly. Both models are validated in simulations according to engineering knowledge and other testing-validated simulators. These two models are respectively effective in describing powertrain dynamics, estimating fuel economy, predicting vehicle performance, and evaluating driveability with adequate fidelity. The simulators provide software test beds for powertrain dynamics analysis and control strategy testing. This allows the designers to exploit tradeoffs between energy storage and conversion systems to achieve optimization in the face of multiple conflicting criteria of fuel economy, performance and driveability.

Evaluating vehicle fuel economy, performance and driveability in simulations and real vehicles requires objective and quantitative measures. Subjective and descriptive metrics cannot be easily implemented in simulations, and these evaluations vary with changing time or evaluators. Fuel economy is usually estimated under various city, highway and some other user-defined driving schedules. Performance criteria consist of acceleration/deceleration performance, gradeability and towing capability. Driveability measures deal with pedal responsiveness, operating smoothness and driving comfort, which include interior noise level, jerk, tip-in/tip-out response, Maximum Transient Vibration Value, acceleration Root Mean Square value and Vibration Dose Value. This dissertation also introduces the numerical references and provides interpretations for these metrics.

The optimal control strategy is designed hierarchically by using Pontryagin's minimum principle instead of the calculus of variations. This is mainly because the system state and control variables are both bounded. Even though dynamic programming provides a global optimal solution, the principle by its nature prohibits real-time applications and thus is not applied in this research. As mentioned earlier, the control strategy for minimum fuel consumption is found first. This has been partitioned into several sub-problems: finding the solution for constant power requests with constant or variable battery parameters with fixed or free to select CVT ratio, for time-varying power requests (e.g., known driving cycles) and for the cases with limited predictable future driving conditions. The control strategy which considers driveability is then tackled based on the investigations on control variables' effects on the fuel economy, performance and driveability measures.

The minimum principle is applied and interpreted in an innovative way when finding the optimal solution for constant power requests with constant battery parameters and fixed CVT ratio. Since there exist two controls leading to the minimum Hamiltonian while either one alone can satisfy the state boundary conditions, the control then takes these two values alternatively as if the dynamic equivalent control can satisfy these conditions. This so-called sliding optimal control is considered as an extension to the conventional minimum principle to deal with the problem where multiple minimum points exist but none of them can satisfy the state boundary conditions by itself. This dissertation introduces both the complete solution for this case and also the theoretical proof of the optimality of the sliding optimal control strategy. This sliding optimal control strategy has been demonstrated to improve fuel economy up to 55% from an engine-powered only counterpart.

When battery parameters depend on the battery SOC, the system state, the optimal control will take two values along time as supported by the conventional minimum principle. The difference of this case compared to the last one lies in the fact that the co-state variable remains constant for the constant battery parameter case and varies in the variable battery parameter case. The Hamiltonian also varies with the co-state variable and thus has different single minimum point when time changes.

When the CVT ratio is not fixed, the optimal control tends to select the highest gear to have the engine operating points concentrate at lower speed and higher torque region. This is exactly the high engine efficiency region.

The optimal solution for time-varying power requests, such as known driving cycles is found numerically. The key issue here is to search for the right initial value of the co-state variable such that splitting the power requests between the engine and the electric machine gives the minimum Hamiltonian in each step and the final value of the state variable is equal to the desired one at the same time.

In the case that the entire trip is unknown in prior but limited future driving information is available, the optimal control strategy is also found numerically. It is expected that the fuel economy is decreased and it is harder to keep the state final value as desired when comparing with the case where all the driving conditions are considered at the beginning of the optimization.

Based on the investigations on the influences of the control variable derivatives on vehicle fuel economy, performance and driveability, this dissertation proposes a strategy which takes tradeoffs among them for the hard-acceleration-deceleration test. Setting the upper limit for the air mass flow rate and the brake torque in addition to both upper and lower limits for the ISA torque significantly improves vehicle fuel economy and driveability, but brings in acceptable degradations in the acceleration time and stopping distance. Research on optimizing vehicle fuel economy, performance and driveability simultaneously is extremely challenging and may not be solvable. Finding the solution to this problem is left as future work.

6.2 Future Work

There exist a few directions to continue this research. On the modeling aspect, the future work will concentrate on model validation using a prototype (such as Future Truck) or the hardware-in-the-loop (HIL) lab [116].

The objective metrics for fuel economy, performance and driveability is not perfectly complete. Finding other effective measures especially for driveability is an on-going task. In addition, defining the measures which can be written as explicit functions of the control variables is highly preferable.

There is more freedom to continue this research regarding to the optimal supervisory control strategy design. Optimizing fuel economy, performance and driveability at the same time is an extremely challenging problem. How good the solution is and whether the problem is solvable depends heavily on the problem formulation. Therefore, formulating a feasible optimization problem to optimize fuel economy, performance and driveability simultaneously is of great interest. Investigations on the influence of prediction window length on the fuel economy improvement and studies on the prediction error effects also provide a rich research topic in the HEV control area. Implementation and validation of the optimal control strategy in real vehicles is critical and interesting as well.

APPENDIX A

ADDITIONAL DRIVING CYCLES AND PERFORMANCE MANEUVERS

<u>Driving Cycles</u>

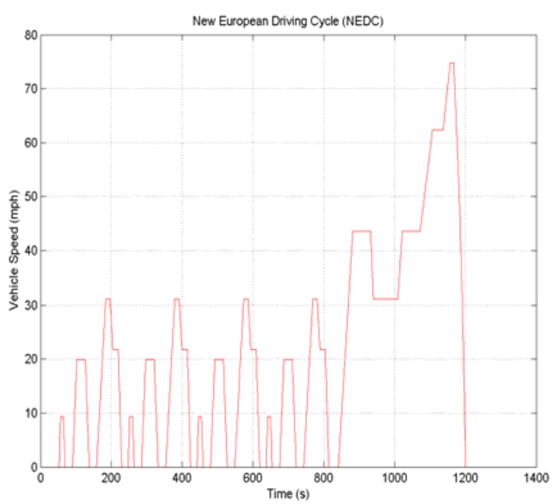

Figure A.1 New European Driving Cycle

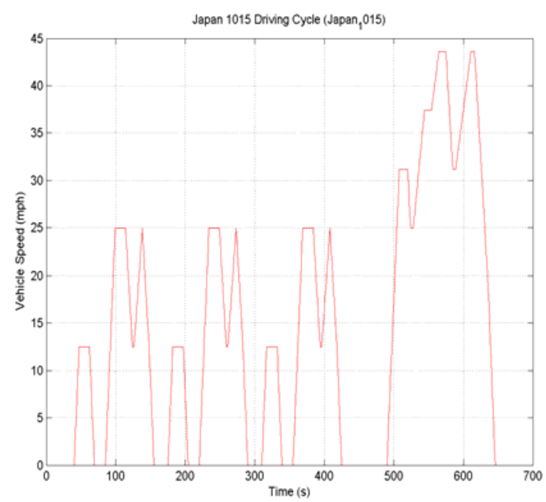

Figure A.2 Japan 1015 Driving Cycle

Performance Maneuvers

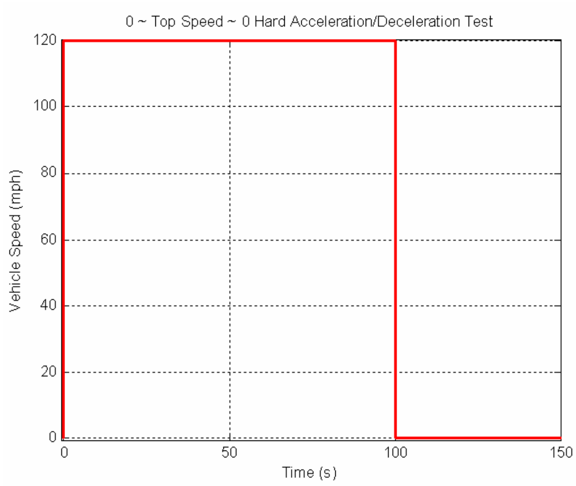

Figure A.3 0 ~ Top Speed ~ 0 Acceleration Test

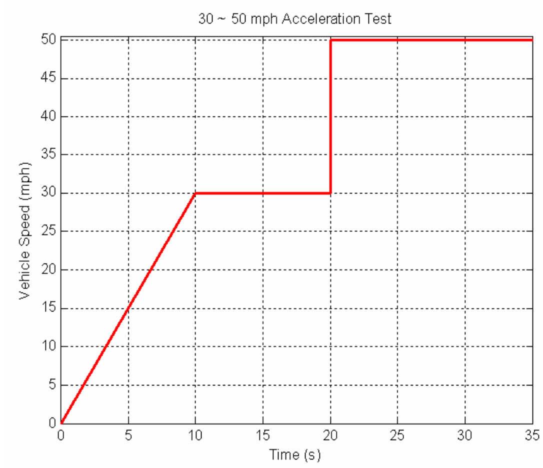

Figure A.4 30 ~ 50 mph Acceleration Test

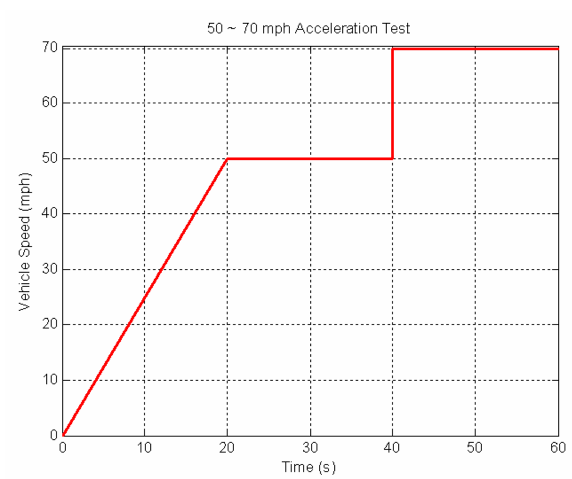

Figure A.5 50 ~ 70 mph Acceleration Test

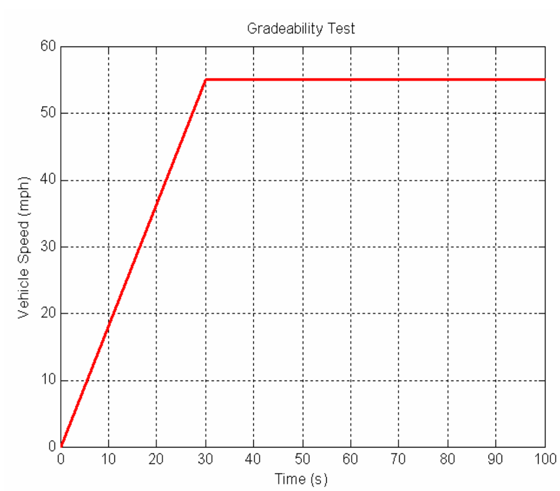

Figure A.6 Gradeability Test

APPENDIX B

MODEL IMPLEMENTATION

The quasi-static and dynamic models described in the chapter #4 are implemented in MATLAB®/SIMULINK®. All the components are programmed as subsystems in a library. In practice, the simulation sampling frequency needs to be about 5 to 10 times of the highest frequency in the system.

This simulator is only applicable for vehicles driving on straight roads without cornering. The objective metrics of fuel economy, performance and driveability used in the dynamic model include fuel economy of standard driving cycles; 0-60, 30-50 and 50-70 mph acceleration time, top speed, stopping distance, gradeability, towing capability; jerk, acceleration profile properties, the VDV, the RMS and the MTVV values.

Besides the official driving cycles, four extra maneuvers are included in the dynamic simulator to evaluate vehicle performance. They are the 0 to top speed then back to 0 mph hard acceleration/deceleration test, the 30~50 mph and the 50~70 mph passing maneuvers, and the gradeability test maneuver (see Appendix A). The hard acceleration/ deceleration test is able to evaluate 0~60 mph acceleration, top speed and stopping distance. This maneuver is designed as two steep ramps close to step functions at the initial time and 100 s, so that the 'Driver' will interpret these two ramp speed commands as full accelerator and brake pedal requests respectively. In the 30~50 mph acceleration test, the vehicle should reach steady state velocity before it starts to accelerate from 30 mph. A moderate ramp from 0 to 30 mph will lead the vehicle to reach 30 mph and it will stabilize at this speed during a 10-second constant speed request period. Then, the vehicle will speed up to track the 30~50 mph steep ramp command. The 50 to 70 mph maneuver is implemented in a similar way.

Due to the causality and the anti-noise concerns, the derivative and the "memory" blocks should appear only if it is inevitable. An anti-windup PID controller is used for the "Driver" block. The *I* term integrates the difference between the desired and the actual speed. If the speed difference has been remained with the same sign for a while, the integral term is accumulated to a relative large value. When the speed difference changes its sign after *I* term became large, it will take long time to bring it back to zero and respond to the current input. This often causes unstable system response and it can be effectively resolved by setting the initial condition of the integrator to zero whenever the speed difference changes sign.

B.1 Parameter Selection

Parameters selected for this mid to full size parallel hybrid electric vehicle are listed in Table B.1 from [117-121]. Neither the powertrain configuration nor the component sizing is optimized.

Component	Parameter Name	Value	Unit
Engine	ETB time constant	0.06	s
	Engine displacement	0.0022	m^3
	Intake manifold volume	0.0022	m^3
	Engine cylinder number	4	
	Engine idle and redline speed	750/6000	rpm
	lumped inertia of engine, ISA and TC pump	0.0843	$N{\cdot}m{\cdot}s^2/rad$
	Engine damping coefficient	0.1	N·m·s/rad
Integrated Starter/Alternator w. Battery	ISA power rating (peak)	30	kW
	ISA time constant	0.01	s
	Battery capacity	7.128	MJ
	Battery initial SOC	0.7	
Torque Converter w. Minimum-Slip Clutch	Pump torque coefficients in torque multiplication mode	0.0034325 0.002221 -0.0046041	
	Turbine torque coefficients in torque multiplication mode	0.0057656 0.0003107 -0.0054323	
	Pump and turbine torque coefficients in torque coupling mode	-0.0067644 0.0320084 -0.0252441	
	Lockup clutch maximum transmitting torque	350	N·m
	Lockup clutch minimum speed difference	50	rev/min
	Lockup clutch engaging time	1	s
Continuously Variable Transmission	CVT ratio range	0.42 ~ 2.15	
	CVT time constant	0.85	s
	CVT efficiency	0.85	
	lumped inertia of TC turbine and CVT primary	0.042	$N{\cdot}m{\cdot}s^2/rad$
	lumped inertia of CVT secondary pulley, final drive and wheels	0.05	$N{\cdot}m{\cdot}s^2/rad$
Final Drive	Final drive ratio	3.7	
	Final drive efficiency	0.95	
Driveshaft	Driveline stiffness	2300	N·m/rad
	Linear driveshaft damping coefficient	0.05	N·m·s/rad
	Quadratic driveshaft damping coefficient	0.005	$N{\cdot}m{\cdot}s^2/rad^2$
Brake-By-Wire	BBW time constant	0.05	s
Vehicle	Vehicle mass	1450	kg
	Frontal area	2.0	m^2
	Drag coefficient	0.3	
	Rolling resistance coefficient	0.01	
	Wheel radius	0.31	m
Driver	PID gains	0.27/0.013/0	

Table B.1 Vehicle Parameters

B.2 Simulation Results and Model Validity

The following results are for the hard acceleration/ deceleration test shown in Figure B.1 where "*s*" denotes the quasi-static model and "*d*" denotes the dynamic model. In order to reveal powertrain excitation dynamics and to estimate the sustainable vehicle top speed, the ISA was shut down abruptly when the vehicle reached a quarter mile (at 17 s). The CVT ratio is set to maintain constant maximum power from the engine during acceleration.

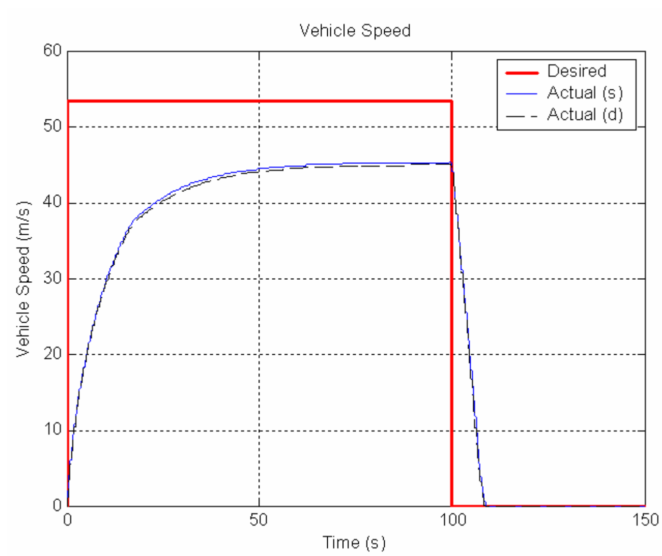

Figure B.1 Actual vehicle velocity in hard acceleration/deceleration test

Performance criteria such as 0 to 60 mph acceleration, top speed and top speed to 0 mph stopping distance of this vehicle in both models are about 8.71 s, 101 mph and 172.8 m as indicated in Figure B.1. This figure also shows that the vehicle speed in two models matches because the vehicle speed depends only on the power in the drivetrain and vehicle dynamics. The delays introduced in the dynamic model are in the order of less than 100 ms and these do not affect the vehicle speed represented in a larger scale.

Figure B.2 and Figure B.3 depicts ISA and BBW torque commands, engine air or torque request and engine speed.

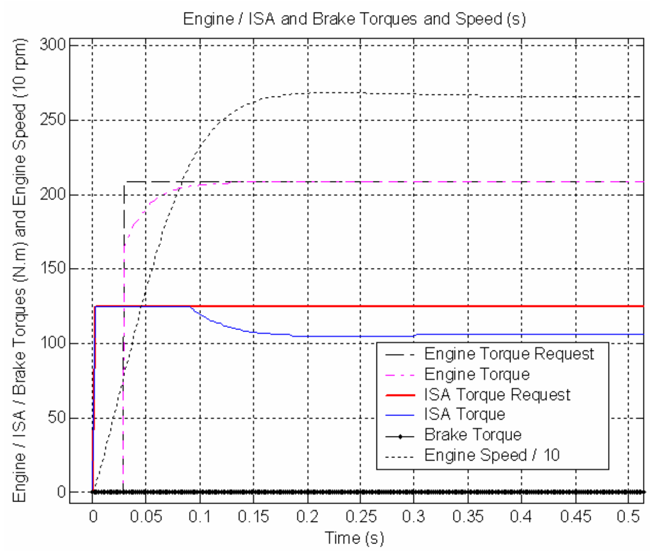

Figure B.2 Vehicle behaviors during launch simulated in the quasi-static model

In the dynamic model, it takes the ISA approximately 70 ms to start the engine, while the engine torque remains negative for another 60 ms after it is started due to the ETB lag and the torque production delay. Actual ISA torque follows the torque request as a first order system and begins to drop when it enters the flux weakening region after 200 ms. The quasi-static model does not show the throttle and the torque production delays. The engine and the ISA torque requests are satisfied immediately. Consequently, the engine speeds up faster than it does in the dynamic model. While the steady state value of the speed and torques in two models are close.

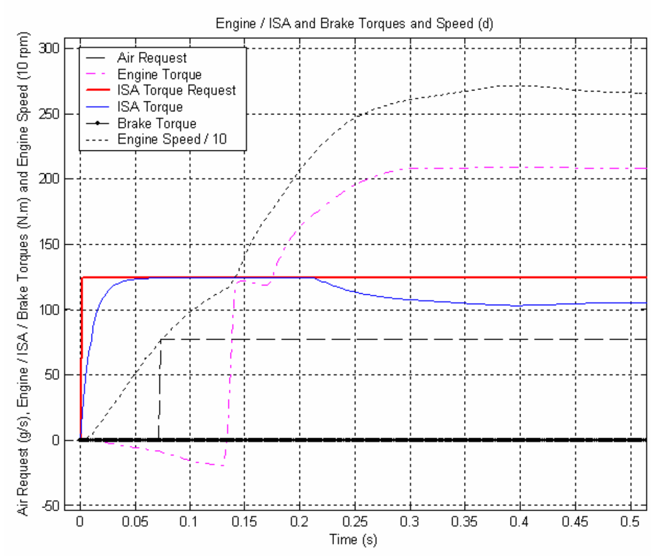

Figure B.3 Vehicle behaviors during launch simulated in the dynamic model

Figure B.4 and Figure B.5 describe CVT behaviors in the two models.

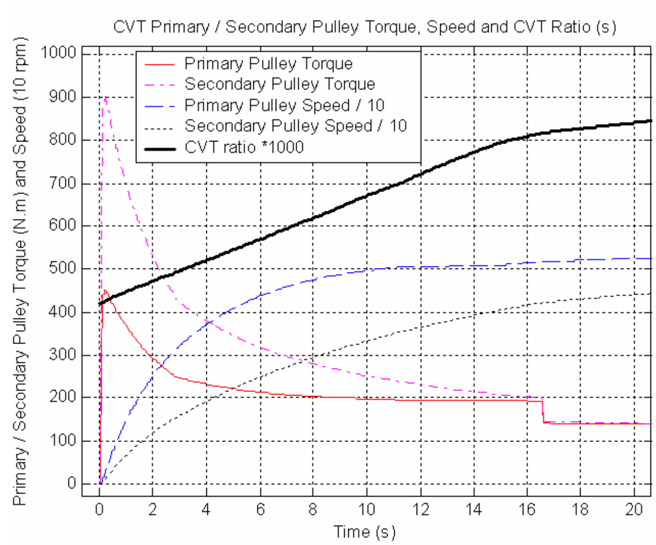

Figure B.4 CVT torques, speeds and ratio simulated in the quasi-static model

Due to sudden introduction and removal of the ISA torque, oscillations of less than 5 Hz in torques and speeds are observed at the very beginning and around 17 s of the test shown in Figure B.4. It is evident that the static model cannot capture the dynamics in the drivetrain and shows no oscillations in Figure B.5.

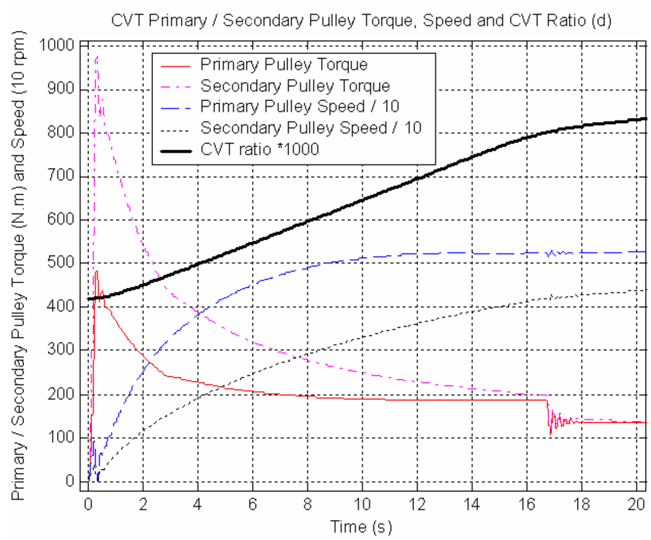

Figure B.5 CVT torques, speeds and ratio simulated in the dynamic model

In Figure B.6, acceleration for the first five seconds simulated in the dynamic model shows both delay and oscillations. Apparently, these oscillations are propagated from the upstream (the engine side). Hard deceleration starting at 100 s causes similar vibrations in the drivetrain. Ultimately, all of these vibrations should be minimized in the control strategy. The maximum acceleration/deceleration is about 0.8/0.65 g, which in turn results in high jerk of more than 50 m/s^3 for less than 50 ms. The VDV and the RMS values of this maneuver are 1.97 $m/s^{1.75}$ (7.33 $m/s^{1.75}$ if normalized to 8 hours) and

0.144 m/s^2. These values for the FUDS and the FHDS are 2.36/1.33 m/s$^{1.75}$ (5.04/3.29 m/s$^{1.75}$ if normalized to 8 hours) and 0.12/0.05 m/s^2, which indicate acceptable overall vibration dosage [30] (see Figure B.7).

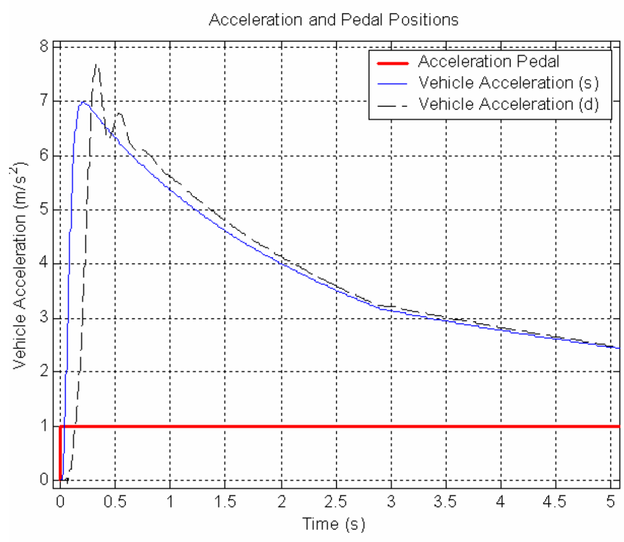

Figure B.6 Vehicle acceleration profile for the first 5 second during lunch

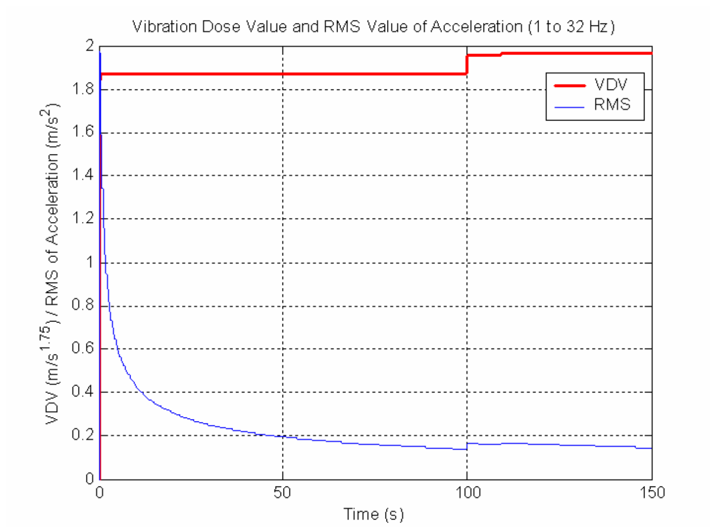

Figure B.7 Vibration dose value and acceleration RMS value

Acceleration profile simulated with the static model is smooth as expected when noticing this model did not reveal any oscillations in the CVT speeds and torques in Figure B.4. Figure B.6 also shows unreal shorter delay in the quasi-static model since the engine and the ISA reach the commands without any delay. Smooth profile with incredible short delay in the vehicle acceleration indicates untruthful driveability measures and proves that the quasi-static model is indeed not sufficient to represent driveability issues. Furthermore, the frequency of the vibrations in the CVT torques and the acceleration is close to that in a real vehicle, proving that this low-frequency dynamic model is an appropriate model to evaluate vehicle driveability.

Figure B.8 shows the battery SOC in the hard acceleration/deceleration test. It is clear that the ISA discharges the battery during the acceleration before 17 s where the vehicle reaches a quarter miles and then recharges the battery during deceleration until the vehicle stops.

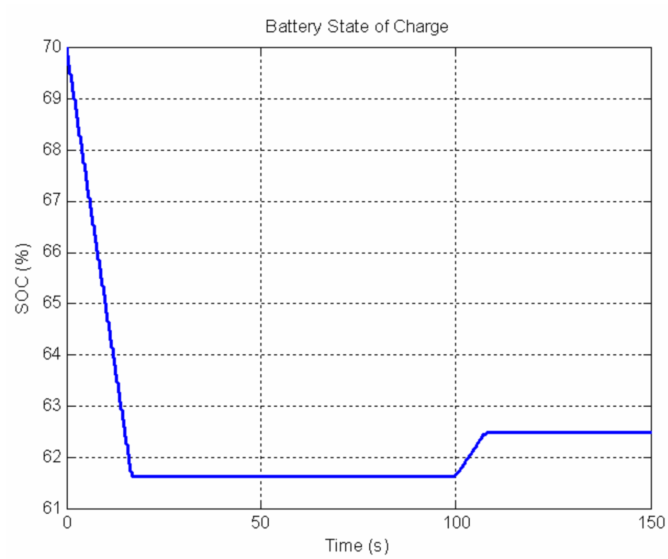

Figure B.8 Battery State of Charge

Vehicle fuel economy is mainly determined by energy flows in the vehicle. Therefore, introducing dynamics in a model does not affect the fuel economy calculation. Estimated city (FUDS) and highway (FHDS) mileage are about 21.7 and 25 mile/gal respectively in both models. Fuel economy could be improved with controller targeting to minimize fuel consumption.

Harmonics of the drivetrain is analyzed in order to verify the frequency components observed in the dynamic simulator. Figure B.9 and Figure B.10 are the frequency response of the drive shaft angular displacement with respect to input shaft torque when the TC is locked or unlocked. System resonance frequencies are listed in Table B.2.

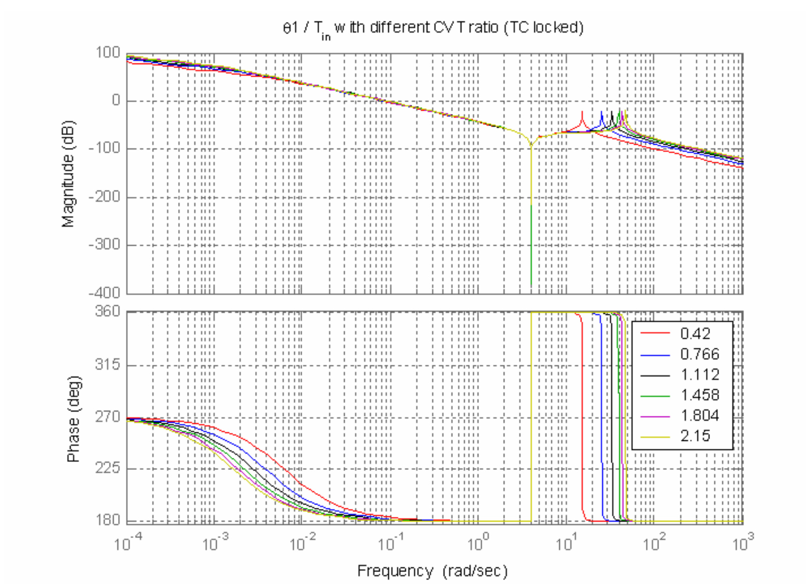

Figure B.9 System frequency analysis when TC is locked

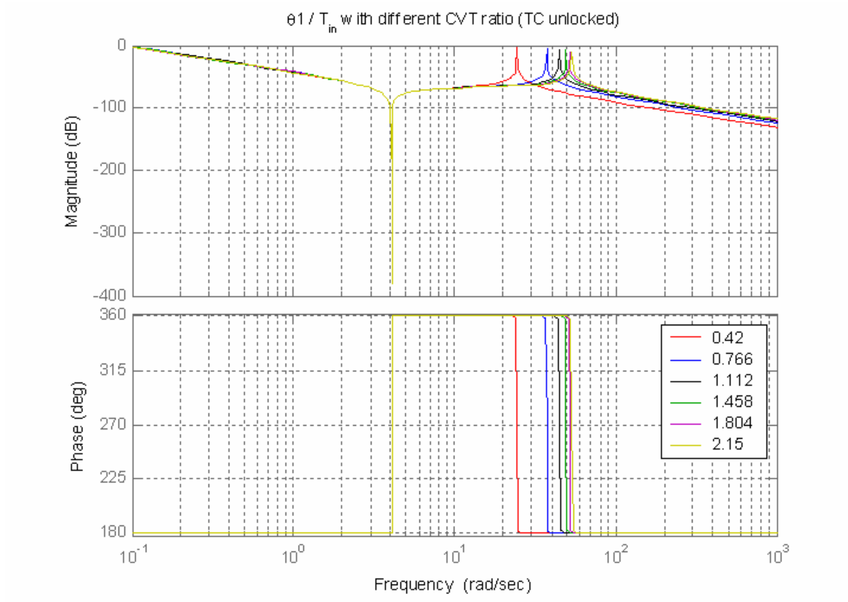

Figure B.10 System frequency analysis when TC is unlocked

Torque Converter Status	System Resonance (Hz)
TC locked	2.45 ~ 7.46
TC unlocked	3.90 ~ 8.51

Table B.2 System Resonances When the TC is Locked or Unlocked

The frequency of the oscillations observed in the drivetrain is in the frequency ranges listed in Table B.2. The minor discrepancies may be resulted from figure-reading inaccuracy and the linear approximation of the driveline nonlinear damper.

The low-frequency nonlinear dynamic model in this paper is effective in describing powertrain dynamics, estimating fuel economy, predicting vehicle performance, and evaluating driveability with adequate fidelity. It allows the designers to exploit tradeoffs between energy storage and conversion systems to achieve optimization in the face of multiple conflicting criteria of fuel economy, performance and driveability. When the optimization objectives only contain fuel economy and performance, a quasi-static model is sufficient without complicating the problem. Simulation results demonstrate that these two models provide good representation of the vehicle for fuel economy and performance or fuel economy, performance and driveability evaluations.

BIBLIOGRAPHY

1. Grava S., 2003, *Urban Transportation Systems Choices for Communities*, McGraw-Hill, New York.

2. Chan C., Chau K., 2001, *Modern Electric Vehicle Technology*, Oxford, New York.

3. Wouk V., 1995, "Hybrids: Then and Now", *IEEE Spectrum*, **33**, July, pp.16-21.

4. Soong W., Ertugrul N., Lovelace E., Jahns T., 2001, "Investigation of Interior Permanent Magnet Offset-Coupled Automotive Integrated Starter/Alternator", *Proceedings of Industry Applications Conference*, **1**, pp. 429-436.

5. Frijlink P., Schaerlaeckens W., Tillaart.E., Haas J., 2001, "Simulation of a Vehicle with an ICE, CVT, and ISG Powertrain – A Pre-study for Concept Evaluation and Dimensioning", *SAE paper 2001-01-3453*.

6. Miyano T., Hubbard M., 1990, "Internal Combustion Engine Intake-Manifold Aspiration Dynamics", *Journal of Dynamic Systems, Measurements, and Control*, **112**, pp. 596-603.

7. Sung N., Song J., Jeong Y., Kim C., 1996, "Flow Modeling for the Branched Intake Manifold Engine", *SAE paper 960079*.

8. Krause P., Wasynczuk O., 1989, *Electromechanical Motion Devices*, McGraw-Hill, New York.

9. Paganelli G., Guezennec Y., Kim H. and Brahma A., 2001, "Battery Dynamic Modeling and Real-Time State-of-Charge Estimation in Hybrid Electric Vehicle Application", *Proceedings of ASME IMECE DSC-7B1*, *New York*.

10. Hrovat D., Tobler W., 1985, "Bond Graph Modeling and Computer Simulation of Automotive Torque Converters", *Journal of Franklin Institute*, **319**, pp. 93-114.

11. Pfiffner R., 2001, "Optimal Operation of CT-Based Powertrains", *Ph.D. Dissertation, Swiss Federal Institute of technology*, Zurich, Switzerland.

12. Kotwicki A., 1982, "Dynamic Models for Torque Converter Equipped Vehicles", *SAE paper 820393*, pp. 103-117.

13. Yurkovich S., Simpson M., 1997, "Comparative Analysis for Idle Speed Control: A Crank-Angle Domain Viewpoint", *Proceedings of American Control Conference, Albuquerque, NM*, pp. 178-283.

14. Butts K., Sivashankar N., Sun J., 1999, "Applications of l_1 Optimal Control to the Engine Idle Speed Control Problem", *IEEE Transactions on Automatic Control*, **34**, pp. 386-396.

15. Sun P., Powell B., Hrovat D., 2000, "Optimal Idle Speed Control of an Automotive Engine", *Proceedings of American Control Conference, Chicago, IL*, pp. 1018-1026.

16. Fekete N., Nester U., Gruden I., Powell J., 1995, "Model-Based Air-Fuel Ratio Control of a Lean Multi-Cylinder Engine", *SAE paper 950846*, pp. 71-83.

17. Liu S., Stefanopoulou A., 2002, "Effects of Control Structure on Performance for an Automotive Powertrain with a Continuously Variable Transmission", *IEEE Transactions on Control Systems Technology*, **10**, pp. 701-708.

18. Rizzoni G., Guezennec Y., Brahma A., Wei X., Miller T., 2000, "VP-SIM: A Unified Approach to Energy and Power Flow Modeling Simulation and Analysis of Hybrid Vehicles", *Proceedings of the 2000 Future Car Congress*, *Arlington, Virginia*.

19. Wipke K., Cuddy M., Burch S., 1999, "ADVISOR 2.1: A User-Friendly Advanced Powertrain Simulation Using a Combined Backward/Forward Approach", *IEEE Transactions on Vehicular Technology*, **48**, pp. 1751-1761.

20. Guzzella L. and Amstutz A., 1999, "CAE-Tools for Quasistatic Modeling and Optimization of Hybrid Powertrains", *IEEE Transactions on Vehicular Technology*, **48**, **6**, pp. 1762-1769.

21. Brahma A., Guezennec Y, Rizzoni G., 2000, "Optimal Energy Management in Series Hybrid Electric Vehicles", *Proceedings of the American Control Conference, Chicago, Illinois*, pp. 60-64.

22. Paganelli G., Ercole G., Brahma A., Guezennec Y, Rizzoni G., 2001, "General Supervisory Control Policy for the Optimization of Charge-Sustaining Hybrid Electric Vehicles", *JSAE 20014505*, pp. 511-518.

23. Jalil N., Kheir N., Salman M., 1997, “A Rule-Based Energy management Strategy for a Series Hybrid Vehicle”, *Proceedings of the American Control Conference*, pp. 689-693.

24. Baumann B., Washington G., Glenn B., Rizzoni G., 2000, “Mechatronics Design and Control of Hybrid Electric Vehicles”, *IEEE/ASME Transactions on Mechatronics*, **5**, pp. 58-72.

25. Momoh J., Wang Y., Elfayoumy M., 1997, “Artificial Neural Network Based Load Forecasting”, *IEEE International Conference on Computational Cybernetics and Simulation*, **4**, pp. 3443-3451.

26. Rubin Z., Munns S., Moskwa J., 1997, “The Development of Vehicular Powertrain System Modeling Methodologies: Philosophy and Implementation”, *SAE paper 971089*.

27. Wei X., Rizzoni G., 2001, “A Scalable Approach for Energy Converter Modeling and Supervisory Control Design”, *Proceedings of ASME International Mechanical Engineering Congress and Exposition 2001, New York, NY*.

28. Schaffnit J., Sinsel S., Isermann R., 1998, “Hardware-in-the-loop Simulation for the Investigation of Truck Diesel Injection Systems”, *Proceedings of American Control Conference, Philadelphia, PA*, pp. 498-502.

29. Hanselmann H., 1996, “Hardware-in-the-loop Simulation Testing and its Integration into a CACSD Toolset”, *Proceedings of the 1996 IEEE International Symposium of Computer-Aided Control System Design, Dearborn, MI*, pp. 152-156.

30. Kwon W., Choi S., “Real-Time Distributed Software-In-the-Loop Simulation for Distributed Control Systems”, *Proceedings of the 1996 IEEE International Symposium of Computer-Aided Control System Design, Hawaii*, pp. 115-119.

31. Cook J, Sun J., Grizzle J., 2002, “Opportunities in Automotive Powertrain Control Applications”, *Proceedings of the 2002 IEEE International Conference on Control Applications, Glasgow, Scotland, UK*.

32. Kojima M., Osawa K., Inoue T., Takaoka T., 2002, “Highly efficient Hybrid Minivan with Super Low Emissions”, *SAE paper 2002-01-0992*.

33. Moore T., 1996, “Tools and Strategies for Hybrid-Electric Drivesystem Optimization”, *SAE paper 961660*, pp. 49-66.

34. www.sts.sae.prg/servicetech/sep-2001/42-v.pdf

35. Liu S., Paden B., 1997, "A Survey of Today's CVT Control", *Proceedings of the 36th Conference on Decision and Control*, *San Diego*, *California*, pp. 4738-4743.

36. Mayer T., Schroeder D., 1996, "Robust Control of a Parallel Drivetrain with a CVT", *SAE paper 960233*, pp. 47-54.

37. Jeon S., Kim K., Jo S., Lee J., 2001, "Driving Simulation of a Parallel Hybrid Electric Vehicle Using Receding Horizon Control", *Proceedings of IEEE International Symposium on Industrial Electronics*, **2**, 1180-1185.

38. Musardo C. and Staccia B., 2004, "Energy Management Strategies for Hybrid Electric Vehicles", *Master thesis at Polytechnic of Milan*, Italy.

39. Johnson V., Wipke K., Rausen D., 2000, "HEV Control Strategy for Real-Time Optimization of Fuel Economy and Emissions", *SAE paper 2000-01-1543*.

40. Piccolo A., Ippolito L., 2001, "Optimization of Energy Flow Management in Hybrid Electric Vehicles via Genetic Algorithms", *Proceedings of IEEE/ASME International Conference on Advanced Intelligent Mechatronics*, *Como*, *Italy*, **1**, pp. 434-439.

41. Kleimaier A., Schroder D., 2000, "Optimization Strategy for Design and Control of a Hybrid Vehicle", *Proceedings of 6th International Workshop on Advanced Motion Control*, pp. 459-464.

42. Fried O., Bargende M., Hotzer D., 2000, "Fuel Consumption Reduction for Electromechanical Powertrains under Driving Conditions", *Stuttgart Symposium*.

43. Rajagopalan A., Washington G., 2002, "Intelligent Control of Hybrid Electric Vehicles Using GPS Information", *2002 Future Car Congress, Arlington, VA*.

44. Quigley C., Ball R., Vinsome A., Jones R., 1996, "Predicting Journey Parameters for the Intelligent Control of a Hybrid Electric Vehicle", *Proceedings of the 1996 IEEE International Symposium on Intelligent Control*, *Dearborn*, *Michigan*, pp. 402-407.

45. Jeon S., Kim K., Jo S., Park Y., Lee J., 2002, "Multi-Mode Driving Control of a Parallel Hybrid Electric Vehicle Using Driving Pattern Recognition", *Journal of Dynamic Systems, Measurement, and Control*, **124**, 141-149.

46. Dongmo J., Salam F., Erten G., 1996, "Adaptive Fuzzy Control of AC Motors for Electric Vehicles and Manufacturing Systems", *Proceedings of the 1996 IEEE International Symposium on Intelligent Control*, *Dearborn*, *Michigan*, pp. 408-413.

47. Hendricks E., Luther J., 2001, "Model and Observer Based Control of Internal Combustion Engines", *Proceedings of the International Workshop on Modeling, Emissions and Control in Automotive Engines (MECA)*, *Fisciano*, *Italy*, pp. 9-21.

48. Baraszu R., Cikanek S., 2002, "Torque Fill-in for an Automated Shift Manual Transmission in a Parallel Hybrid Electric Vehicle", *Proceedings of the American Control Conference, Anchorage, Arkansas*, pp. 1431-1436.

49. Davis R., Lorenz R., 2002, "Engine Torque Ripple Cancellation with an Integrated Starter Alternator in a Hybrid Electric Vehicle: Implementation and Control", *Proceedings of the 37th Industry Application Conference*, **3**, pp. 2016-2020.

50. Nakano K., Ochiai S., 2000, "Development of the Motor Assist System for the Hybrid Automobile – the Insight", *SAE paper 2000-01-0079*, pp. 543-552.

51. Ciesila C., Jennings M., 1995, "A Modular Approach to Powertrain Modeling and Shift Quality Analysis", *SAE paper 950419*, pp. 139-147.

52. Schwab M., 1990, "Electronically-Controlled Transmission Systems – Current Position and Future Developments", *SAE paper 901156*, pp. 335-342.

53. Lee H., Sul S., Cho H., Lee J., 1998, "Advanced Gear Shifting and Clutching Strategy for a Parallel Hybrid Vehicle with Automated Manual Transmission", *Proceedings of the 33rd Industry Applications Conference,* **3**, pp. 1709-1714.

54. Kasai Y., Morimoto Y., 1988, "Electronically Controlled Continuously Variable Transmission (ECVT II)", *International Congress on Transportation Electronics*, pp. 33-42.

55. Jantos J., 2001, "Control of the Transmission Ratio Derivative in Passenger Car Powertrain with CVT", *SAE paper 2001-01-1159*.

56. Guzzella L., Schmid A., 1995, "Feedback Linearization of Spark-Ignition Engines with Continuously Variable Transmissions", *IEEE Transactions on Control Systems Technology*, **3**, pp. 54-60.

57. Foley D., Sadegh N., Barth E., Vachtsevanos., 2001, "Model Identification and Backstepping Control of a Continuously Variable Transmission System", *Proceedings of the American Control Conference, Arlington, Virginia*, pp. 4591-4596.

58. Kim W., Vachtsevanos., 2000, "Fuzzy Logic Ratio Control of a CVT Hydraulic Module", *Proceedings of the15th IEEE International Symposium on Intelligent Control, Rio, Patras, Greece*, pp. 151-156.

59. Kirk D., 1974, *Optimal Control Theory: An Introduction*, Prentice-Hill, Englewood Cliffs, New Jersey.

60. Stengel R., 1986, *Stochastic Optimal Control: Theory and Application*, John Wiley & Sons, New York.

61. Dorey R., Holmes C., 1999, "Vehicle Driveability – Its Characterization and Measurement", *SAE paper 1999-01-0949*.

62. Dorey R., McLaggan J., Harris J., Clarke D., Gondre B., 2001, "Transient Calibration on the Testbed for Emissions and Driveability", *SAE paper 2001-01-0215*.

63. Schoeggl P., Ramschak E., 2000, "Vehicle Driveability Assessment Using Neural Networks for Development, Calibration and Quality Tests", *SAE paper 2000-01-0702*.

64. Dorey R., Martin E., 2000, "Vehicle Driveability – The Development of an Objective Methodology", *SAE paper 2000-01-1326*.

65. Megli T., Haghgooie M., Colvin D., 1999, "Shift Characteristics of a 4-Speed Automatic Transmission", *SAE paper 1999-01-1060*.

66. www.chevron.com/prodserv/fuels/bulletin/motorgas/tech_fuels_bull.pdf

67. www.epa.gov

68. www.fueleconomy.gov/feg/info.shtml

69. www.fueleconomy.gov/feg/FEG2003.pdf

70. www.metricmind.com/data/cycles.pdf

71. www.dieselnet.com/standards/cycles

72. Dembski N., Guezennec Y., Soliman A., 2002, "Analysis and Experimental Refinement of Real-World Driving Cycles", *SAE paper 2002-01-0069*.

73. www.arb.gov/msei/on-road/downloads/pwbs/ucc-crcs.pdf

74. www.scottsdalelaw.com/shepston/braking.html

75. Electric vehicle Acceleration, Gradeability, and Deceleration, Test Procedure - SAE J1666 MAY93

76. www1.mn.man.de/manted/aufbaurichtlinien/gb_f10.html#Anchor-14210

77. www.cardirect.com/research/new_cars/buying_guides

78. www.consumersearch.com/www/automotive/suvs/comparisonchart.html

79. www.thecarplace.com/main.htm

80. www.sdt.com.au/STOPPINGDUSTANCE.htm

81. www.jasperjeep.com/images/dodgecars.pdf

82. www.hillerford.com/Web%20Pages/resource%20library/2002/2002cars

83. www.flippedit.net/F150/powertes.doc

84. www.s10planet.com/History/history_ss.htm

85. www.minivansearch.com/pontiac_montana.htm

86. www.edmunds.com/reviews/comparison/articles/46418/page025.html

87. www.epinions.com/auto-review-15A9-260ABE7-38C3F7CF-prod9

88. www.syty.org/old/d&e.html

89. 198.65.230.227/html/feat_8.asp

90. turva.me.tut.fi/iloagri/fore/vib2.htm

91. www.atsb.gov.au/road/rpts/cr203/std_vib.cfm

92. www.ergotech.co.za/vib_wbv.htm

93. www.fra.dot.gov/rdv/volpe/pubs/reports/hsr2fils/hsr2chp3.html

94. hyperphysics.phy-astr.gsu.edu/hbase/sound/intens.html

95. www.hse.gov.uk/hthdir/noframes/vibrate/vdv.htm

96. www.CivilEngineeringVibrations.com/vibration.pdf

97. www.dibdenterminal.co.uk/SUMMARY/FAWLEYBL/APENDA.pdf

98. Wicke V., Brace C., Vaughan N., 2000, "The potential for Simulation of Driveability of CVT Vehicles", *SAE paper 2000-01-0830*.

99. Chen Y., 1995, "Effect of Communication Delays on the Performance of Vehicle Platoons", *M.S. Dissertation, University of California, Berkeley*, Berkeley, CA.

100. vdcl.hanyang.ac.kr/research/0102.pdf

101. www.moderanracer.com/tips/brakingdistance.html

102. Wicke V., Brace C., Deacon M., Vaughan N., 1999, "Preliminary Results from Driveability Investigations of Vehicles with Continuously Variable Transmissions", *Proceedings of the International Congress on Continuously Variable Power Transmission, Eindhoven, Netherlands,* pp. 9-14.

103. Heywood J., 1988, *Internal Combustion Engine Fundamentals*, McGraw-Hill, New York.

104. Rizzoni G., Guzzella L., Baumann B., 1999, "Modeling and Design Optimization of Hybrid Vehicles", *IEEE / ASME Transactions on Mechatronics*, **4**, pp. 246-257.

105. Kahlon G., Mohan R., Liu N., Rehman H., 1999, "A Case Study of Starting Power Requirement for Visteon Integrated Starter-Alternator System", *Proceedings of Digital Avionics Systems Conference*, **2**, pp. 8.B.4-1 – 8.B.4-7.

106. Keyhani A., 1999, "Modern Control of Industrial Electrical Machinery", *Class Notes of course EE 744 at the Ohio State University, Columbus, OH*.

107. Rizzoni G., 2000, "Powertrain Dynamics", *Class Notes of course ME 781 at the Ohio State University, Columbus, OH*.

108. Vroemen B., 2001, "Component Control for the Zero Inertia Powertrain", *Ph.D. dissertation, Technische Universiteit Eindhoven, The Netherlands*.

109. www.wfw.wtb.tue.nl/em/pdf/poster02/p02drogen.pdf

110. ca.autos.yahoo.com/030402/11/shrz.html

111. Streib H., Bischof H., 1996, "Electronic Throttle Control (ETC): A Cost Effective System for Improved Emissions, Fuel Economy, and Driveability", *SAE paper 960338*, pp. 169-176.

112. Wit C., Kolmanovsky I., Sun J., 2001, "Adaptive Pulse Control of Electronic Throttle", *Proceedings of American Control Conference, Arlington, VA*, pp. 2872-2877.

113. Hiramatsu T., Akagi T., Yoneda H., 1985, "Control Technology of Minimal Slip-Type Torque Converter Clutch", *SAE paper 850460*, pp. 127-135.

114. Ross P., 2003, "Top 10 Techno-Cool Cars", *IEEE Spectrum*, pp. 30-35.

115. Aidemark J., Vinter J., Folkesson P., Karlsson J., 2002, "Experimental Evaluation of Time-Redundant Execution for a Brake-by-Wire Applications", *IEEE Proceedings of the International Conference on Dependable Systems and Networks*.

116. Powell B., Sureshbabu N., Bailey K., Dunn M., 1998, "Hardware-In-The-Loop Vehicle and Powertrain Analysis and Control Design Issues", *Proceedings of American Control Conference, Philadephia, PA*, pp. 483-492.

117. www.bgsoflex.com/airdragchart.html

118. www.teknett.com/pwp/drmayf/dragcd~1.hrm

119. www.school-for-champions.com/science/frictionrolling2.htm

120. www.toyota.com/html/shop/vehicles/prius/spec/prius_specs.html

121. www.oldsmobile.com/alero/features/specifications.htm